CHARACTERIZATION AND REMEDIATION OF A CONTROLLED DNAPL RELEASE: FIELD STUDY AND UNCERTAINTY ANALYSIS

By

MICHAEL CARSON BROOKS

A DISSERTATION PRESENTED TO THE GRADUATE SCHOOL
OF THE UNIVERSITY OF FLORIDA IN PARTIAL FULFILLMENT
OF THE REQUIREMENTS FOR THE DEGREE OF
DOCTOR OF PHILOSOPHY

UNIVERSITY OF FLORIDA

2000

ACKNOWLEDGEMENTS

I would like to thank my committee members: Drs. Paul Chadik, Wendy D. Graham, P. Suresh C. Rao, and Michael D. Annable; and my committee chair: William R. Wise for their professional dedication. They have continually been an inspirational source of guidance and assistance. I have also benefited from discussions with Drs. Kirk Hatfield, A. Lynn Wood and Carl G. Enfield, and I thank them for their assistance. I would also like to recognize and thank my fellow graduate students, for they too have served as an invaluable resource in my education. This study involved numerous people, and this dissertation would not be possible without their work. I wish to specifically thank Dr. Wise for his guidance with the material presented in Chapters 2 and 3, and Dr. Annable for his work and assistance with Chapters 4 and 5 (including the tracer degradation correction work he completed). Chapter 5 has benefited from several reviews by Drs. Annable, Rao, Wise, Wood, and Enfield, as well as reviews by Dr. James Jawitz, and I thank them all for their helpful comments. I would also like to specifically thank Irene Poyer and Jaehyun Cho for their work in the laboratory, and Dr. Andrew James for producing the graphical display of the MLS data in Chapter 5. Finally, most of all, I would like to thank my family for their love and support.

TABLE OF CONTENTS

page

ACKNOWLEDGMENTS ii

LIST OF TABLES vi

LIST OF FIGURES viii

ABSTRACT xii

CHAPTERS

1 INTRODUCTION 1

2 GENERAL METHODS FOR ESTIMATING UNCERTAINTY IN TRAPEZOIDAL RULE-BASED MOMENTS 5

Introduction 5
Theory 8
General Expressions 8
Systematic Errors 11
Random Errors 11
Validation and Analysis Using a Synthetic Data Set 18
Results and Discussion 19
Systematic Errors 19
Random Errors 22
Conclusions 27

3 UNCERTAINTY IN NAPL VOLUME ESTIMATES BASED ON PARTITIONING TRACERS 29

Introduction 29
A Review of Partitioning Tracer Tests 29
Sources of Uncertainty and Errors 30
Uncertainty-Estimation Method 37
General Equations 37
Systematic Errors 38

Random Errors 38
Results and Discussion 42
Systematic Errors 42
Random Errors 45
Applications 46
Conclusions 50

4 PRE- AND POST-FLUSHING PARTITIONING TRACER TESTS ASSOCIATED WITH A CONTROLLED RELEASE EXPERIMENT 52

Introduction 52
Site Description 52
Background Sorption Tracer Test 55
Controlled Release Conducted by EPA 55
Partitioning Tracer Tests 59
Results and Discussion 61
Extraction Wells 61
Comparison to Release Locations and Volumes 68
Summary of Post-Flushing Partitioning Tracer Test 69
Discussion 71
Conclusions 75

5 FIELD-SCALE COSOLVENT FLUSHING OF DNAPL FROM A CONTROLLED RELEASE 77

Introduction 77
Methods 80
PCE Volume Initially Present 80
System Description 81
Performance Monitoring 83
Results and Discussion 84
System Hydraulics 84
Mass Recovery 87
Ethanol Recovery 92
PCE Recovery 93
Treatment Efficiency 97
Changes in Aqueous PCE Concentrations 100
Recycling Treatment 100
Conclusions 102

6 CONCLUSIONS 103

APPENDICES

A SYSTEMATIC ERRORS 108

B RANDOM ERRORS IN MOMENT CALCULATIONS 116

C DELTA METHOD FORMULAS 126

REFERENCES 140

BIOGRAPHICAL SKETCH 147

LIST OF TABLES

Tables		page
1-1.	Sequence of activities completed in the cell	4
2-1.	Comparison of mass and swept volume CV (%) based on Monte Carlo (M.C.) simulations and semi-analytical calculations (S.A)	25
3-1.	Summary of errors and their impact on partitioning tracer test predictions	32
3-2.	Comparison of the CV (%) estimated from Monte Carlo (M.C.) simulations and semi-analytical procedure (S.A) for three cases	46
4-1.	Summary of results from the background sorption tracer test	56
4-2.	Volume of PCE (L) added and removed from the cell	58
4-3.	Partitioning coefficients for tracers used in the pre- and post-flushing partitioning tracer tests	62
4-4.	Summary of results for common non-reactive lower and upper zone tracers from the pre-flushing test	64
4-5.	Pre-flushing partitioning tracer test, common lower zone partitioning tracer results	64
4-6.	Pre-flushing partitioning tracer test, upper-zone reactive tracer (n-heptanol) results. The corrected mass recovery is based on a first-order degradation model	65
4-7.	Pre-flushing partitioning tracer test, summary of unique tracer pairs injected into wells 45 and 55	69
4-8.	Post-flushing partitioning tracer test summary	72
4-9.	Comparison in NAPL volume (L) estimates based on four schemes of log-linear BTC extrapolation	74

5-1. Phases of the flushing demonstration 83

5-2. Summary of PCE volumes predicted from pre- and post-flushing PITTs..... 97

LIST OF FIGURES

Figures page

2-1. Relative error between trapezoidal and true values, expressed as a function of the number of intervals used in the numerical integration. The normal probability density function was used in the comparison (average = 1, standard deviation = 1, and integrated from -4 to 6). Shown on the graph are the absolute first moment by equation (2-5) (◇) and equation (2-4a) (□), and the absolute second moment by equation (2-5) (Δ) and equation (2-4a) (x) 10

2-2. Relative errors in the zeroth moment (solid line) and the normalized first moment (dashed line) for a) constant systematic volume errors, and b) proportional systematic volume errors. The volume errors are benchmarked to the swept volume 20

2-3. Relative error in zeroth moment (solid line) and normalized first moment (dashed line) as a function of the ratio of constant systematic concentration errors to injection concentration 23

2-4. BTCs for the synthetic non-reactive and reactive tracers, as well as "measured" non-reactive (crosses) and reactive (circles) BTCs generated from one Monte Carlo realization. Both volume standard deviation and concentration CV were equal to 0.15 25

2-5. Coefficient of variation (%) of the a) zeroth and b) normalized first moments as a function of the ratio of volume standard deviation to swept volume. Each line represents concentration CV of 0.0 (o), 0.5 (□), 0.10 (◇), 0.15 (Δ), 0.20 (*), 0.25 (x) and 0.30 (+), respectfully 26

2-6. Coefficient of variation for the zeroth moment (closed symbols) and the normalized first moment (open symbols) for a range in concentration detection-limit coefficient of variation (CV_{DL}) values. Results are shown for maximum-concentration

coefficient of variation (CV_{max}) values of 5% (◇), 10% (□), and 15% (Δ). Volume error was neglected 28

3-1. The effects of systematic errors on retardation (solid line), saturation (short-dashed line), and NAPL volume (long-dashed line) are illustrated for the case of a) constant systematic volume errors, b) proportional systematic volume errors, and c) constant systematic concentration errors. The retardation factor was 1.5 in each case, and the BTCs were composed of 100 data points 43

3-2. NAPL volume CV as a function of retardation factor for volume and concentration measurement errors of 0.05 (diamonds), 0.15 (squares), and 0.30 (triangles). BTCs with 100 data points were used to generate the figure 47

3-3. NAPL volume coefficient of variation as a function of dimensionless volume errors for BTCs of 50 (diamonds), 100 (squares), and 350 (triangles) volume-concentration data points. The figure is based on a retardation factor of 1.5 47

3-4. Retardation (triangles), NAPL saturation (squares), and NAPL volume (circles) CV as a function of the concentration detection limit CV. The CV of the maximum concentrations were 5% (open symbols) and 15% (closed symbols). The figure is based on 100 volume-concentration data points, and a retardation factor of 1.5 49

3-5. Impacts of background-retardation uncertainty. The NAPL volume CV is presented as a function of retardation for background retardation CVs of 5% (circles), 15% (triangles), and 30% (squares). The curves with the open symbols are based on a partitioning coefficient of 8, and the curves with the closed symbols are based on a partitioning coefficient of 200 49

4-1. Cell instrumentation layout 54

4-2. a) Double five-spot pumping pattern used in the background sorption tracer test and the ethanol flushing demonstration (discussed in Chapter 5), and b) inverted, double five-spot pumping pattern used in the pre- and post-flushing tracer test 56

4-3. PCE injection locations and volumes (plan view). The number inside the circles indicates the release volume (L) per location 58

4-4. Selected EW 51 BTCs from the pre-flushing partitioning-tracer test. a) Common lower zone tracers: methanol (closed diamonds) and 2-octanol (open diamonds), b) unique lower zone tracers: isobutanol (closed circles) and 3-heptanol (open circles), and c) upper zone tracers: isopropanol (closed squares) and n-heptanol (open squares) 63

4-5. Pre-flushing PITT estimate of a) upper zone and b) lower zone spatial distribution of NAPL based on extraction well data 70

4-6. DNAPL volume estimated from the pre- and post-partitioning tracer tests as a function of the tracer partitioning coefficient 73

4-7. Average and standard deviation in NAPL volume from four different extrapolation schemes 74

5-1. Cumulative volume injected into a) the lower zone, and b) the upper zone. Injected fluid consists of new ethanol (triangles), recycled ethanol (squares), and water (circles) for the lower zone; and re-cycled water (squares) and water (circles) for the upper zone 85

5-2. PCE concentrations (squares) and ethanol percentages (triangles) from a) upper zone extraction well 45A, and b) lower zone extraction well 45B. 88

5-2. continued. PCE concentrations (squares) and ethanol percentages (triangles) from c) upper zone extraction well 55A, and d) lower zone extraction well 55B..... 89

5-3. Ratio of PCE concentration to PCE solubility limit for upper zone (plus signs) and lower zone (circles) samples from extraction wells a) 45 and b) 55. The PCE solubility limits are a function of ethanol content, and were based on values reported by VanValkenburg (1999)..... 90

5-4. Aqueous PCE distribution based on MLS samples from the end of the flushing demonstration. The concentration contours were created using an inverse distance contouring method in the TechPlot software package. 95

5-5. Removal efficiency for a) upper zone: 45A (plus symbols) and 55A (triangles); and b) lower zone: 45B (minus symbol), 55B (circles), and 51B (x)..... 99

5-6. DNAPL removal effectiveness versus reduction in PCE concentrations 101

Abstract of Dissertation Presented to the Graduate School
of the University of Florida in Partial Fulfillment of the
Requirements for the Degree of Doctor of Philosophy

CHARACTERIZATION AND REMEDIATION OF A CONTROLLED DNAPL RELEASE: FIELD STUDY AND UNCERTAINTY ANALYSIS

By

Michael Carson Brooks

December, 2000

Chair: William R. Wise
Major Department: Environmental Engineering Sciences

A dense non-aqueous phase liquid (DNAPL) source zone was established within an isolated test cell through the controlled release of 92 L of perchloroethylene (PCE) by EPA researchers. The purpose of the release was to evaluate innovative DNAPL characterization and remediation techniques under field conditions. Following the release, a partitioning-tracer test to characterize the DNAPL, a cosolvent flood to remediate the DNAPL, and a second partitioning tracer test to characterize the remaining DNAPL were conducted by University of Florida researchers who had no knowledge of the volume, the method of release, nor the resulting spatial distribution.

The pre-flushing, partitioning tracer test predicted 60 L of PCE, or 70% of the 86 L of PCE estimated in the cell at the start of the tracer test. The estimate of 86 L was based on the release information and the amount of PCE removed by activities conducted between the PCE release and the tracer test. The partitioning tracer test estimate was

complicated by tracer degradation problems. During the cosolvent flood, the cell was flushed with an ethanol-water solution for approximately 40 days. Alcohol solution extracted from the cell was recycled after treatment using activated-carbon and air-stripping. Based on the release information and the amount of PCE removed by all prior activities, it was estimated that 83 L of PCE was in the cell at the start of the flood. The amount of PCE removed during the alcohol flushing demonstration was 53 L, which represents a flushing effectiveness, defined as the percent mass of PCE removed, of 64%. The mass balance from the cosolvent flood indicated that 30 L of PCE remained in the test cell prior to the final tracer test, but the results from this test only predicted 5 L.

The majority of the data from these tests was analyzed using moments calculated from breakthrough curves. General stochastic methods were investigated whereby the uncertainty in volume and concentration measurements were used to estimate the uncertainty of the zeroth and normalized first moments. These methods were based on the assumption that moments are calculated from the breakthrough curves by numerical integration using the trapezoidal rule. The uncertainty associated with the NAPL volume estimates using partitioning tracers was then quantified by propagating uncertainty in moments to NAPL volume estimates.

CHAPTER 1
INTRODUCTION

Groundwater contaminants originate from a number of sources in modern society, including: fuels for transportation and heating, solvents and metals from commercial and industrial activities, herbicides and pesticides from farming activities, and spent nuclear material from nuclear power and weapons production. While an awareness for the need to preserve and protect natural resources can be traced back to the late 1800s, it is only within the last 30 years that society has taken steps, in the form of federal laws, to protect groundwater resources, and correct adverse impacts on ground-water resources. Most environmental protection regulations in the United States (US) were not established until the 1970s, starting with the basic environmental policy act, the National Environmental Policy Act (NEPA), in 1969. Specific water protection and restoration regulations were established by the Federal Water Pollution Control Act of 1972, which was later amended to become the Clean Water Act in 1977, the Safe Drinking Water Act in 1974, the Resource Conservation and Recovery Act (RCRA) in 1976, and the Comprehensive Environmental Response, Compensation, and Liability Act in 1980.

These regulations ultimately provided the driving force for the work in the area of groundwater contaminant characterization and remediation within the US since the late 1970s. In turn, from this work emerged a better understanding of the complexity of groundwater contamination characterization and remediation issues. It became apparent that new methods would be necessary to economically characterize and remedy source-

zone contamination. Persistent organic contaminant plumes have a source, which typically consists of non-aqueous phase liquid (NAPL). Dense, non-aqueous phase liquids (DNAPLs) have densities greater than water and are particularly difficult to characterize and remove because of their subsurface behavior in complex geology. Within the last 5 years, efforts have focused on new and innovative techniques to deal with source-zone contamination.

Partitioning tracers are among the new characterization techniques for source-zone contamination. The technique originated in the petroleum industry as a means to estimate oil saturations in reservoirs, and has been applied to groundwater characterization to estimate the amount of NAPL present. Likewise, cosolvent flushing is among the new source-zone remediation techniques, and it too has roots in the petroleum industry (Rao et al., 1997). These techniques have been successfully demonstrated in laboratory experiments and pilot studies, and partitioning tracers have been used in full-scale operations.

Due to the challenges associated with DNAPL characterization and remediation, the performance of innovative techniques is still uncertain. A jointly sponsored demonstration was undertaken to investigate the ability of six different techniques to remediate DNAPLs. The demonstration discussed herein was the first of these techniques. The tests were conducted at the Dover National Test Site (DNTS), located at Dover Air Force Base (AFB) in Dover, Delaware. The DNTS is a field-scale laboratory, designed as a national test site for evaluating remediation technologies (Thomas, 1996). Each demonstration is to follow a similar test protocol. Researchers from the Environmental Protection Agency (EPA) begin each test by releasing a known quantity

of PCE into an isolated test cell. However, the amount and spatial distribution of the release are not revealed to the researchers conducting the demonstration until they have completed the characterization and remediation components of their test protocol. After a release, a partitioning tracer test is completed to characterize the volume and distribution of PCE, followed by the remedial process, and finally, a post-remediation partitioning tracer test is conducted to evaluate the remedial performance. Since multiple technologies were planned for each test cell, DNAPL characterization using soil cores was not feasible. The University of Florida was involved in two of the demonstrations. The first demonstration, enhanced dissolution by ethanol flushing, was completed between July 1998 and June 1999. The sequence of activities for this demonstration is summarized in Table 1-1.

In the course of analyzing the data from the demonstration, it became of interest to estimate the uncertainty associated with the results. This was of particular interest due to the unique feature of this demonstration: a controlled contaminant release into a native medium. However, it is easily understood that the uncertainty of a result is of fundamental importance to the proper use of that result, and many introductory texts on measurement uncertainty or error propagation provide illustrative examples of this point. There are limited references to quantifying the uncertainty of NAPL estimates from partitioning tracer tests. For that matter, there are limited references to the more general problem of estimating uncertainty for moments based on breakthrough curves (BTCs). Consequently, procedures to estimate the uncertainty of the demonstration results were investigated.

Table 1-1. Sequence of activities completed in the cell.

Activity	Date	Purpose
Hydraulic Test	September 5 - 8, 1997	Estimate cell-average hydraulic conductivity.
Pre-Release Partitioning Tracer Test (PITT)	May 28 - June 4, 1998	Investigate cell hydraulics and background retardation.
Controlled PCE Release	June 10 – 12, 1998	Release known PCE volume at specified locations.
Conservative Interwell Tracer Test (CITT)	June 18 – 25, 1998	Investigate PCE dissolution characteristics.
Pre-Demonstration PITT	July 1 – 12, 1998	Estimate PCE distribution.
Ethanol Flushing Demonstration	February 2 - March 19, 1999	DNAPL remediation by ethanol flushing.
Post-Demonstration PITT	May 7 – 19, 1999	Estimate remaining PCE distribution.

Chapter 2 presents the methods investigated to estimate the uncertainty in moments calculated from BTCs, and Chapter 3 presents the method used to estimate uncertainty in NAPL volume estimates. Chapter 4 presents the results from the pre- and post-flushing partitioning tracer tests, and Chapter 5 presents the results from the ethanol-flushing test. Chapter 6 is the conclusion.

CHAPTER 2
GENERAL METHODS FOR ESTIMATING UNCERTAINTY IN TRAPEZOIDAL RULE-BASED MOMENTS

Introduction

There are many instances in hydrology and engineering where tracers are used to characterize system hydrodynamics. This typically involves measuring the system response to an injected tracer in the form of a breakthrough curve (BTC). Subsequent BTC analysis has varied, but has generally followed one of two methods: moment analysis or model analysis. Model analysis typically consists of a procedure whereby model parameters are determined such that the mathematical model prediction matches the tracer response (curve fitting), and hydrodynamic properties of the system are characterized by the model parameters. It has been reported that curve-fitting techniques produce more accurate results compared to the use of moments (Fahim and Wakao, 1982; Haas et al., 1997). The mathematical model must be based on the physical and chemical nature of the hydrodynamic system. The inability of mathematical models to accurately describe the physical and chemical nature of complex hydrodynamic systems is a disadvantage of this approach. In moment analysis, hydrodynamic properties of the system are investigated using moments calculated from the BTCs. For example, the zeroth moment of the BTC is a measure of the tracer mass recovered from the system, the first moment is a measure of the travel time through the system, and the second moment is a measure of the mixing in the system. Moments can be estimated from the BTCs

either by direct numerical integration, or by fitting a curve to the BTC and then subsequent analysis is based on moments estimated from the mathematical curve (Jin et al., 2000, Haas et al., 1997, Helms, 1997). In the latter case, it is not necessary for the model to be an accurate representation of the physical system, all that is necessary is for the curve to accurately describe the shape of the breakthrough curve. Helms (1997) showed that nonlinear regression methods were more reliable for estimating BTC moments than direct integration for imperfect BTCs. However, assuming an adequate number of data points are available to define a BTC, direct numerical integration of the BTC has been found to satisfactorily predict moments (Helms, 1997; Jin et al., 1995). With this qualification, direct integration using the trapezoidal rule to estimate moments from BTCs is advantageous due to its simplicity.

Skopp (1984) stated that the accurate estimation of moments is prevented for two reasons. "First, the data obtained is invariably noisy; second, at some point the data must be truncated." Noisy data is the result of measurement error, and is inherent in any experimental procedure. The uncertainty associated with each measurement can be divided into what has traditionally been referred to as systematic and random errors. Systematic errors are generally defined as errors that affect the measurement in a consistent manner, and if identified can be corrected by applying an appropriate correction factor (Massey, p. 67, 1986). Systematic errors can be further classified as constant or proportional errors (Funk et al., 1995). Constant systematic errors have a magnitude that is independent of the measurement magnitude, while proportional systematic errors are scaled to the measurement magnitude. Random errors result from unidentifiable sources, and must be handled using stochastic methods. The accuracy of a

measurement is therefore a function of both systematic and random errors, and the precision of multiple measurements is a function of random errors.

The uncertainty in an experimental result due to random measurement error can best be estimated by conducting statistical analysis on results from multiple trials of the same experiment. However, in many cases, it is not practical to conduct multiple trials of the same experiment, as in the case of large field-scale experiments. In such situations, it is necessary to estimate experimental uncertainty by other means, such as error-propagation techniques. This basically consists of measuring or estimating uncertainty for fundamental variables, and then propagating the uncertainties through to the final experimental result. For moments based on direct numerical integration of the BTCs, fundamental variables consist of time or volume, and concentration. Eikens and Carr (1989) used error-propagation methods to estimate the uncertainty in statistical moments of chromatographic peaks. Their method was based on several simplifying assumptions, which limited application to temporal moments based on evenly spaced data and constant concentration uncertainty. Specifically, they presented formulas for the absolute zeroth, first normalized, and second normalized moments under the stated conditions.

This chapter presents analytical and semi-analytical equations to estimate the uncertainty in moments resulting from systematic and random measurement errors. The method is based on the assumption that moments are estimated from experimentally measured BTCs by numerical integration using the trapezoidal rule. It is also assumed that a finite tracer pulse is used in the tracer test. However, the same methods could be used to develop uncertainty equations if tracer is introduced into the system by a step change in concentration. A synthetic data set is used to demonstrate uncertainty

estimates with the equations. Uncertainly predictions resulting from random measurement errors are compared to results from a Monte Carlo analysis for validation. Finally, the equations are used to investigate general relationships between uncertainty in measurements and estimated moments.

Theory

General Expressions

An experimentally measured BTC can be represented by a series of volume and concentration measurements:

$$V_1, \ldots, V_{i-1}, V_i, V_{i+1}, \ldots, V_n, \text{ and } c_1^d, \ldots, c_{i-1}^d, c_i^d, c_{i+1}^d, \ldots, c_n^d \quad (2\text{-}1)$$

where V_i = i^{th} cumulative volume measurement [L^3], and c_i^d = i^{th} dimensioned concentration measurement [ML^{-3}]. Each dimensioned concentration, c_i^d, is converted to a dimensionless concentration, c_i, by dividing by the tracer injection concentration (c_0):

$$c_i = \frac{c_i^d}{c_0} . \quad (2\text{-}2)$$

The absolute k^{th} moment, m_k [$L^{3(k+1)}$], of the BTC based on volume measurements is defined as

$$m_k = \int_0^\infty cV^k dV , \quad (2\text{-}3)$$

and can be approximated using the trapezoidal rule by

$$m_k \cong \sum_{i=1}^{n-1} \overline{cV_i^k} \Delta V_i , \quad (2\text{-}4a)$$

where $\Delta V_i = (V_{i+1} - V_i)$, and $\overline{cV_i^k} = (c_i V_i^k + c_{i+1} V_{i+1}^k)/2$. Note that the numerical approximation methods used herein employ a forward difference scheme starting with i = 1. The absolute zeroth moment of the breakthrough curve, m_0 [L^3] is

$$m_0 = \int_0^\infty c dV \cong \sum_{i=1}^{n-1} \bar{c}_i \Delta V_i \qquad (2\text{-}4b)$$

where $\bar{c}_i = (c_i + c_{i+1})/2$. The zeroth moment is a measure of the mass associated with the breakthrough curve, and is typically used to measure the tracer mass recovered, or to measure contaminant mass removed during treatment processes. The absolute first moment of the breakthrough curve, m_1 [L^6], can be approximated by

$$m_1 = \int_0^\infty cV dV \cong \sum_{i=1}^{n-1} \overline{cV_i} \Delta V_i \ , \qquad (2\text{-}4c)$$

where $\overline{cV_i} = (c_i V_i + c_{i+1} V_{i+1})/2$.

Haas (1996) discussed the difference between approximating moments using equation (2-4a) and

$$m_k = \int_0^\infty c V^k dV \cong \sum_{i=1}^{n-1} \bar{c}_i \bar{V}_i^k \Delta V_i \ , \qquad (2\text{-}5)$$

where $\bar{V}_i^k = (V_i^k + V_{i+1}^k)/2$. He concluded that equation (2-4a) produced a less biased estimate of the moments, and therefore should be used in preference to equation (2-5). As an illustration of this point, Figure 2-1 shows the percent difference between the first and second absolute moments of the normal probability density function estimated using equations (2-4a) and (2-5), as a function of the number of intervals used in the trapezoidal rule. The percent difference between the first absolute moments is practically

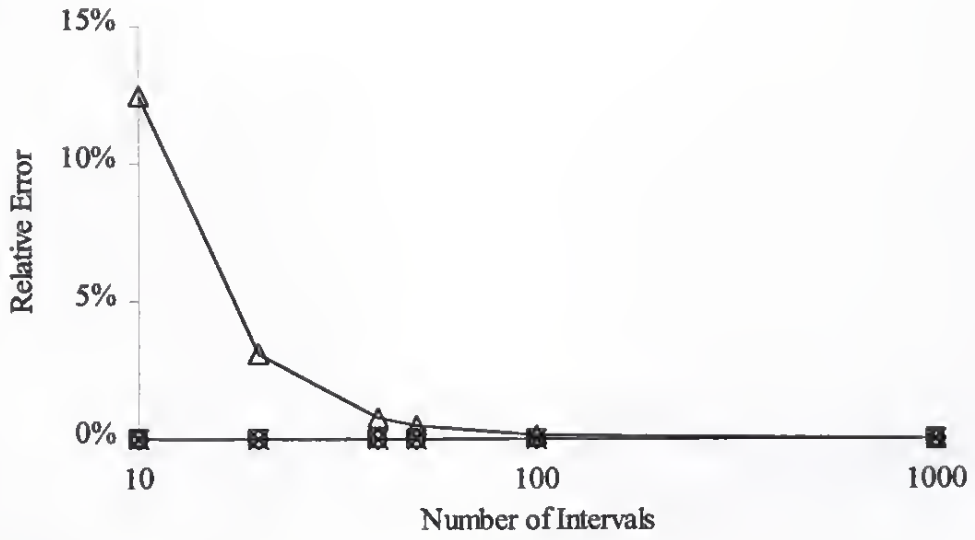

Figure 2-1. Relative error between trapezoidal and true values, expressed as a function of the number of intervals used in the numerical integration. The normal probability density function was used in the comparison (average = 1, standard deviation = 1, and limits of integration = -4 to 6). Shown on the graph are the absolute first moment by equation (2-5) (◇) and equation (2-4a) (□), and the absolute second moment by equation (2-5) (Δ) and equation (2-4a) (x).

insignificant for 10 or more intervals. However, significant differences are observed for the higher moment. At least 80 intervals are needed to ensure the percent difference between the second absolute moments is less than 1%. Equation (2-5) is considered accurate enough for use herein because this work is limited to the zeroth and first absolute moments, and the BTCs typically consist of 50 or more volume-concentration pairs.

The pulse-corrected, normalized first moment, μ_1' [L^3] is defined as

$$\mu_1' = \frac{m_1}{m_0} - \frac{V_p}{2}, \qquad (2\text{-}6)$$

where V_p = tracer pulse volume [L^3]. The normalized first moment for a non-reactive tracer is a measure of the volume through which the tracer was carried. This is generally referred to as the mean residence volume, or for groundwater tracer tests, the swept pore volume.

Systematic Errors

The effect of systematic errors can be estimated in a deterministic manner by deriving the moment equations using equation (2-1), modified to include systematic errors in volume and concentration measurements. The resulting equations accounting for constant and proportional systematic errors in volume and concentration measurements are presented in Appendix A.

Random Errors

Absolute moments. The effects of random errors in volume and concentration measurements on equations (2-1) through (2-6) were estimated by the application of conventional stochastic formulas for variance propagation. The procedure is presented below for the zeroth moment, and in Appendix B for the first absolute moment.

Each measurement is assumed to have a zero-meaned, random error such that

$$\alpha = \alpha^t + e_\alpha \ , \tag{2-7}$$

where α = measured value, α^t = true value, and e_α = zero-meaned, random measurement error. The expectation, or mean, μ_x, of a random variable x is defined as

$$\mu_x = E[x] = \int_{-\infty}^{\infty} x p_x(x) dx \ , \tag{2-8a}$$

where x = random variable, and $p_x(x)$ = probability density function of x. The variance of x, referred to as either var[x] or σ_x^2, is defined as

$$\sigma_x^2 = \text{var}[x] = \int_{-\infty}^{\infty}(x-\mu_x)^2 p_x(x)dx = E[x^2] - \mu_x^2 \ . \qquad (2\text{-}8b)$$

Applying equations (2-8a) and (2-8b) to equation (2-7) results in

$$E[\alpha] = \alpha^t \ , \text{and} \qquad (2\text{-}9a)$$

$$\text{var}[\alpha] = \text{var}[e_\alpha] \ , \qquad (2\text{-}9b)$$

respectively. Each dimensioned concentration is converted to a dimensionless concentration as shown in equation (2-2). Generally, the value of c_0 has less uncertainty than c_i^d because c_0 is a controlled concentration produced at the start of tracer tests, and because multiple samples from the injection volume are generally collected and analyzed. Therefore, the error associated with c_0 is neglected, and the error associated with c_i is assumed equal to the error associated with c_i^d, scaled by c_0. The variance of ΔV_i can be expressed in terms of the variance in the i^{th} and $(i+1)^{th}$ volume measurements by

$$\sigma^2_{\Delta V[i]} = \sigma^2_{V[i]} + \sigma^2_{V[i+1]} . \qquad (2\text{-}10)$$

Note that equation (2-10) reflects that the volume measurements are independent of one another. To avoid double subscripts, the notation V[i] is used to represent V_i. Likewise, the variance in the average concentration over the i^{th} interval in terms of the variance in the i^{th} and $(i+1)^{th}$ dimensionless concentration is given by

$$\sigma^2_{\bar{c}[i]} = \frac{1}{4}\sigma^2_{c[i]} + \frac{1}{4}\sigma^2_{c[i+1]} \ . \qquad (2\text{-}11)$$

Equation (2-11) reflects that concentration measurements (for a given tracer) are also independent from one another. Formally, the expected value of a function, g(x,y), with two random variables x and y is

$$E[g(x,y)] = \int_{-\infty}^{\infty}\int_{-\infty}^{\infty} g(x,y)p_{x,y}(x,y)dxdy \qquad (2\text{-}12a)$$

where $p_{x,y}(x,y)$ is the joint probability density function. If x and y are independent, then the expected value of the function is

$$E[g(x,y)] = \int_{-\infty}^{\infty}\int_{-\infty}^{\infty} g(x,y)p_x(x)p_y(y)dxdy \qquad (2\text{-}12b)$$

where $p_x(x)$ and $p_y(y)$ are the probability density functions for random variables x and y, respectively. The variance of g(x,y) is defined as

$$\text{var}[g(x,y)] = E\left[\{g(x,y)\}^2\right] - \left\{\mu_{g(x,y)}\right\}^2 . \qquad (2\text{-}13)$$

Assuming volume and concentration measurements are independent, equations (2-12b) and (2-13) can be used to derive the following variance equation for the i^{th} product $\Delta V\bar{c}$:

$$\sigma^2_{\Delta V\bar{c}[i]} = (\Delta V_i)^2\sigma^2_{\bar{c}[i]} + \sigma^2_{\Delta V[i]}\bar{c}_i^2 + \sigma^2_{\Delta V[i]}\sigma^2_{\bar{c}[i]} . \qquad (2\text{-}14)$$

The variance of the sum of the i^{th} and $(i+1)^{th}$ products of differential volumes and average concentrations is given by

$$\text{var}[\Delta V_i\bar{c}_i + \Delta V_{i+1}\bar{c}_{i+1}] = \text{var}[\Delta V_i\bar{c}_i] + \text{var}[\Delta V_{i+1}\bar{c}_{i+1}] + 2\,\text{cov}[\Delta V_i\bar{c}_i, \Delta V_{i+1}\bar{c}_{i+1}] . \qquad (2\text{-}15)$$

The i^{th} and $(i+1)^{th}$ products of differential volumes and average concentrations are not independent since they both use the $(i+1)^{th}$ measure of cumulative volume and concentration. The general definition of covariance is

$$\sigma_{xy} = \text{cov}[x,y] = E[(x-\mu_x)(y-\mu_y)] = E[xy] - \mu_x\mu_y . \qquad (2\text{-}16)$$

Applying equation (2-16) to the i^{th} and $(i+1)^{th}$ products of differential volumes and average concentrations yields

$$\mathrm{cov}\left[\Delta V_i \bar{c}_i, \Delta V_{i+1} \bar{c}_{i+1}\right] = E\left[\Delta V_i \bar{c}_i \Delta V_{i+1} \bar{c}_{i+1}\right] - \Delta V_i^t \bar{c}_i^t \Delta V_{i+1}^t \bar{c}_{i+1}^t \ , \tag{2-17}$$

which results in the following equation after expansion and subsequent simplification using the fact that the expected value of a zero-meaned random variable is zero (see Appendix B):

$$\mathrm{cov}\left[\Delta V_i \bar{c}_i, \Delta V_{i+1} \bar{c}_{i+1}\right] = \frac{1}{4}\Delta V_i^t \Delta V_{i+1}^t \sigma^2_{c[i+1]} - \bar{c}_i^t \bar{c}_{i+1}^t \sigma^2_{V[i+1]} - \frac{1}{4}\sigma^2_{c[i+1]}\sigma^2_{V[i+1]} \ . \tag{2-18}$$

The variance of the absolute zeroth moment estimate using the trapezoidal rule is then given by the sum of all n-1 products of differential volume and average concentration:

$$\mathrm{var}\left[m_0\right] = \sum_{i=1}^{n-1} \mathrm{var}\left[\Delta V_i \bar{c}_i\right] + 2\sum_{i=1}^{n-2} \mathrm{cov}\left[\Delta V_i \bar{c}_i, \Delta V_{i+1} \bar{c}_{i+1}\right] \ . \tag{2-19}$$

The derivation for the variance of the first absolute moment is complicated by the addition of the average-volume term (see equation (2-5) with k = 1), but follows the same basic outline completed for the zeroth moment. The final equation for the absolute first moment variance is similar to equation (2-19), but the covariance expression (analogous to equation (2-18) for the zeroth moment) contains 15 terms, and each variance of the product $\Delta V_i \bar{V}_i \bar{c}_i$ must account for the corresponding covariance between the differential and average volumes. The complete derivations are presented in Appendix B.

An alternative method to estimating BTC moment uncertainty is the delta method (Kendall and Stuart, pg. 246, 1977; Papoulis, 1991; Lynch and Walsh, Appendix A, 1998). This method uses Taylor series expansions to estimate the statistical moments of random variables. Higher accuracy is obtained by including higher-order terms in the

Taylor series. The first-order approximation to the variance of the k^{th} absolute moment based on numerical integration using the trapezoidal rule is

$$\sigma^2_{m[k]} \cong \sum_{i=1}^{2n} \sigma^2_{x[i]} \left(\frac{\partial m_k}{\partial x_i} \right)^2 , \tag{2-20a}$$

and the second-order approximation is

$$\sigma^2_{m[k]} \cong \sum_{i=1}^{2n} \sigma^2_{x[i]} \left(\frac{\partial m_k}{\partial x_i} \right)^2 + \sum_{i=1}^{2n} \sum_{j>1}^{2n} \sigma^2_{x[i]} \sigma^2_{x[j]} \left(\frac{\partial^2 m_k}{\partial x_i \partial x_j} \right)^2 . \tag{2-20b}$$

Equations (2-20a) and (2-20b) are based on the assumption that all x_i random variables are independent, and equation (2-20b) is based on the additional assumption that the random variables have symmetric probability distributions. An overview of the delta method is presented in Appendix C, and the method is applied to estimate the uncertainty in the absolute zeroth and first moments. As shown in Appendix C, the second-order expression for the zeroth-moment variance is an exact expression, and is therefore equivalent to the variance given by equation (2-19). A second-order expression for the first absolute moment is also given in Appendix C. However, this is an approximation to the true variance since it ignores third-order mixed derivative terms.

Normalized moment. To estimate the uncertainty associated with the k^{th} normalized moment, it is necessary to estimate the variance of the ratio of the k^{th} absolute moment to the zeroth moment. The exact analytical solution is obtained by the evaluation of equation (2-12a) and (2-13), with g(x,y) defined as m_k/m_0. The difficulty in evaluating the resulting integrals, however, makes approximation methods more practical. The delta method is often used to estimate the uncertainty of a ratio of two

random variables. Winzer (2000) discussed the accuracy of error propagation related to the ratio of two numbers using the delta method, which in general can be expressed as

$$\sigma_{b/a}^2 = \left(\frac{b}{a}\right)^2 \left(\frac{\sigma_a^2}{a^2} + \frac{\sigma_b^2}{b^2} - \frac{2\sigma_{a,b}}{ab}\right) . \tag{2-21}$$

For the ratio of the absolute k^{th} to the zeroth moment,

$$\sigma_{\mu[k]}^2 = \left(\frac{m_k}{m_0}\right)^2 \left(\frac{\sigma_{m[0]}^2}{m_0^2} + \frac{\sigma_{m[k]}^2}{m_k^2} - \frac{2\sigma_{m[0]m[k]}}{m_0 m_k}\right) . \tag{2-22}$$

Equations (2-21) and (2-22) are first-order approximations because all terms in the Taylor series expansion with second- and higher-order derivatives are neglected (See Appendix C). The zeroth and k^{th} absolute moments are not independent since they are based on the same measurements of volume and concentration. Therefore, the covariance between the two is needed to apply equation (2-22). Due to the complexity of an analytical solution, a delta method approximation to the covariance is also used. For two random variables a and b, which are functions of random variables x_1 to x_m, the first-order approximation to $\sigma(a,b)$ is (see Appendix C)

$$\sigma(a,b) \cong \sum_{i=1}^{m}\sum_{j=1}^{m} \sigma(x_i,x_j)\left(\frac{\partial a}{\partial x_i}\right)\left(\frac{\partial b}{\partial x_j}\right) . \tag{2-23}$$

For the covariance between the zeroth and k^{th} absolute moments, equation (2-23) becomes

$$\sigma(m_0,m_k) \cong \sum_{i=1}^{2n}\sum_{j=1}^{2n} \sigma(x_i x_j)\left(\frac{\partial m_0}{\partial x_i}\right)\left(\frac{\partial m_k}{\partial x_j}\right) . \tag{2-24a}$$

The second-order approximation to $\sigma(m_0,m_k)$ is (see Appendix C)

$$\sigma(m_0,m_k) \cong \sum_{i=1}^{2n} \sigma_{x[i]}^2 \frac{\partial m_0}{\partial x_i}\frac{\partial m_k}{\partial x_i} + \sum_{i=1}^{2n}\sum_{j>1}^{2n} \sigma_{x[i]}^2\sigma_{x[j]}^2 \frac{\partial^2 m_0}{\partial x_i \partial x_j}\frac{\partial^2 m_k}{\partial x_i \partial x_j} . \tag{2-24b}$$

Equation (2-24b) is based on the assumptions that all x_i random variables are independent and that they have symmetric probability distributions. Since the zeroth and first-absolute moments are calculated using the trapezoidal rule, the variables x_1 through x_{2n} in equation (2-24) are the measured volume and concentration values:

$$\{x_1,...,x_i,...,x_n\} = \{V_1,...,V_i,...,V_n\} \text{ , and} \tag{2-25a}$$

$$\{x_{n+1},...,x_{i+n},...,x_{2n}\} = \{c_1,...,c_i,...,c_n\} \text{ .} \tag{2-25b}$$

Appendix C also presents the derivation of the first-normalized moment uncertainty. The uncertainty of the pulse-corrected, first-normalized moment is

$$\sigma^2_{\mu[1]'} = \sigma^2_{\mu[1]} + \sigma^2_{V[p]}, \tag{2-26}$$

where $\sigma^2_{V[p]}$ is the variance of one-half the tracer-pulse volume, which is estimated from the field methods employed in the tracer test.

Special case: constant flow rate. For the case where the flow rate is constant over the duration of the test, moments can be calculated on a temporal basis rather than a volumetric basis. From a practical standpoint, random errors in measuring time can be neglected, and the equations for estimating moment uncertainty can be simplified. In this case, the uncertainty for the k^{th} temporal moment ($m_{k,t}$) can be written as

$$\sigma^2_{m[k,t]} = \frac{1}{4}\Delta t_1^2 t_1^{2k}\sigma^2_{c[1]} + \sum_{i=1}^{n-2}\left[\frac{1}{4}\left(\Delta t_i^2 + \Delta t_{i+1}^2\right)\left(t_{i+1}^{2k}\sigma^2_{c[i+1]}\right)\right] + \frac{1}{4}\Delta t_n^2 t_n^{2k}\sigma^2_{c[n]} \text{ .} \tag{2-27a}$$

Under the additional condition of constant Δt, equation (2-27a) becomes

$$\sigma^2_{m[k,t]} = \frac{1}{4}\Delta t^2\left[t_1^{2k}\sigma^2_{c[1]} + 2\sum_{i=2}^{n-2}\left[t_i^{2k}\sigma^2_{c[i]}\right] + t_n^{2k}\sigma^2_{c[n]}\right] \text{ ,} \tag{2-27b}$$

and under the further condition of constant σ_c, equation (2-27b) reduces to

$$\sigma^2_{m[k,t]} = \frac{1}{4}\Delta t^2 \sigma_c^2 \left[t_1^{2k} + 2\sum_{i=2}^{n-2} \left[t_i^{2k} \right] + t_n^{2k} \right] . \qquad (2\text{-}27c)$$

For the zeroth moment, equation (2-27c) becomes

$$\sigma^2_{m[0,t]} = \frac{1}{2}(n-1)\Delta t^2 \sigma_c^2 . \qquad (2\text{-}28)$$

(The equation for the zeroth-temporal moment reported by Eikens and Carr (1989) under the same conditions (constant Δt and σ_c) was $n\Delta t^2 {\sigma_c}^2$. The difference between their equation and that reported in equation (2-28) results from a difference in the formulation of the numerical approximation to the moment integral). The uncertainty in the flow rate is then used to estimate the uncertainty in the k^{th} volumetric moment:

$$\sigma^2(Qm_{k,t}) = Q^2 \sigma^2_{m[k,t]} + \sigma_Q^2 m^2_{k,t} + \sigma_Q^2 \sigma^2_{m[k,t]} , \qquad (2\text{-}29)$$

where Q = the volumetric flow rate [L^3T^{-1}], and σ_Q^2 [L^6T^{-2}] is the variance of the flow rate. Equation (2-29) is based on the assumption of independence between measurement errors in the flow rate and temporal moments.

Validation and Analysis Using a Synthetic Data Set

A synthetic data set was generated to validate the method for estimating moment uncertainty and to investigate the impact of measurement uncertainty on moment calculations. The synthetic data set was generated using the solution to the one-dimensional advective-dispersive transport equation, subject to the initial condition of $c(x,0) = 0$ for $x \geq 0$, and the boundary conditions of $c(0,t) = c_0$ for $t \geq 0$, and $c(\infty,t) = 0$ for $t \geq 0$ (Lapidus and Amundson, 1952; Ogata and Banks, 1961). The nondimensional form of the solution, accounting for retardation, is

$$c(\tau, R, P_e) = \left(\frac{1}{2}\right)\left\{erfc\left[\sqrt{\frac{P_e}{4R\tau}}(R-\tau)\right] + \exp(P_e)erfc\left[\sqrt{\frac{P_e}{4R\tau}}(R+\tau)\right]\right\}, \quad (2\text{-}30)$$

where c is the dimensionless concentration (c^d/c_0), τ is the dimensionless pore volume (τ = vt/L, where v = pore velocity [LT^{-1}], t = time [T], and L = linear extent of the flow domain [L]), R = retardation factor ($R = 1+(SK_{NW})/(1-S)$, where S = NAPL saturation and K_{NW} = NAPL partitioning coefficient), and P_e = Peclet number (P_e = vL/D, where D = dispersion coefficient [L^2T^{-1}]). Note that for the nonreactive tracer, R = 1. This solution is for a step input of tracer, and was used to generate a pulse-input solution by superposition, lagging one step-input solution by the tracer pulse-input length and subtracting it from another. The nondimensional pulse length (defined as $\tau_p = vt_p/L$, where t_p is the pulse duration [T]) was 0.1, and the Peclet number was 10. The nonreactive and reactive breakthrough curves represented the known, or true data set. The synthetic data set was chosen such that the zeroth moment of the tracers was 1, and the normalized first moment of the non-reactive tracer was 10. Unless noted otherwise, a total of 100 volume-concentration data points were used to represent the BTCs, and a retardation factor of 1.5 was used to generate the reactive breakthrough curve.

Results and Discussion

Systematic Errors

Constant systematic volume errors. The impact of constant systematic errors in volume measurements on the absolute zeroth moment and the normalized first moment are illustrated in Figure 2-2a. The volume error shown on the abscissa in Figure 2-2a is expressed as a fraction of the pore volume, as predicted by the non-reactive normalized

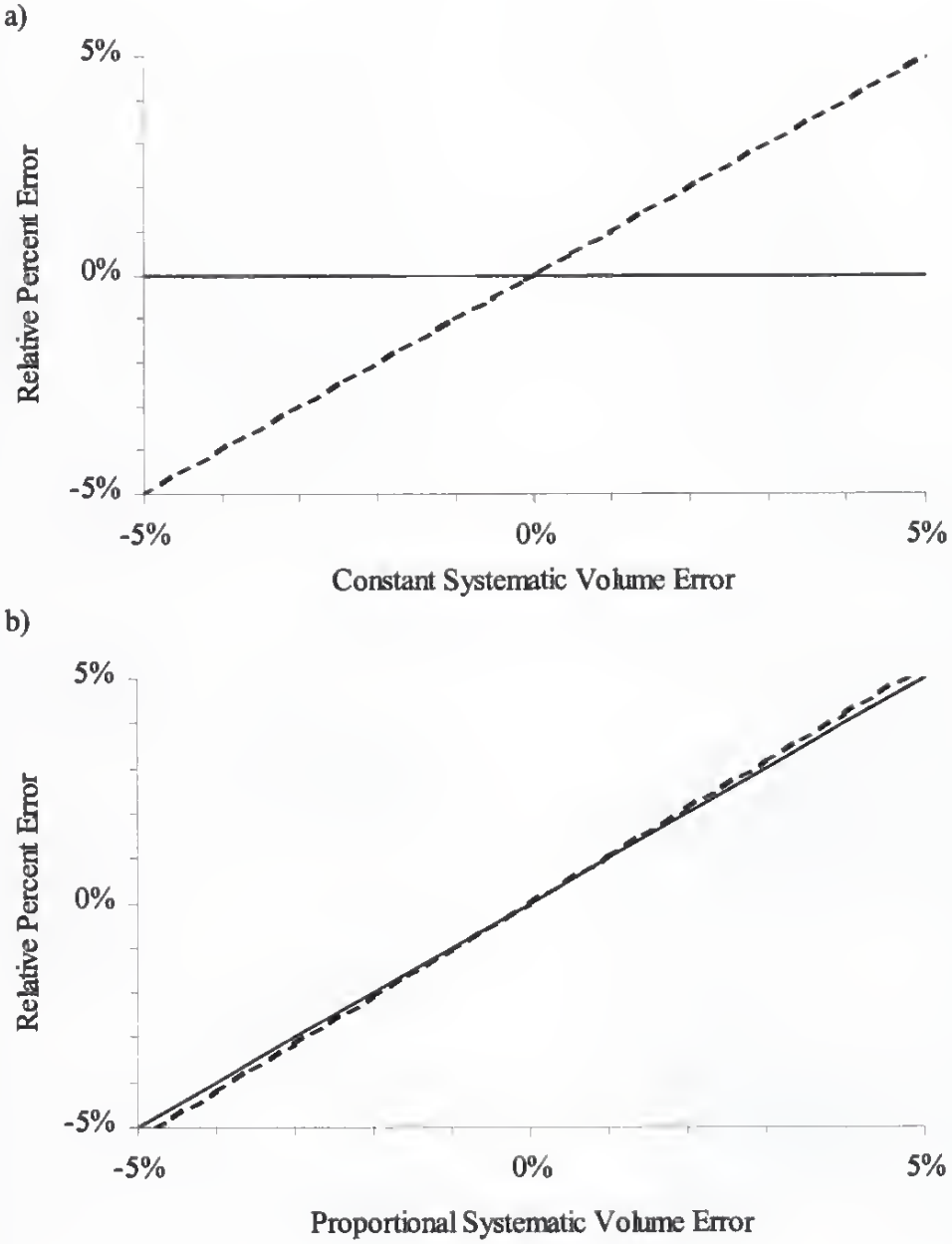

Figure 2-2. Relative errors in the zeroth moment (solid line) and the normalized first moment (dashed line) for a) constant systematic volume errors, and b) proportional systematic volume errors. The volume errors are benchmarked to the swept volume.

first moment. Constant systematic errors in volume measurements have no impact on the zeroth moment because this moment is based on a volume differential, and consequently the error is eliminated. However, higher-order moments, like the first-normalized moment (see Figure 2-2a), will be affected because of the volume dependency in the numerator of the moment calculation (see equation (2-4a) or (2-5)). As shown in Figure 2-2a, the normalized first moment is directly proportional to the constant systematic volume error.

Proportional systematic volume errors. The impact of proportional systematic errors in volume measurements on the absolute zeroth moment and normalized first moment are illustrated in Figure 2-2b. The error shown on the abscissa in Figure 2-2b is defined in the same manner above for the constant systematic volume error. Proportional systematic errors in volume measurements directly impact both the absolute zeroth moment and the normalized first moment. As shown in Figure 2-2b, the zeroth moment is directly proportional to the proportional systematic volume error. The normalized first moment is also directly proportional to the proportional systematic volume error, and the difference between the lines in Figure 2-2b is due to the correction of one-half the pulse volume. Errors in pulse volume were neglected in this analysis.

Constant systematic concentration errors. For this analysis, constant systematic errors are limited to magnitudes equal to or less than method detection limits, based on the assumption that larger values would be readily identified by typical quality assurance procedures used in the laboratory. Assuming typical values for alcohol tracers, i.e., injection concentrations on the order of 1000 mg/L and method detection limits on the order of 1 mg/L, dimensionless concentration errors could range from –0.001 to

+0.001. The impacts of errors in this range on the absolute zeroth moment and normalized first moment are shown in Figure 2-3. It is noted that the effects of these types of errors will be more pronounced for smaller injection concentrations, but they would also be easier to identify. For example, dimensionless errors ranging from –0.001 to +0.001 produce errors in the zeroth moment ranging from –7% to +7%. Mass recoveries ranging from 93% to 107% are not unrealistic, and do not necessarily indicate analytical problems. However, dimensionless concentration errors ranging from –0.01 to +0.01 (1 mgL^{-1} /100 mgL^{-1}) produce errors in the zeroth moment ranging from -70% to +70%. Mass recoveries less than 90% or greater than 110% should be used with caution, and certainly, mass recoveries as low as 30% or as large as 170% would clearly reflect a serious problem with the tracer data.

Proportional systematic concentration errors. As shown by equations (A-20a) through (A-20c) in Appendix A, the impact of proportional systematic errors in concentration measurements is eliminated by using dimensionless concentrations. Therefore, proportional systematic concentration errors do not impact moments.

Random Errors

Method validation. The variance of the zeroth and absolute first moments calculated by the analytical expressions were compared to variances estimated by the delta method. The zeroth-moment variance calculated by the two methods is the same since both expressions are exact. The first-absolute moment variance calculated by the two methods were similar, and the slight differences between the two were attributed to the delta-method approximation.

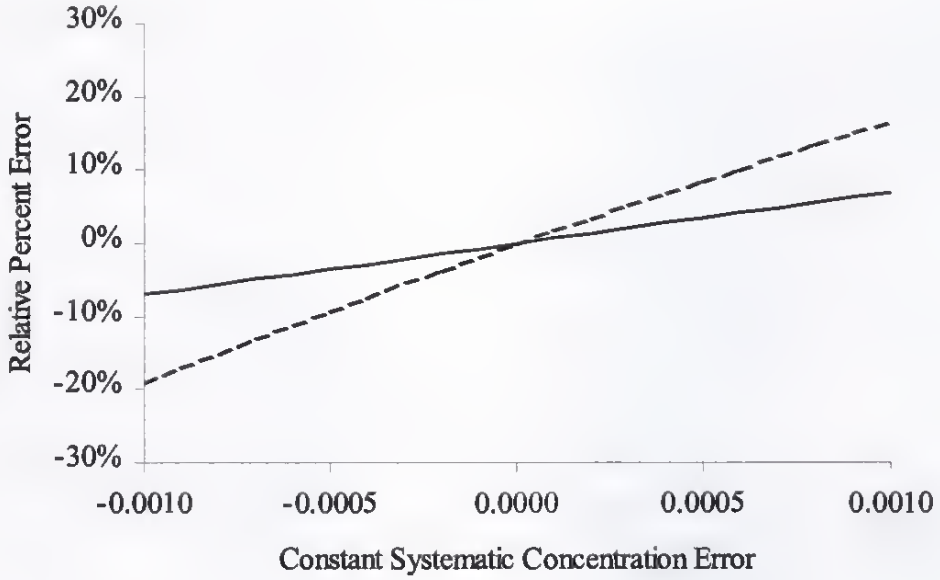

Figure 2-3. Relative error in zeroth moment (solid line) and first-normalized moment (dashed line) as a function of the ratio of constant systematic concentration errors to injection concentration.

Monte Carlo analysis (see, for example, Gelhar, 1993) was used to verify normalized moment uncertainty estimates. Measurement uncertainty was assumed to be a normally distributed random variable with a zero mean. Concentration-measurement uncertainty was assigned using a coefficient of variation (CV), defined as the ratio of standard deviation to true measurement, between 0 and 0.15. Volume-measurement uncertainty was assigned by equating volume standard deviation to a value less than or equal to one-half the interval between volume measurements (a constant interval was used). A unique measurement error was applied to each volume and concentration value in the synthetic data set. Moment calculations were then completed on the "measured" BTC. This process was repeated 10,000 times, and the averages and standard deviations

of the moments were computed. Convergence of Monte Carlo results was tested by completing three identical simulations, each with 10,000 iterations; the CV for the moments differed by no more than 0.02%. Figure 2-4 shows BTCs for the synthetic non-reactive and reactive tracers, as well as "measured" BTCs generated from one Monte Carlo realization with the volume standard deviation and concentration CV defined as 0.15.

Table 2-1 compares the absolute zeroth and normalized first moment CVs using the semi-analytical equations to those estimated from the Monte Carlo simulation. Three cases are presented: the first with volume uncertainty (standard deviation) equal to 0.35 and no concentration uncertainty, the second with no volume uncertainty and concentration uncertainty equal to 0.15, and the third case with volume uncertainty equal to 0.35 and the concentration uncertainty equal to 0.15. The second-order covariance expression between the zeroth and absolute first moments (equation (2-24b)) provided much better agreement with the Monte Carlo results, and was therefore used in the semi-analytical method rather than the first-order covariance expression (equation (2-24a)). As shown in Table 2-1, the agreement between the two methods demonstrates that the semi-analytical method correctly accounts for the uncertainly in volume and concentration measurements.

Application. Based on the CV of the moments, concentration errors have a greater impact on the results than volume errors. This is illustrated in Figure 2-5, which shows the CV for the zeroth and normalized first moments as a function of volume and concentration errors. Concentration errors are expressed as CV, and volume errors are expressed as the ratio of the volume measurement standard deviation to the swept

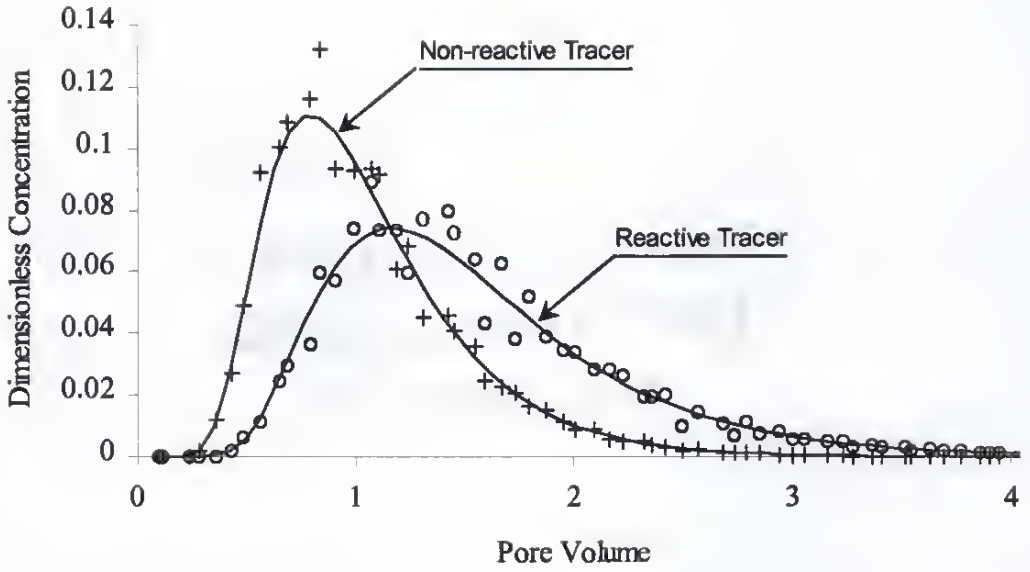

Figure 2-4. BTCs for the synthetic non-reactive and reactive tracers, as well as "measured" non-reactive (crosses) and reactive (circles) BTCs generated from one Monte Carlo realization. Both volume standard deviation and concentration CV were equal to 0.15.

Table 2-1. Comparison of mass and swept volume CV (%) based on Monte Carlo (M.C.) simulations and semi-analytical calculations (S.A).

	S. A.	M. C.
Case A		
Mass	1.8	1.8
Swept Volume	0.9	0.9
Case B		
Mass	3.4	3.5
Swept Volume	1.1	1.0
Case C		
Mass	4.1	4.1
Swept Volume	1.4	1.4

Case A: volume error = 0.35 and concentration CV = 0; Case B: volume error = 0 and concentration CV = 0.15; and Case C: volume error = 0.35 and concentration CV = 0.15.

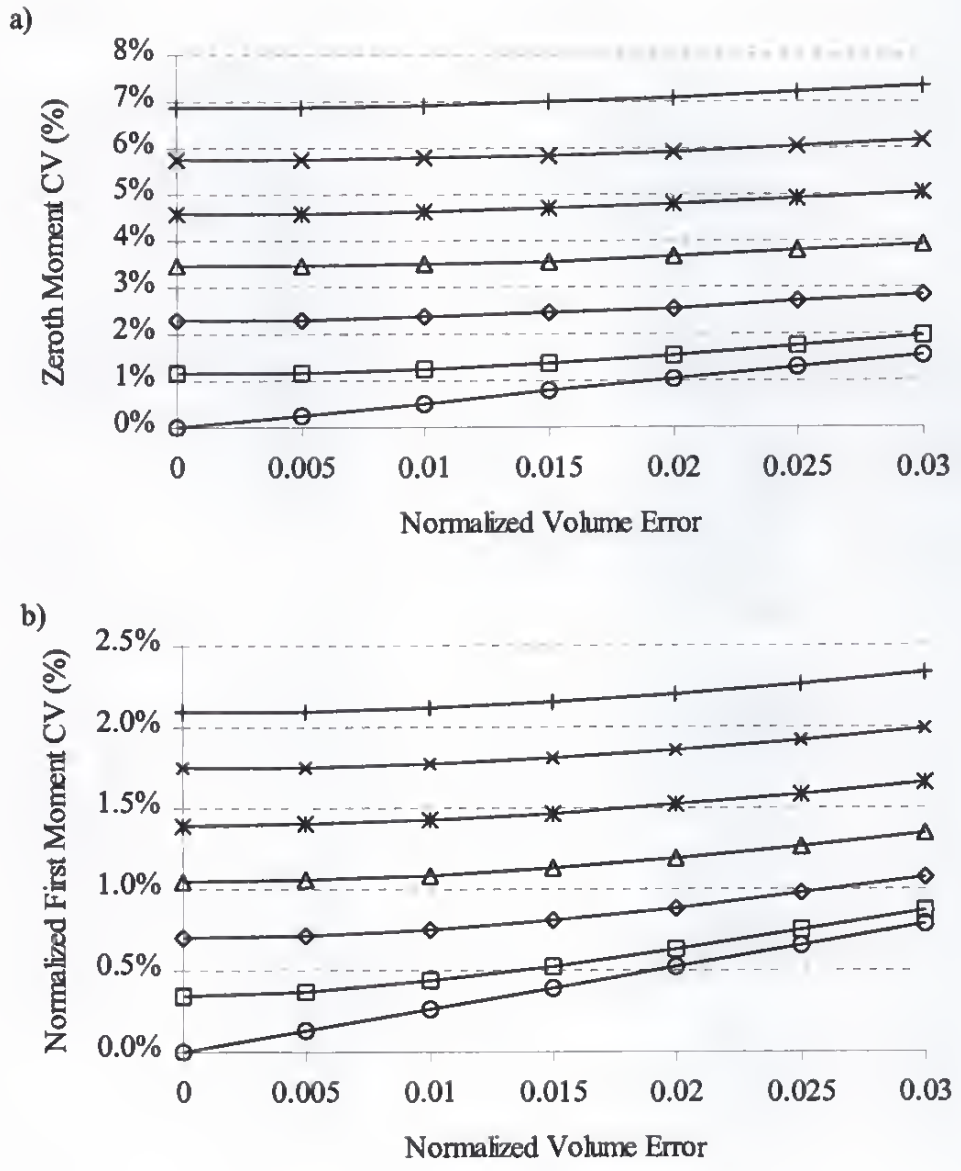

Figure 2-5. Coefficient of variation (%) of the a) zeroth and b) normalized first moments as a function of the ratio of volume standard deviation to swept volume. Each line represents concentration CVs of 0.0 (o), 0.05 (□), 0.10 (◇), 0.15 (Δ), 0.20 (*), 0.25 (x) and 0.30 (+), respectfully.

volume. The robust nature of moment calculations is exemplified by the fact that relative uncertainty in moments is less than the relative uncertainty in volume and concentration measurements. In addition, measurement uncertainty has less impact on the first-normalized moment than the zeroth moment, which results from the fact that normalized moments are a function of the ratio of absolute moments.

It could be argued that the uncertainties in concentrations near the detection limit are higher than the uncertainties in concentrations near the largest concentration measurements on the BTC. To investigate the impact of variable concentration uncertainty, it was assumed that the concentration CV varied linearly between the CV of the maximum concentration (CV_{max}) and the CV of the detection-limit concentration (CV_{DL}). A detection limit of 0.001 (1 mg/L in 1,000 mg/L) was assumed for this analysis, and all concentrations equal to, or less than this value were assigned CV_{OL}. Figure 2-6 shows the CV for the zeroth and normalized first moments for $50\% < CV_{OL} < 200\%$, and for CV_{max} = 5%, 10% and 15%. Volume errors were neglected in this analysis. The zeroth moment CV varies from 4 to 15%, and the normalized first moment CV varies from 2% to 7%. These results provide further support for the conclusion that the relative uncertainty in moments is less than the relative uncertainty in concentration measurements.

Conclusions

This chapter presented a generalized method for estimating the uncertainty of BTC moments calculated by numerical integration using the trapezoidal rule. The method can be applied to either temporal or volumetric moments, and in the latter case, explicitly accounts for errors in volume measurements. The complexity of the

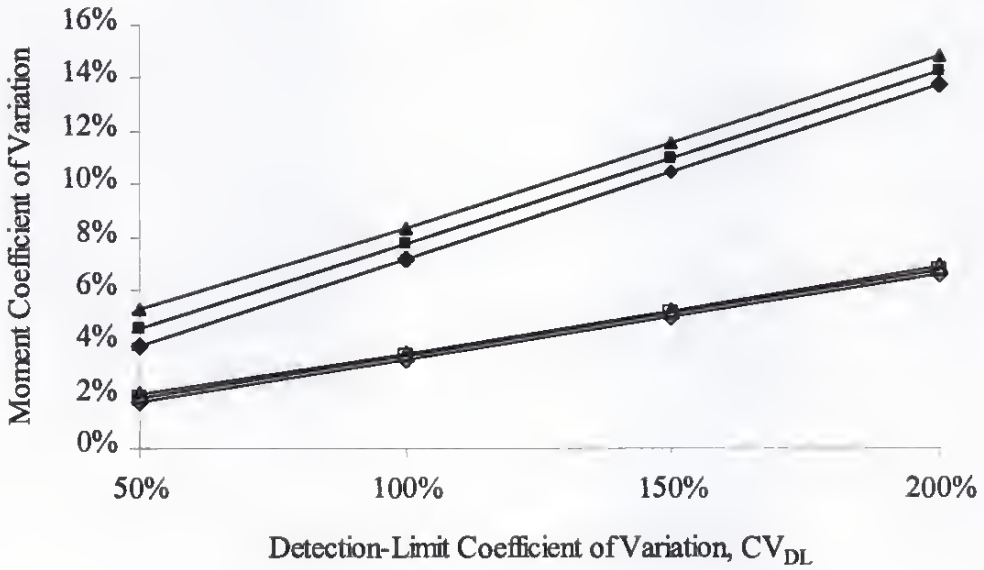

Figure 2-6. Coefficient of variation for the zeroth moment (closed symbols) and the normalized first moment (open symbols) for a range in concentration detection-limit coefficient of variation (CV_{DL}) values. Results are shown for maximum concentration coefficient of variation (CV_{max}) values of 5% (◇), 10% (□), and 15% (Δ). Volume error was neglected.

calculations for the zeroth moment is comparable to that associated with the typical propagation-of-errors formula. However, the formulae for higher moments, as exemplified by the first-absolute moment formulae, are substantially more complex than the typical propagation of errors formula. The results have shown that the relative moment uncertainty is less than the relative volume and concentration measurement uncertainties, and that the normalized first moment is impacted less than the zeroth moment. Moment uncertainties are more sensitive to concentration uncertainties as opposed to volume uncertainties.

CHAPTER 3
UNCERTAINTY IN NAPL VOLUME ESTIMATES BASED ON PARTITIONING TRACERS

Introduction

This chapter begins with a review of partitioning tracer tests and the errors and uncertainties that can affect their results. A method is then presented for estimating the uncertainty in NAPL volume estimates using partitioning tracers. It is based on the assumption that moments are calculated from the experimentally measured BTCs using the trapezoidal rule for numerical integration. The method for estimating uncertainty from random errors is based on standard stochastic methods for error propagation, and is verified through a comparison of uncertainty predictions to those made by Monte Carlo simulations using a synthetic data set. Systematic errors are also addressed. Finally, the methods are used to develop some general conclusions about NAPL volume measurement and uncertainty.

A Review of Partitioning Tracer Tests

Partitioning tracers were first used in the petroleum industry to estimate oil saturation. The first patents related to partitioning tracers were issued in 1971 (Cooke, 1971; Dean, 1971). Tang (1995) reviewed the application of partitioning tracers in the petroleum industry, and reported that over 200 partitioning tracer tests had been conducted in the petroleum industry since 1971. The first publication discussing the

application of the method to groundwater contaminant, source-zone characterization occurred in 1995 (Jin et al., 1995), in which the theory of partitioning tracers for source-zone contamination characterization was described and supported by experiments and model simulations. The first field application to a NAPL-contaminated aquifer took place at Hill AFB in 1994 (Annable et al., 1998). Other field applications have been described by Cain et. al. (2000), Sillan et al. (1999), Hayden and Linnemeyer (1999), and Nelson and Brusseau (1996). Dwarakanath et al. (1999) report that over 40 field demonstrations of the technique had been completed at that time. Rao et al. (2000) and Brusseau et al. (1999a) review partitioning tracer test methods, applications and reliability. Patents for source-zone characterization using partitioning tracers were issued in 1999 (Pope and Jackson, 1999a and 1999b).

Sources of Uncertainty and Errors

General sources of errors. Uncertainty in partitioning tracer predictions can result from two major sources: uncertainty in meeting underlying assumptions (modeling uncertainty), and uncertainty in measured values used in the partitioning tracer technique (measurement uncertainty). As discussed in Chapter 2, measurement uncertainty can be divided into systematic and random errors.

In general, a partitioning tracer is retarded relative to a non-partitioning tracer due to its interaction with NAPL, and the NAPL saturation can be estimated based on the extent of retardation. NAPL saturation can also be estimated using two partitioning tracers, provided the partitioning coefficients differ enough to ensure the retardation of one relative to the other can be sufficiently measured. Partitioning-tracer tests are based on several assumptions, and they can be summarized broadly as: retardation of the

partitioning tracer results solely from the NAPL, partitioning tracers are in equilibrium contact with all the NAPL within the swept zone, and the partitioning relationship between the NAPL and the tracer can be accurately described by a linear equilibrium relationship (Jin et al., 1995). Uncertainty in tracer predictions can result when these assumptions are not sufficiently satisfied. Table 3-1 summarizes the different types of errors that can occur in partitioning tracer tests.

Dwarakanath et al. (1999) discussed errors caused by the background retardation of tracers due to tracer adsorption onto porous media. This will cause a systematically larger prediction in NAPL saturation due to the increase in tracer retardation. This error can be corrected by subtracting the background retardation factor from the partitioning tracer retardation factor, assuming that the total retardation of the partitioning tracer is the sum of background retardation and NAPL retardation. However, it should be recognized that in certain circumstances the total retardation may not be the sum of background retardation and NAPL retardation. Nelson et al. (1999) investigated the effect of permeability heterogeneity, variable NAPL distribution, and sampling methods on partitioning tracer predictions. Observations in laboratory experiments indicated that flow by-passing, resulting from both low conductivity regions and relative permeability reductions due to NAPL saturation, resulted in lower predictions of NAPL saturation. They also noted that the mixing in sampling devices of streamlines that have passed through a heterogeneous NAPL distribution resulted in under-predictions of NAPL saturation. Errors from these processes (flow by-passing, and streamline mixing) could result in a systematically lower prediction of NAPL saturation by partitioning tracers.

Table 3-1. Summary of errors and their impact on partitioning tracer test predictions.

Error	Type of Error	References
Nonlinear partitioning	Systematically larger	Wise et al. (1999), Wise (1999)
Rate-limited mass transfer	Systematically lower	Willson et al. (2000), Nelson and Brusseau (1996)
Non-reversible partitioning	Systematically lower or larger	Brusseau et al. (1999a)
Background retardation	Systematically larger	Dwarakanath et al. (1999)
Flow by-passing	Systematically lower	Nelson et al. (1999), Dwarakanath et al. (1999), Brusseau et al. (1999a), Jin et al. (1995)
Nonequilibrium partitioning	Systematically lower	Dwarakanath et al. (1999), Brusseau et al. (1999a)
Tracer mass loss	Systematically lower or larger	Brusseau et al. (1999a), Brusseau et al. (1999b)
Measurement Error	Systematically lower or larger, and random	Dwarakanath et al. (1999)
Variable NAPL characteristics	Systematically lower or larger, and random	Dwarakanath et al. (1999), Brusseau et al. (1999a)
Effects from remedial flushing solution	Systematically lower or larger	Lee et al. (1998)

A linear, reversible equilibrium relationship is usually used to describe the partitioning relationship between the tracer and the NAPL. Brusseau et al. (1999a) qualitatively discuss errors due to mass-transfer limitations and non-reversible partitioning. Dwarakanath et al. (1999) suggested results from laboratory column experiments could be used to select tracer residence times large enough to ensure partitioning is adequately described by equilibrium relationships. Lee et al. (1998) reported differences in partitioning coefficients measured from batch and column experiments, and suggested that the discrepancy in measurements could have resulted

from diffusion limitations of the tracer in the NAPL. Willson et al. (2000) investigated the effect of mass-transfer rate limitations on partitioning tracer tests. They conducted column laboratory experiments using TCE as the NAPL, isopropanol as the non-partitioning tracer, and 1-pentanol and 1-hexanol as the partitioning tracers. Experimental results were modeled using an advective-dispersive model, where mass transfer between the NAPL and aqueous phase were estimated using terms to describe boundary layer mass transfer resistance and internal-NAPL diffusion resistance. Modeling results successfully matched the experimental results. However, it was noted that the method-of-moments analysis also reasonably agreed with the experimental results. Valocchi (1985) showed that nonequilibrium does not effect the normalized first moment for diffusion physical, first-order physical, and linear chemical nonequilibrium models. If nonequilibrium partitioning of the tracer into the NAPL is adequately described by one of these models, then it could be concluded that nonequilibrium will not effect NAPL volume estimates. If nonequilibrium partitioning does occur, it should result in less tracer retardation, and therefore produce a systematically lower prediction of NAPL saturation and volume.

Wise et al. (1999) reported that partitioning between tracers and NAPL was inherently nonlinear, and showed that an unfavorable form of the Langmuir partitioning relationship effectively predicts the partitioning behavior. Error associated with using a linear equilibrium model in place of a nonlinear equilibrium model, as well as steps to minimize this error were discussed by Wise (1999). It was reported that this type of error produced systematically larger predictions of the NAPL saturation, and could be minimized by avoiding large injection concentrations for partitioning tracers.

Additional uncertainty in partitioning tracer tests can result from the interaction of tracers to resident remediation flushing solutions (such as cosolvent or surfactant solutions) if the partitioning tracer test is conducted after remediation efforts. Lee et al. (1998) investigated the impact of changes in NAPL characteristics from cosolvent flushing on tracer partitioning coefficients. They found that preferential dissolution of more soluble NAPL components during cosolvent flushing to enhance NAPL dissolution decreased the tracer-partitioning coefficient. This resulted in NAPL-volume estimates lower than the actual NAPL volume. Spatially variable NAPL characteristics could also impact partitioning-tracer behavior, and Dwarakanath et al. (1999) discussed the resulting uncertainty in partitioning coefficients using a model relating partitioning coefficients to NAPL composition.

The loss of tracer mass, and its affect on partitioning tracer tests was qualitatively discussed by Brusseau et al. (1999a). Brusseau et al. (1999b) investigated the effect of linear and non-linear degradation on the moments of a pulse-input of contaminant, the results of which can be applied to tracers as well. It was reported that the first moment for the case of linear degradation is reduced relative to the first moment for the case without degradation. Nonlinear degradation was investigated using a Monod equation. It was reported that the first moment with non-linear degradation was at first less than, and then greater than the first moment without degradation.

Previous uncertainty estimations. Helms (1997) compared techniques for estimating moments associated with imperfect data sets of tracer BTCs. Nonlinear least-squares regression was found to be an effective method for working with imperfect data; methods to estimate standard deviations and confidence intervals of temporal moments

based on a nonlinear regression technique were presented. However, the uncertainty analysis was not extended to NAPL-volume estimates.

Jin et al. (1997), Dwarakanath et al. (1999) and Jin et al. (2000) discussed errors and uncertainty related to partitioning tracer tests. The method discussed in the latter two papers is based on the propagation of random errors in the retardation factor and the partitioning coefficient through to NAPL saturation. Dwarakanath et al. (1999) also investigated the impact of systematic measurement errors in volume and concentration measurements on NAPL volume predictions. Systematic errors in volume measurements were reported to have limited impact on NAPL volume estimates, and systematic errors in concentration measurements were shown to inversely effect NAPL volume estimates. Random errors in retardation factors were characterized using nonlinear regression analysis to estimate the variance between collected BTC data and a theoretical model. Random errors in the measurement of the partitioning coefficient were assessed using the standard deviation of the isotherm slope from batch partitioning experiments, or by calculating the standard deviation of results from multiple experiments when the partitioning coefficient was estimated from column experiments. It was concluded that random errors in the retardation factor and in the partitioning coefficient result in an error of approximately 10% in the NAPL saturation when tests yield retardation factors greater than 1.2. Jin et al. (2000) made a similar presentation regarding the uncertainty in NAPL saturation as a function of retardation factor and partitioning coefficient uncertainty. However, they also include a formula for the uncertainty in the retardation factor as a function of the non-partitioning and partitioning first moments. However, no discussion of estimating these uncertainties is presented. As a further point of interest, Jin et al.

(2000) also present a formula for the normalized temporal moment, as a function of BTC extrapolation. Specific application of this formula for uncertainty analysis was not presented.

The technique used by Dwarakanath et al. (1999) and Jin et al. (2000) is based on the first-order Taylor series expansion for error propagation (delta method), and assumes that errors in the retardation factor and the partitioning coefficient are independent. The error in the retardation factor and normalized moments is based on the residual error between the measured data and the curve used to fit the data. The limitation in the method presented by Dwarakanath et al. (1999) is that the uncertainty in retardation and partitioning coefficient can only be propagated through to NAPL saturation. The uncertainty in NAPL volume cannot be estimated without the uncertainty in the swept volume (provided by the normalized first moment), and the correlation between the swept volume and saturation. Jin et al. (2000) provide an estimate of the non-partitioning normalized first moment uncertainty, which is based on the residual error between data points and the curve fit. However, the uncertainty in NAPL volume still requires the correlation between the swept volume and NAPL saturation. Furthermore, the uncertainty in the normalized moments and retardation does not explicitly account for measurement uncertainty, but is more accurately a measure of how well the curve fits the measured data. Curve-fitting techniques that explicitly include measurement uncertainty could be used with the procedure outlined by Dwarakanath et al. (1999) and Jin et al. (2000) to better estimate partitioning tracer test uncertainty.

Uncertainty-Estimation Method

General Equations

An outline of the equations used to estimate NAPL saturations and volumes from tracer information is presented as an introduction into the uncertainty equations. The retardation factor, R is defined as

$$R = \frac{\mu_1^{R'}}{\mu_1^{NR'}}, \tag{3-1a}$$

where $\mu_1^{NR'}$ [L^3] and $\mu_1^{R'}$ [L^3] are pulse-corrected, normalized first moments for the non-partitioning and partitioning tracers, respectively. The partitioning tracer may be retarded relative to the non-partitioning tracer due to adsorption onto the aquifer matrix (background retardation). If background retardation (R_B) has been measured, it can be accounted for using

$$R = \frac{\mu_1^{R'}}{\mu_1^{NR'}} - (R_B - 1), \tag{3-1b}$$

where R_B is defined as the ratio of the pulse-corrected normalized first moment of the partitioning tracer in the absence of NAPL to the pulse-corrected normalized first moment of the non-partitioning tracer. Assuming a linear equilibrium partitioning coefficient (K_{NW}), and pore space occupied by water (or air) and NAPL only, the saturation (S) can be calculated from

$$S = \frac{R-1}{R-1+K_{NW}}, \tag{3-2}$$

and the volume of NAPL, V_N, is given by

$$V_N = \mu_1^{NR'} S \quad . \tag{3-3}$$

Systematic Errors

The effect of systematic errors can be estimated in a deterministic manner by developing equations (3-1) through (3-3) with systematic errors in volume and concentration measurements. This was done for both constant and proportional systematic errors in volume and concentration measurements; those derivations and resulting formulae are presented in Appendix A.

Random Errors

To estimate the random uncertainty in R, it is necessary to estimate the covariance between the partitioning and non-partitioning normalized first moments, since they are based on the same volume measurements. Furthermore, it is possible for correlation to exist between the non-partitioning and partitioning tracer concentrations. The covariance is estimated using a first-order delta method approximation (see equation (2-23) in Chapter 2), which can be expressed as

$$\sigma\left(\mu_1^{NR'},\mu_1^{R'}\right)\cong\left[\sum_{i=1}^{2n}\sum_{j=1}^{2n}\sigma\left(x_i,x_j\right)\left(\frac{\partial\mu_1^{NR'}}{\partial x_i}\right)\left(\frac{\partial\mu_1^{R'}}{\partial x_j}\right)\right]+\sigma_{V[p]}^2\left(\frac{\partial\mu_1^{NR'}}{\partial V_p}\right)\left(\frac{\partial\mu_1^{R'}}{\partial V_p}\right) \quad . \qquad (3\text{-}4a)$$

The last term on the right-hand side on equation (3-4a) describes the covariance resulting from a common tracer-pulse volume. It is assumed that the tracer-pulse volume uncertainty is negligible due to the controlled conditions generally used in its measurement, and this term will be ignored in subsequent analysis. Since errors in volume and concentration measurements are assumed independent, equation (3-4a) can be written as

$$\sigma\left(\mu_1^{NR'},\mu_1^{R'}\right)\cong\sum_{i=1}^{n}\sigma^2\left(V_i\right)\left(\frac{\partial\mu_1^{NR'}}{\partial V_i}\right)\left(\frac{\partial\mu_1^{R'}}{\partial V_i}\right)+\sum_{i=1}^{n}\sigma\left(c_i^{NR},c_i^{R}\right)\left(\frac{\partial\mu_1^{NR'}}{\partial c_i^{NR}}\right)\left(\frac{\partial\mu_1^{R'}}{\partial c_i^{R}}\right) \quad , \qquad (3\text{-}4b)$$

or expressing the derivatives of the normalized first moments in terms of the zeroth and absolute first moments:

$$\sigma\left(\mu_1^{NR'},\mu_1^{R'}\right)\cong\sum_i^n\sigma^2\left(V_i\right)\left[\frac{m_0^{NR}\frac{\partial m_1^{NR}}{\partial V_i}-m_1^{NR}\frac{\partial m_0^{NR}}{\partial V_i}}{\left(m_0^{NR}\right)^2}\right]\left[\frac{m_0^{R}\frac{\partial m_1^{R}}{\partial V_i}-m_1^{R}\frac{\partial m_0^{R}}{\partial V_i}}{\left(m_0^{R}\right)^2}\right]+$$

$$\sum_i^n\sigma\left(c_i^{NR},c_i^{R}\right)\left[\frac{m_0^{NR}\frac{\partial m_1^{NR}}{\partial c_i^{NR}}-m_1^{NR}\frac{\partial m_0^{NR}}{\partial c_i^{NR}}}{\left(m_0^{NR}\right)^2}\right]\left[\frac{m_0^{R}\frac{\partial m_1^{R}}{\partial c_i^{R}}-m_1^{R}\frac{\partial m_0^{R}}{\partial c_i^{R}}}{\left(m_0^{R}\right)^2}\right], \quad (3\text{-}4c)$$

where $\sigma(c^{NR}, c^{R})$ is the covariance between the non-partitioning and partitioning concentrations. One possible approach to approximating the covariance is to assume a linear correlation between the non-partitioning and partitioning concentrations, in which case,

$$\sigma\left(c_i^{NR},c_i^{R}\right)=K\left[\mathrm{var}\left(\sigma_{c[i]}^{NR}\right)\right], \quad (3\text{-}5)$$

where K is estimated as the ratio of the i^{th} partitioning and non-partitioning concentrations. If it is assumed that there is no correlation between the non- partitioning and partitioning concentrations, then the second terms on the right-hand side of equations (3-4b) and (3-4c) are zero. The derivatives of the zeroth and absolute first moments with respect to volume and concentration measurements are the same as those used to estimate the covariance between the zeroth and absolute first moments from Chapter 2 (see Appendix C for a listing of those derivative expressions). Using a first-order delta method approximation to the uncertainty of the ratio of two random variable (see equation (2-21) in Chapter 2) the retardation variance, σ^2_R is approximated as

$$\sigma_R^2 = \left(\frac{\mu_1^{R'}}{\mu_1^{NR'}}\right)^2 \left[\frac{\sigma^2\left(\mu_1^{R'}\right)}{\left(\mu_1^{R'}\right)^2} + \frac{\sigma^2\left(\mu_1^{NR'}\right)}{\left(\mu_1^{NR'}\right)^2} - \frac{2\sigma\left(\mu_1^{R'}, \mu_1^{NR'}\right)}{\mu_1^{R'}\mu_1^{NR'}}\right]. \tag{3-6}$$

Likewise, equation (2-21) is used to estimate the uncertainty in saturation. The variance of the numerator in equation (3-2) is

$$\sigma_{R-1}^2 = \sigma_R^2 \ , \tag{3-7a}$$

and the variance of the denominator in equation (3-2) is

$$\sigma_{R-1+K[NW]}^2 = \sigma_R^2 + \sigma_{K[NW]}^2 \ . \tag{3-7b}$$

Note that equation (3-7b) reflects the assumption that the retardation factor and the partitioning coefficient are independent, which is the same assumption made by Dwarakanath et al. (1999) and Jin et al. (2000) in their analysis of NAPL saturation uncertainty. It could be argued that R and K_{NW} are correlated since the partitioning coefficient controls the degree of retardation. For this analysis, however, it is assumed that R and K_{NW} are independent because the random errors incurred in measuring either R or K_{NW} are independent. Accounting for the fact that R occurs in the numerator and denominator, the variance of the saturation, σ_S^2 becomes

$$\sigma_S^2 = \frac{(R-1)^2}{(R-1+K_{NW})^2}\left[\frac{\sigma_R^2}{(R-1)^2} + \frac{\left(\sigma_R^2 + \sigma_{K[NW]}^2\right)}{(R-1+K_{NW})^2} - \frac{2\sigma_R^2}{(R-1)(R-1+K_{NW})}\right], \tag{3-7c}$$

which reduces to

$$\sigma_S^2 = \frac{K_{NW}^2\sigma_R^2 + (R-1)^2\sigma_{K[NW]}^2}{(R-1+K_{NW})^4} \ . \tag{3-7d}$$

Equation (3-7d) is equivalent to that presented by Dwarakanath et al. (1999) and Jin et al. (2000).

The uncertainty of the NAPL volume must account for the correlation between the normalized first moment of the non-partitioning tracer and the saturation, since they are both based on the same volume and non-partitioning concentration measurements. Likewise, it must account for the correlation in non-partitioning and partitioning concentrations if present. The covariance between the two is estimated using the delta-method approximation (equation (2-23)):

$$\sigma\left(S,\mu_1^{NR'}\right)\cong\sum_{i=1}^{2n}\sum_{j=1}^{2n}\sigma\left(x_i,x_j\right)\left(\frac{\partial S}{\partial x_i}\right)\left(\frac{\partial \mu_1^{NR'}}{\partial x_j}\right). \tag{3-8}$$

The x values in equation (3-8) are the same as those stated in equations (2-25a) and (2-25b). The derivative of $\mu_1^{NR'}$ with respect to x_i in terms of the zeroth and absolute first moments is given in equation (3-4c). The derivative of S with respect to measurement x_i in terms of the zeroth and absolute first moments is

$$\frac{\partial S}{\partial x_i}=\frac{K_{NW}}{\left(R-1+K_{NW}\right)^2\left(\mu_1^{NR'}\right)^2}*$$
$$\left\{\mu_1^{NR'}\left[\frac{m_0^R\frac{\partial m_1^R}{\partial x_i}-m_1^R\frac{\partial m_0^R}{\partial x_i}}{\left(m_0^R\right)^2}\right]-\mu_1^{R'}\left[\frac{m_0^{NR}\frac{\partial m_1^{NR}}{\partial x_i}-m_1^{NR}\frac{\partial m_0^{NR}}{\partial x_i}}{\left(m_0^{NR}\right)^2}\right]\right\} \tag{3-9}$$

The derivatives of the zeroth and first absolute moments are listed in Appendix C. The covariance terms $\sigma(x_i,x_j)$ in equation (3-8) include the covariance between the volume and concentration measurements used in S and $\mu_1^{NR'}$. The volume and non-partitioning concentrations measurements are the same, consequently, the covariance is simply the volume variance and the non-partitioning concentration variance. The covariance between the non-partitioning and partitioning concentrations can be estimated using equation (3-5), but is assumed negligible for this analysis. With the covariance between

the NAPL saturation and the non-partitioning normalized first moment known, the variance in the volume estimate of NAPL is given by

$$\sigma^2_{V[N]} = \left(\bar{\mu}_1^{NR'}\right)^2\sigma_S^2 + \bar{S}^2\sigma\left(\bar{\mu}_1^{NR'}\right)^2 + \left[\sigma\left(\mu_1^{NR'},S\right)\right]^2 + 2\bar{\mu}_1^{NR'}\bar{S}\,\sigma\left(\mu_1^{NR'},S\right) + \sigma\left(\bar{\mu}_1^{NR'}\right)^2\sigma_S^2 \quad (3\text{-}10)$$

Results and Discussion

Systematic Errors

Constant systematic volume errors. The impact of constant systematic errors in volume measurements on retardation, saturation, and NAPL volume are illustrated in Figure 3-1a. The error shown on the abscissa in Figure 3-1a is expressed as a percent of the pore volume, as predicted by the non-partitioning normalized first moment. Constant systematic errors in volume measurements impact the retardation estimate to a lesser extent because the volume error occurs in both the numerator and denominator, and the saturation estimate to a greater extent because the magnitude of the partitioning coefficient relative to the error reduces the effect of the error in the denominator of equation (3-2). Interestingly, the final error in NAPL volume is relatively small due to the offsetting errors in saturation and the normalized first moment. This result agrees with that presented by Dwarakanath et al. (1999).

Proportional systematic volume errors. The impact of proportional systematic errors in volume measurements on retardation, saturation, and NAPL volume are illustrated in Figure 3-1b. The error shown on the abscissa in Figure 3-1b is the percent volume error. Proportional systematic errors in volume measurements have minimal

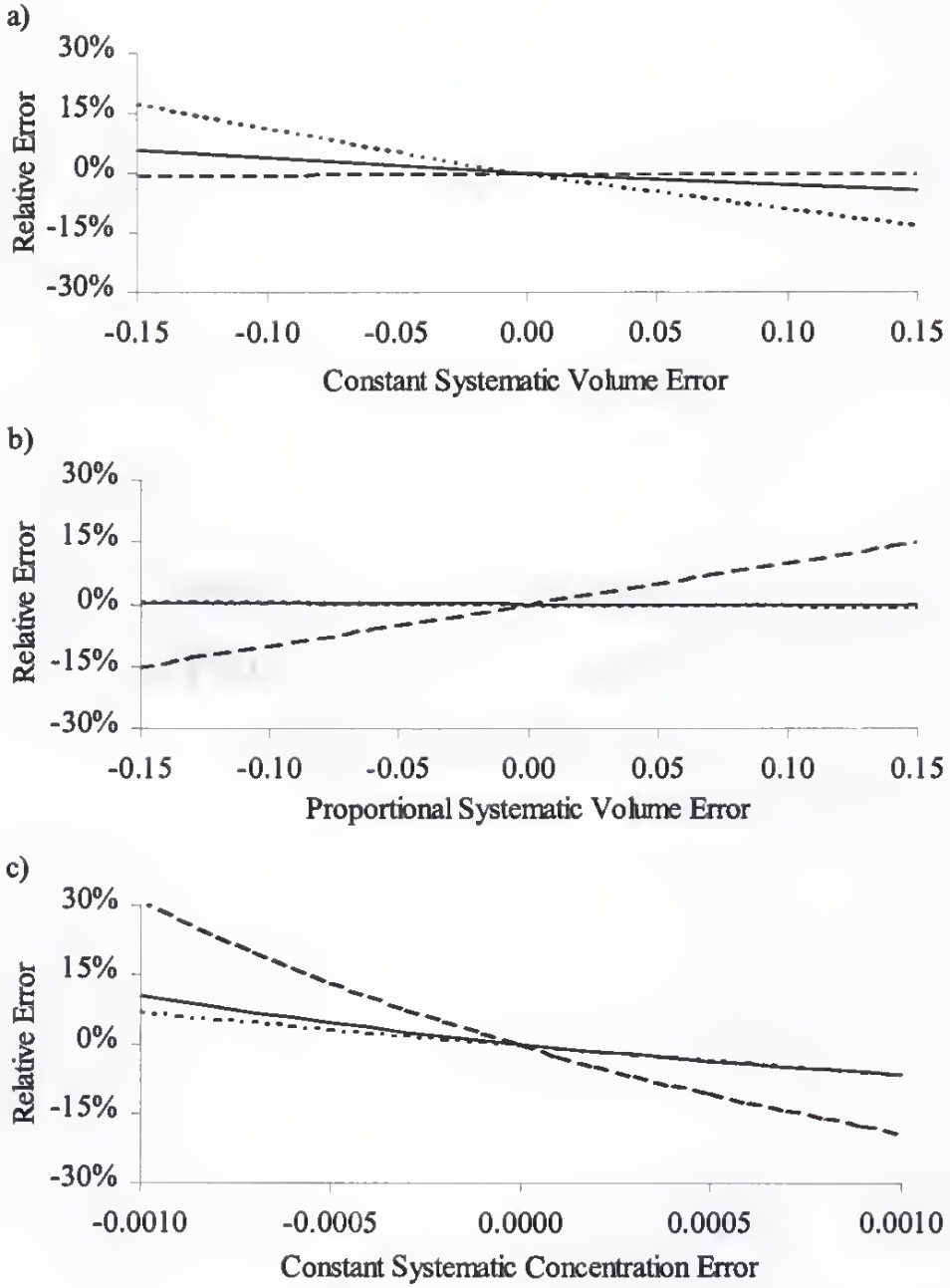

Figure 3-1. The effects of systematic errors on retardation (solid line), saturation (short-dashed line), and NAPL volume (long-dashed line) are illustrated for the case of a) constant systematic volume errors, b) proportional systematic volume errors, and c) constant systematic concentration errors. The retardation factor was 1.5 in each case, and the BTCs were composed of 100 data points.

impact on retardation and saturation estimates, because the error occurs in both the numerator and denominator of these terms. However, this type of systematic error has a larger impact on the NAPL volume estimate because of its impact on the swept volume (see Figure 2-2b).

Constant systematic concentration errors. The range of constant systematic errors is limited to magnitudes equal to or less than method detection limits, based on the assumption that larger errors would be more readily identified by typical quality assurance procedures used in the laboratory. Assuming typical values for alcohol tracers, i.e., injection concentrations on the order of 1000 mg/L and method detection limits on the order of 1 mg/L, dimensionless concentration errors could range from –0.001 to +0.001. The impact of errors in this range on the retardation, saturation, and NAPL volume are shown in Figure 3-1c. It was assumed that the systematic error was the same for both non-partitioning and partitioning concentrations. As shown in Figure 3-1c, these types of errors have the largest impact on NAPL volume estimates, and smaller, but similar impacts on retardation and NAPL saturation estimates. Comparable estimates were obtained when the results from Figure 3-1c for NAPL volume errors were compared to NAPL volume errors estimated by the formula presented by Dwarakanath et al. (1999).

Proportional systematic concentration errors. As shown by equations (A-20a) through (A-20c) in Appendix A, the impact of proportional systematic errors in concentration measurements on the moment calculations is eliminated by using dimensionless concentrations. Therefore, proportional systematic concentration errors do not impact retardation, NAPL saturations, or NAPL volume estimates.

Random Errors

A Monte Carlo analysis was used as a means to verify uncertainty estimates from the error-propagation equations. For the Monte Carlo analysis in this work, measurement uncertainty was estimated as a normally distributed random variable with a zero-mean, and an assumed standard deviation. Concentration measurement uncertainty was estimated using a coefficient of variation (CV), ranging from 0 to 0.15. Volume measurement uncertainty was estimated by assuming the volume standard deviation ranged from 0 to one-half the interval between volume measurements. A unique measurement error was applied to each volume and concentration value in the synthetic data set. Moment calculations were then completed on the "measured" BTC. This process was repeated 10,000 times, and the averages and standard deviations of the retardation, NAPL saturation, and NAPL volume were computed. Convergence of Monte Carlo results was tested by completing three identical simulations, each with 10,000 iterations; the coefficient of variation for the moments, retardation, NAPL saturation, and NAPL volume differed by no more than 0.0002.

Table 3-2 compares the coefficient of variation for retardations, NAPL saturations, and NAPL volumes estimated using the semi-analytical approach to those estimated from the Monte Carlo simulation. Three cases are presented: the first with the volume standard deviation equal to 0.35 and no concentration CV, the second with no volume standard deviation and concentration CV equal to 0.15, and the third with volume standard deviation equal to 0.35 and the concentration CV equal to 0.15.

The agreement shown in Table 3-2 demonstrates that the semi-analytical method correctly accounts for the uncertainly in volume and concentration measurements, based

Table 3-2. Comparison of the CV (%) estimated from Monte Carlo (M.C.) simulations and the semi-analytical procedure (S.A) for three cases.

	Case A		Case B		Case C	
	S. A.	M. C.	S. A.	M. C.	S. A.	M. C.
Retardation	0.8	0.8	1.4	1.4	1.6	1.6
Saturation	2.2	2.2	4.0	4.0	4.8	4.8
NAPL Volume	1.4	1.5	3.1	3.2	3.8	3.8

Case A: volume standard deviation = 0.35, and concentration CV = 0; Case B: volume standard deviation = 0, and concentration CV =0.15; and Case C: volume standard deviation = 0.35, and concentration CV = 0.15.

on the assumption of independence between all measurements. Based on the coefficient of variation of the retardation, NAPL saturation, and NAPL volume, concentration errors have a greater impact on PITT results than volume errors.

Applications

The NAPL volume CV is shown in Figure 3-2 as a function of retardation for several combinations of volume errors (standard deviation) and concentration errors (CV). As indicated by Figure 3-2, the uncertainty in NAPL volume estimates is high for low retardation values, and the uncertainty decreases as retardation increases. This result agrees with that presented by Jin et al. (1995). For reliability, estimates of saturation and NAPL volume should be based on retardation values of 1.2 or greater. In contrast, there is a high degree of uncertainty associated with the conclusion that little or no NAPL is present based on small retardation values. Figure 3-3 shows the NAPL volume coefficient of variation as a function of the dimensionless volume error for breakthrough curve resolutions of 50, 100, and 350 volume-concentration data points. The intent of

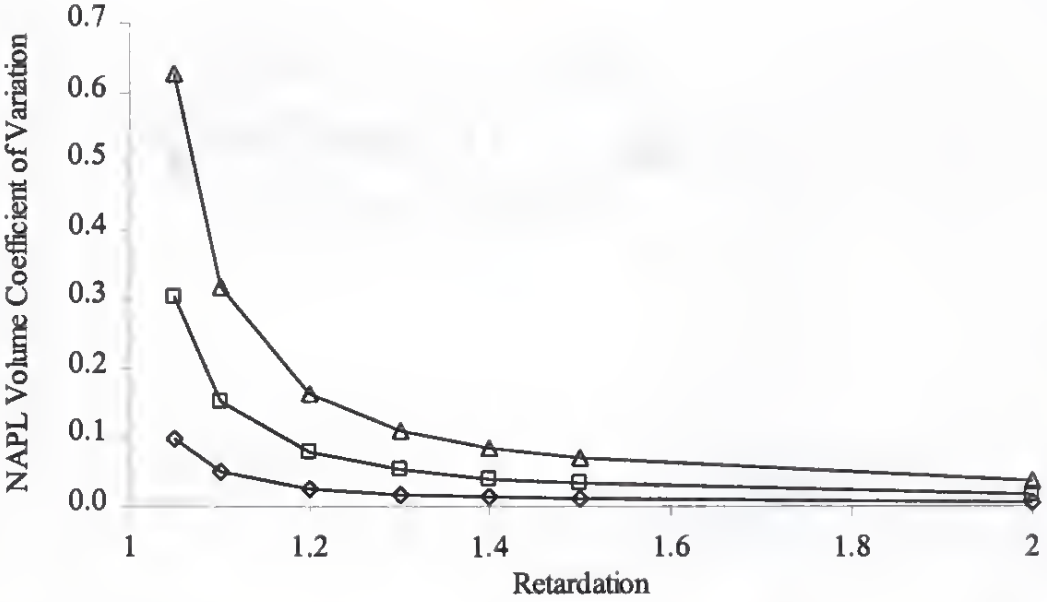

Figure 3-2. NAPL volume CV as a function of retardation factor for volume or concentration measurement errors of 0.05 (diamonds), 0.15 (squares), and 0.30 (triangles). BTCs with 100 data points were used to generate the figure.

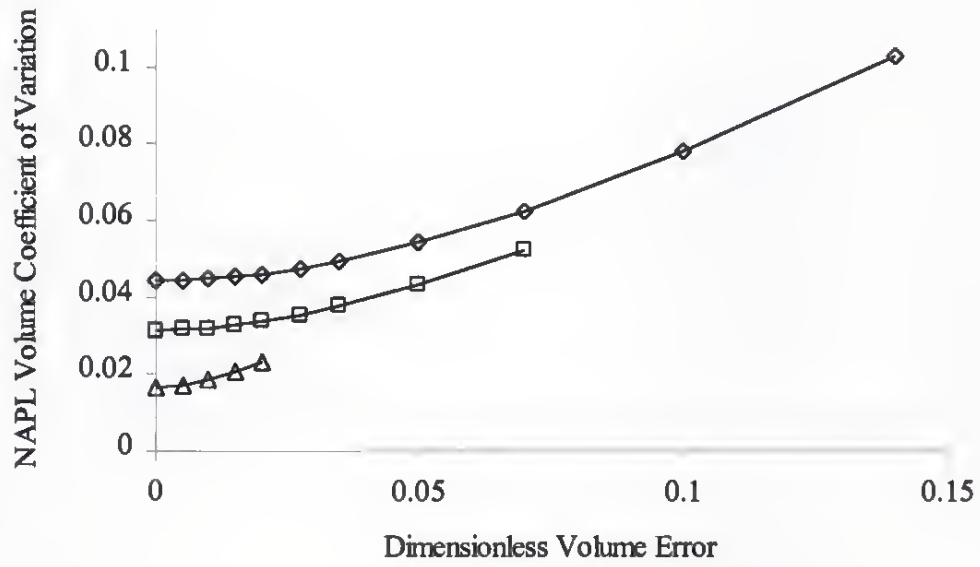

Figure 3-3. NAPL volume coefficient of variation as a function of dimensionless volume error for BTCs of 50 (diamonds), 100 (squares), and 350 (triangles) volume-concentration data points. The figure is based on a retardation factor of 1.5.

this figure is to quantify NAPL volume uncertainty as a function of BTC resolution. The data used in the figure is based on a concentration CV of 0.15, and a retardation factor of 1.5. The dimensionless volume error used on the abscissa in Figure 3-3 is the ratio of volume standard deviation to the normalized first moment. It is apparent from the figure that the uncertainty decreases as the resolution increases, which is a reasonable result since more points should serve to better define the BTCs.

Figure 3-4 shows the impact of variable concentration uncertainty on retardation, NAPL saturation, and NAPL volume. The analysis was based on the same conditions used in Chapter 2: uncertainty in volume measurements was neglected, concentration uncertainty varied linearly from the uncertainty of the detection limit concentration to the uncertainty of the peak concentration, and a dimensionless detection limit of 0.001 was assumed. The uncertainty of the peak concentration, defined using concentration CV, was 0.05 and 0.15. The uncertainty of the detection limit concentration was varied using CV values ranging from 0.5 to 2.0. As illustrated in Figure 3-4, the uncertainty in the peak concentration has less impact than uncertainty in the detection limit concentration. However, even with the detection limit uncertainty set as high as $CV_{DL} = 2.00$, the uncertainties (expressed as CVs) in NAPL volume are only approximately 20%.

The impact of uncertainty in background retardation on NAPL volume uncertainty is shown in Figure 3-5. This figure was based on equations (3-1b), (3-7d), and (3-10) with all variances equal to zero except the variance of the background retardation. Partitioning coefficients of 8 and 200, and background uncertainties (defined as CV) of 0.05, 0.15 and 0.30 were used to produce the figure. By comparison to Figure

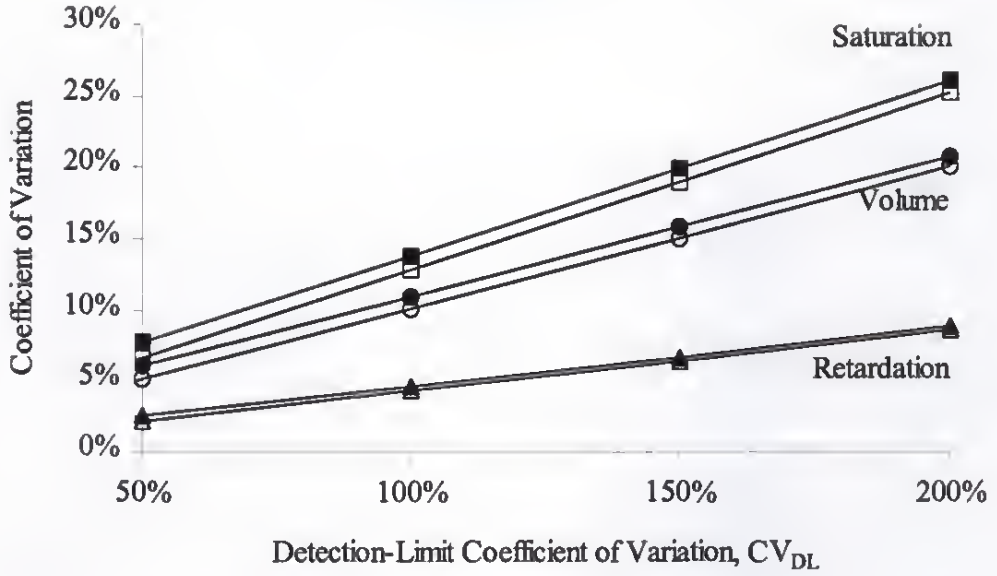

Figure 3-4. Retardation (triangles), NAPL saturation (squares), and NAPL volume (circles) CV as a function of the concentration detection limit CV. The CV of the maximum concentrations were 5% (open symbols) and 15% (closed symbols). The figure is based on 100 volume-concentration data points, and a retardation factor of 1.5.

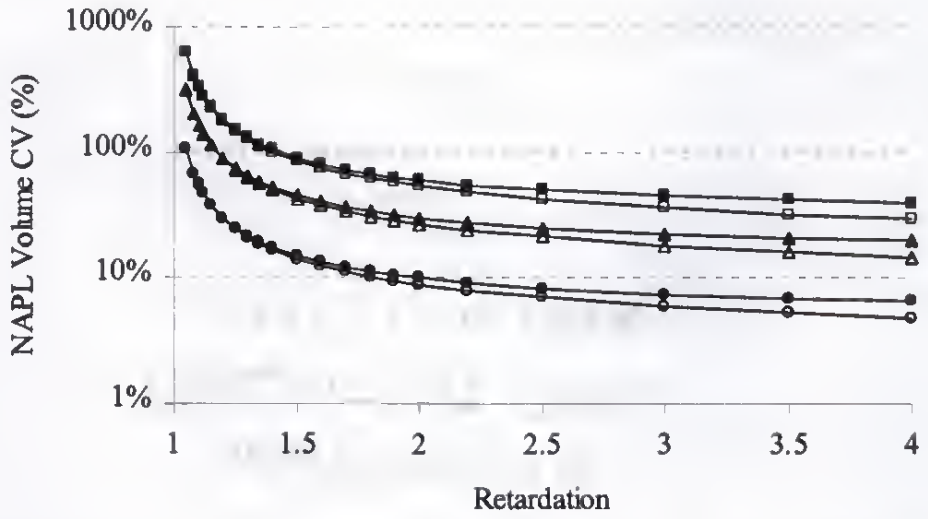

Figure 3-5. Impacts of background-retardation uncertainty. The NAPL volume CV is presented as a function of retardation, for background retardation CVs of 5% (circles), 15% (triangles), and 30% (squares). The curves with the open symbols are based on a partitioning coefficient of 8, and the curves with the closed symbols are based on a partitioning coefficient of 200.

3-2, it is evident that NAPL volume uncertainty is more sensitive to background retardation uncertainty compared to its uncertainty from volume- and concentration-measurement uncertainty.

Conclusions

This chapter presented a method of estimating uncertainties associated with partitioning tracer tests. The method differs from previous work on measurement uncertainty in that retardation, saturation, and NAPL volume uncertainty are based on the uncertainty in volume and concentration measurements, rather than uncertainty based on the difference between measurements and model predictions. Uncertainty in the NAPL volume estimate has also been presented, which was not discussed in previous work. The method is equally applicable to volumetric and temporal moments, and in the case of the former, accounts for volume-measurement uncertainty. Results from this chapter quantitatively indicate how the uncertainty in NAPL volume grows as the retardation factor decreases. In other words, the conclusion that NAPL is not present based on partitioning tracer test results has a high degree of uncertainty, simply because of measurement uncertainty. This suggests that using partitioning tracers as a means to detect small volumes of NAPL is not a reliable technique, or at least, if used as such, should be done so with great care.

It should be clearly stated that the methods presented in this chapter, as well as those presented by Dwarakanath et al. (1999) and Jin et al. (2000) provide estimates of the uncertainty associated with partitioning tracer tests arising from measurement error. These errors have been found to be relatively small; less than 10% for retardation factors

greater than approximately 1.2. As discussed in the next chapter, however, caution is still advised when qualifying the uncertainty (and reliability) of partitioning tracer results.

CHAPTER 4
PRE- AND POST-FLUSHING PARTITIONING TRACER TESTS ASSOCIATED WITH A CONTROLLED RELEASE EXPERIMENT

Introduction

This chapter describes the partitioning tracer tests conducted in the cell at the DNTS before and after the ethanol-flushing demonstration. A tracer test was conducted prior to the release of PCE in order to characterize the background retardation of the tracers, and results from that test, as well as a description of the controlled PCE release, are included. The chapter begins with a description of the site geology and cell instrumentation, and this is followed by a description of the background sorption test, controlled PCE release, and pre- and post-partitioning tracer tests. Results based on extraction well BTCs are presented, and a comparison is made between the volume of PCE predicted by the partitioning-tracers and the volume released into the cell. The uncertainty of the tracer-test results is quantified using the methods presented in Chapters 2 and 3. However, for the sake of clarity, uncertainty quantifications are limited to PCE-volume estimates since this is the measure used to compare tracer-test results to release information.

Site Description

Site geology. The permit application for the demonstration (Noll et al., 1998) provided detailed information on the site geology and the cell installation and instrumentation. The following summary provides information relevant to tests discussed

herein. The site geology consists of the Columbia Formation, characterized by silty, poorly sorted sands. This is underlain by the Calvert Formation, the upper portion of which is characterized by silty clay with thin layers of silt and fine sand. This layer forms the aquitard for the surficial aquifer. Noll et al. (1998) reported that the average hydraulic conductivity of the surficial aquifer ranges from 2.4 m/day to 10.4 m/day based on pump tests. The hydraulic conductivity ranged from 2.4 m/day to 3.0 m/day based on the hydraulic gradient measured under steady flow during initial hydraulic tests in the cell. Ball et al. (1997) and Liu and Ball (1999) provide additional descriptions of the geology at the Dover AFB. Boring logs from the wells installed in the cell generally indicated alternating layers of silty sand, poorly sorted sand, and well sorted sand. The average depth to clay was approximately 12 m below grade based on the well boring logs. The grade elevation varied by 0.2 m across the cell; consequently all references to grade are based on an average grade elevation. The minimum observed clay depth was 11.8 m below grade at well 52 (Figure 4-1), and the maximum observed clay depth was 12.5 m below grade at well 56.

Cell instrumentation. The 3-m by 5-m by 12-m cell was constructed by driving Waterloo sheet piling with interlocking joints (Starr et al., 1992, 1993) through the surficial aquifer into the confining unit. A second enclosure of sheet piling was also installed to act as a secondary containment barrier. Hydraulic tests were performed after the installation of the cell to ensure containment integrity. In addition, an inward hydraulic gradient was maintained during the tests, and DNTS personnel conducted frequent groundwater compliance sampling to safeguard against contaminant migration. The cell was instrumented with 12 wells, 18 release points, and 18 multi-level sampling

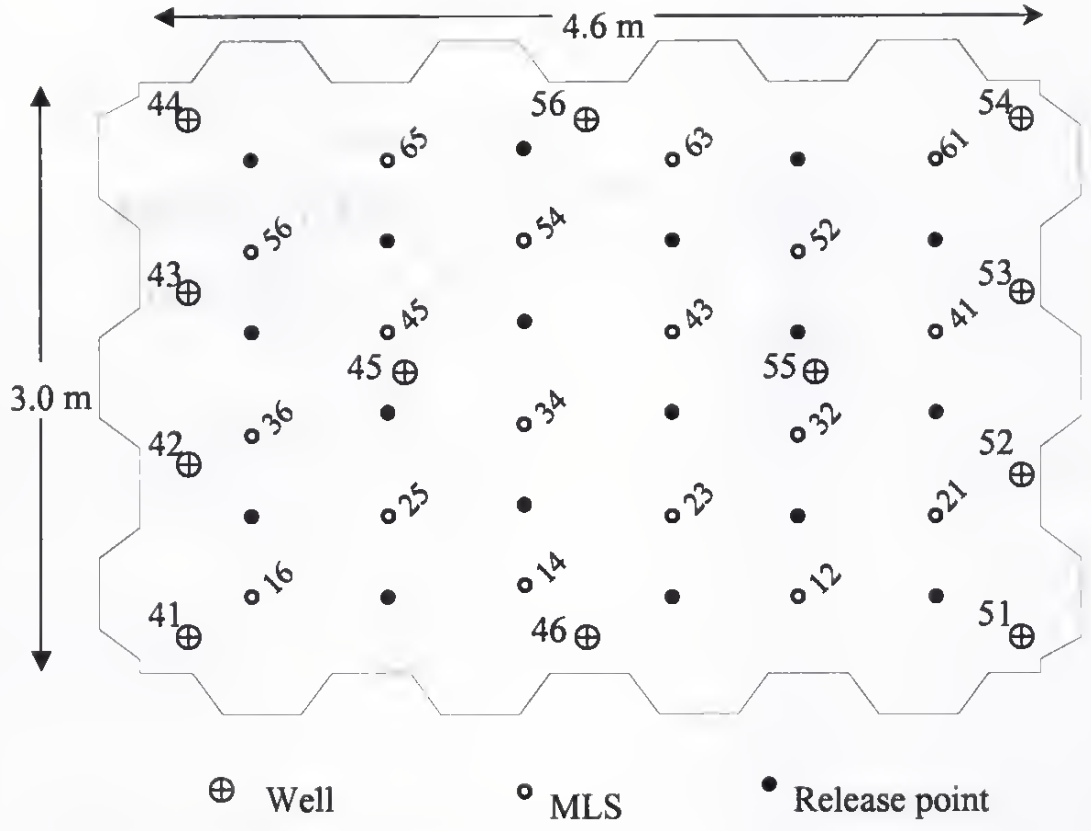

Figure 4-1. Cell instrumentation layout.

(MLS) locations (Figure 4-1). Each well was approximately 5 cm in diameter, and screened from 6.1 m to 12.5 m below grade. A 0.3 m section of casing was installed below each screen and served as a sump for collecting DNAPL in the event it entered the wells. The release points terminated at 10.7 m below grade. Each release point had a sampler installed above it at approximately 9.9 m. Each MLS had 5 vertical sampling points spaced 0.3 m apart, distributed over the bottom 1.5 m of the cell. MLSs were distributed within the cell on a tetrahedral grid.

Background Sorption Tracer Test

Prior to release of PCE into the cell, a partitioning tracer test was conducted to assess background sorption of tracers onto aquifer materials. Alcohol tracers, methanol, 2,4-dimethyl-3-pentanol (DMP), and n-octanol, along with bromide were injected into six wells at the corners and sides of the cell and extracted from the two wells in the center of the cell (double five-spot pumping pattern, as shown in Figure 4-2a). Background sorption was quantified by moment analysis of the extrapolated tracer breakthrough responses, and the results are summarized in Table 4-1. Retardation of DMP (K_{NW} = 30) in both wells was approximately 1.13, which is equivalent to a background PCE saturation of 0.004, or a total volume of PCE in the cell of approximately 50 L. However, retardation of the most hydrophobic tracer, n-octanol (K_{NW} = 170) was less than 1. The tail of the BTC for this tracer declined significantly relative to the other tracers, suggesting n-octanol may have degraded during the test. The effective porosity in the cell was estimated at approximately 0.2 based on moment analysis of the methanol non-reactive tracer. Bromide was retarded relative to methanol by a factor of 1.3. Brooks et al. (1998) showed that bromide-mineral interaction could retard bromide when used as a groundwater tracer, which may explain its retardation in this test.

Controlled Release Conducted by EPA

The release of PCE into the cell was designed to produce a DNAPL distribution within the target-flow zone between 10.7 and 12.2 m below ground surface (bgs). The approach used was intended to minimize pooling of the DNAPL on the clay confining

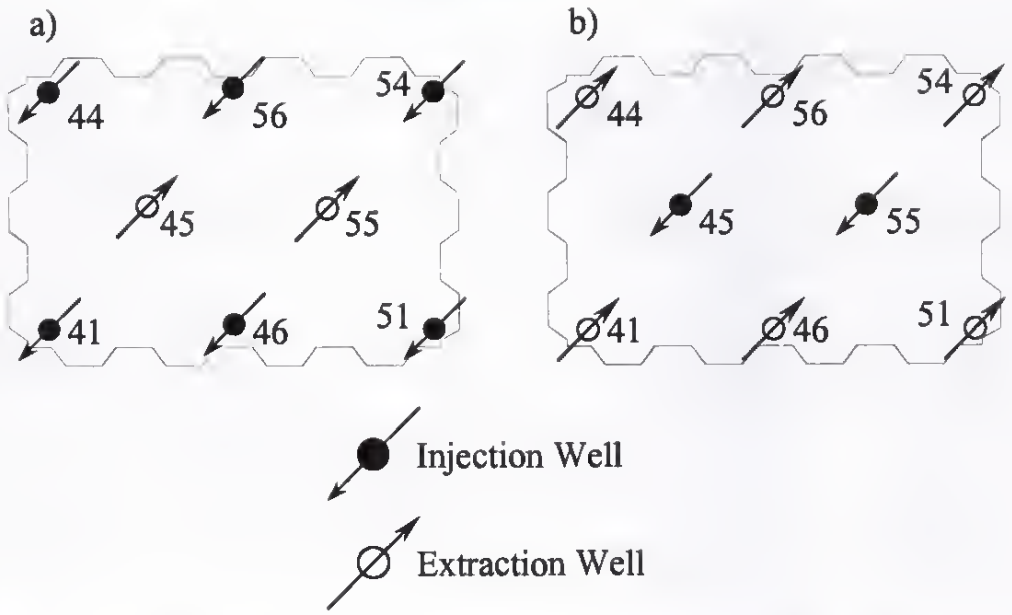

Figure 4-2. a) Double five-spot pumping pattern used in the background sorption tracer test and the ethanol-flushing demonstration (discussed in Chapter 5), and b) inverted, double five-spot pumping pattern used in the pre- and post-flushing tracer test.

Table 4-1. Summary of results from the background sorption tracer test.

Tracer	Mass Recovery		Swept Volume (L)		Retardation [1]	
	EW 45	EW 55	EW 45	EW 55	EW 45	EW 55
Methanol	107%	94%	6440	5340		
Bromide	124%	106%	8700	6740	1.35	1.26
2,4-DM-3-P [2]	115%	101%	7300	5980	1.13	1.12
n-Octanol	96%	88%	4500	4420	0.70	0.83

[1]Retardation relative to methanol.
[2]2,4-DM-3-P = 2,4-Dimethyl-3-pentanol

unit, which was undesirable because of the increased potential for downward migration of PCE through natural fractures in the clay or openings produced during sheet-pile installation. The water table was lowered 0.3 m below the release elevations (11.0 m below grade) prior to PCE injection. EPA researchers conducted the release by pumping selected volumes of PCE down the release tubes at a typical flow rate of 0.6 L/min. Immediately following the release, the water table was lowered further to facilitate vertical spreading of the DNAPL between the release points and the clay confining unit. When the water table reached approximately 11.9 m below grade, groundwater extraction was terminated and water injection was initiated to raise the water table back to the pre-release elevation (8.5 m below grade).

The target release volume was 92 L. The uncertainty associated with the release volume was estimated assuming the tolerance of a one-liter graduated cylinder (5 mL) was equivalent to the standard deviation of a 1-L measurement. The target release volume was 92 L, therefore the uncertainty was 0.5 L. EPA researchers estimated that between 0 and 0.5 L of PCE remained in the containers used during the release as residual fluid. Therefore, it was assumed that 0.3 L of PCE remained in the containers, and the uncertainty of this number was 0.2 L. Therefore, the best estimate of the volume of PCE in the cell and its uncertainty was 91.7 ± 0.5 L. Figure 4-3 shows the volume of PCE released at specific release locations. As indicated in Chapter 1, this information was withheld until after the remedial demonstration. Table 4-2 summarizes the estimated volume of PCE in the cell over the entire demonstration based on the release information and the volume of PCE removed by each subsequent activity.

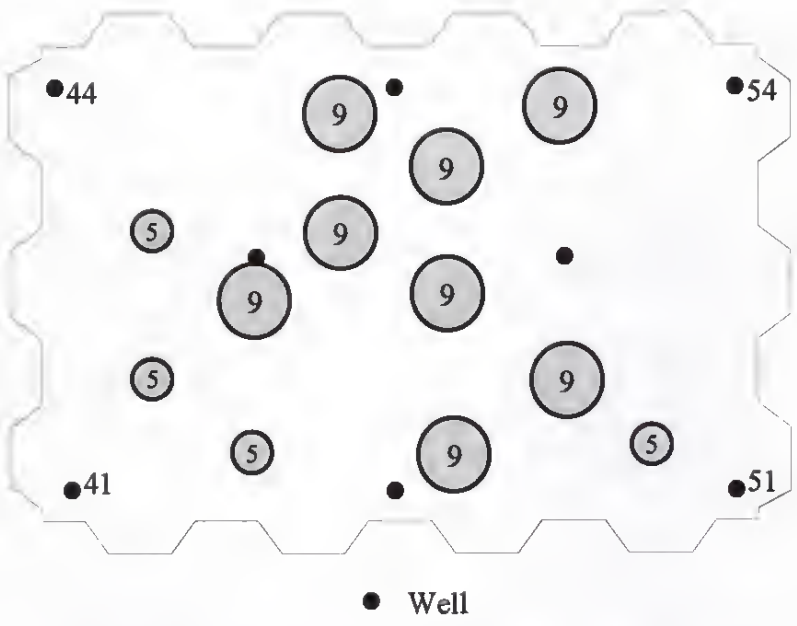

Figure 4-3. PCE injection locations and volumes (plan view). The number inside the circles indicates the release volume (L) per location.

Table 4-2. Volume of PCE (L) added and removed from the cell.

PCE Addition or Removal	Volume in Cell	Change	Error Estimate
DNAPL released into the cell	91.7		0.5
Amount at the start of the CITT	91.7		0.5
Removed by dissolution from EWs		3	0.1
Removed by dissolution from MLSs		0.1	0.03
DNAPL removed from EW 56 [1]		2.8	0.2
Amount at the start of the first PITT	85.8		0.5
Removed by dissolution from EWs		2.5	0.1
Removed by dissolution from MLSs		0.1	0.03
DNAPL removed by MLSs prior to flood [2]		0.2	0.05
Amount at the start of the ethanol flood	83.0		0.6
Total removed during flood through EWs		52.6	0.7
Total removed during flood through MLSs		1.2	0.1
DNAPL removed through MLSs		0.08	0.04
PCE injected through recycling		-0.5	0.04
Net PCE removed		53.4	0.7
Amount at the start of the second PITT	29.6		0.9

[1]This volume was removed from the well before the first PITT.
[2]This includes the DNAPL removed during the CITT and the first PITT

Partitioning Tracer Tests

Following the release of PCE into the cell, two tracer tests were conducted. The first tracer test took place two weeks after the release. The goal of this test was to investigate non-reactive transport characteristics in a line drive flow pattern (injection through wells 51, 53, and 54, and extraction from wells 41, 42, 43,and 44) using bromide as a tracer. The transition from a static system to steady flow was studied including the changes in PCE concentration in extraction wells (EWs) and multilevel samplers. EPA researchers conducted this test and the results were not used by UF in the design or interpretation of the partitioning tracer test. Approximately 5 pore volumes of water were flushed through the cell, and 3.0 L of PCE were removed through dissolution. The EPA provided this estimate and an uncertainty analysis was not completed. However, assuming relative uncertainties of 0.15 for volume and concentration measurements, Figure 2-4a indicates the uncertainty of this mass removal estimate is probably on the order of 5%. Further results of the line-drive tracer test are not discussed here.

Two weeks after the line-drive tracer test, UF researchers conducted the post-release partitioning tracer test. The test was designed to estimate the volume and distribution of PCE released in the cell by monitoring the tracer breakthrough at the extraction wells and multilevel samplers. Each monitoring well was checked for free-phase PCE using an interface probe prior to conducting the test. Well 56 had the only PCE present. A peristaltic pump was used to remove 2.8 ± 0.2 L of PCE from the well. This may indicate that PCE was pooled on the clay confining unit; however, the PCE may also have entered the well by migrating on a layer present in the target flow zone.

An inverted, double five-spot pattern was employed for the tracer test (Figure 4-2b), which consisted of six extraction wells (41, 44, 46, 51, 54, and 56) located around the perimeter of the cell and two injection wells (45 and 55) located in the center. This pattern was used because it provided the highest spatial resolution of PCE distribution from the extraction well breakthrough responses. Of the 108 potential multilevel sampling locations, approximately 35 yielded breakthrough responses adequate for moment analysis to determine partitioning tracer retardation. Approximately 60 samplers failed due to faulty valves and system leaks. These problems were later corrected such that all 108 samplers worked for the post-flushing partitioning-tracer test.

In an effort to increase the measured partitioning tracer retardation at the extraction wells, the flow domain was segregated into upper and lower zones. Inflatable packers were used in the injection wells to segregate fluid into the upper and lower portions of the wells. The average saturated thickness of the flow domain was 4.3 m so the center of the packers were placed at 1.8 m above the clay dividing the flow domains approximately in half. The average flow rate injected into the upper and lower zones was 3.7 L/min and 3.0 L/min, respectively. This approach was intended to deliver a suite of tracers into the lower zone in order to focus tracer flow though the NAPL contaminated zone. This would then produce higher retardation for the lower zone tracers than if a single tracer suite was employed. In the upper zone, very low retardation was expected. In an effort to provide further spatial resolution of the PCE distribution, unique tracer pairs were employed in the lower zones of the two injection wells (45 and 55). The unique non-partitioning and partitioning tracers allowed the flow domain to be segregated

into eight zones based on the extraction well data. The tracers used as common or unique to the upper and lower zones for both pre- and post-tests are listed in Table 4-3.

The tracer test was conducted over an 11-day period maintaining a steady total flow of 6.7 L/min based on injection rate measurements. A tracer pulse of 8 hours was applied in the lower zone and 9.4 hours in the upper zone. Samples were collected from the six extraction wells and all functioning multilevel samplers to measure tracer BTCs. The water level in the cell was maintained at 7.9 m bgs producing a saturated zone of approximately 4.3 m. Up-coning and drawdown in the injection and extraction wells were approximately one meter but this was assumed to be local to each well. The wells were installed by direct push using a 30-ton cone penetrometer truck and therefore had no sand pack that would reduce head loss at the well.

Results and Discussion

Extraction Wells

Each of the six extraction wells yielded 11 BTCs from the suite of tracers used. Figure 4-4 shows selected non-reactive and reactive BTCs at EW 51. Moments were calculated and the results for the non-reactive tracer are summarized in Table 4-4 and the partitioning tracers in Table 4-5. All BTCs were extrapolated to provide best estimates of the true moments (Jin et al., 1995), and background sorption was neglected. Iodide results (not listed in Table 4-4) showed similar trends in mass recovery and swept volume per extraction well as those shown by methanol, however the total mass recovered was 95%, and the total swept volume estimate was 3,920 L. Compared to the swept volume estimated from methanol, the iodide was retarded by a factor of 1.02. The

Table 4-3. Partitioning coefficients for tracers used in the pre- and post-flushing partitioning tracer tests.

Tracer	Pre-Flushing PITT	Post-Flushing PITT
Lower Zone Common		
Iodide	0	0
Methanol	0	0
n-Hexanol	6	6
2,4-Dimethyl-3-pentanol	30	30
2-Octanol	120	120
3,5,5-Trimethyl-1-Hexanol	-	265
Lower Zone Unique Well 45		
Tert-butyl Alcohol	0	-
n-Octanol	170	-
Lower Zone Unique Well 55		
Isobutyl Alcohol	0	-
3-Heptanol	31	-
Upper Zone Common		
Isopropal Alcohol	0	-
n-Heptanol	32	32
Isobutyl Alcohol	-	0
2-Ethyl-1-Hexanol	-	140

iodide may have been retarded due to mineral interaction, analogously to bromide retardation discussed by Brooks et al. (1998). Due to the possible retardation and smaller mass recovery of iodide relative to methanol, results from the latter were used in NAPL volume calculations. Wells 51 and 56 had the highest average NAPL saturation at 1%. This is a very low average saturation and produced a retardation over 2 for 2-octanol, which provided a reasonable measure of the saturation (Jin et al., 1995). The BTCs are shown on a log scale and indicate that the retardation was primarily in the tailing portion of the BTC. This indicated that the NAPL was non-uniformly distributed since a uniform distribution would produce a simple offset of the non-reactive and partitioning tracer BTCs (Jawitz et al., 1998). The total volume of NAPL estimated in the lower swept zone

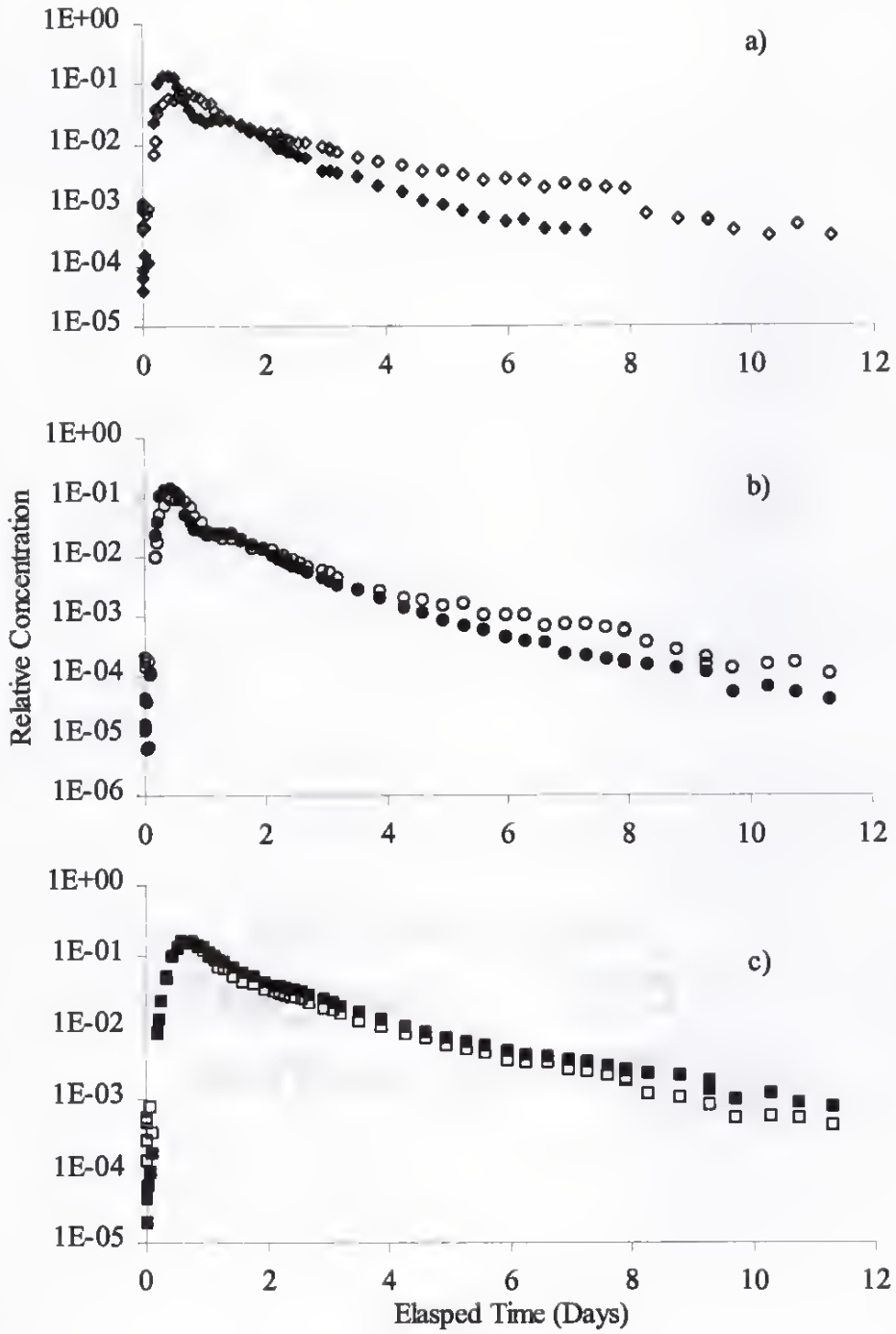

Figure 4-4. Selected EW 51 BTCs from the pre-flushing tracer test. a) Common lower zone tracers: methanol (closed diamonds) and 2-octanol (open diamonds), b) unique lower zone tracers: isobutanol (closed circles) and 3-heptanol (open circles), and c) upper zone tracers: isopropanol (closed squares) and n-heptanol (open squares).

Table 4-4. Summary of results for common non-reactive lower and upper zone tracers from the pre-flushing test.

Well	Mass Recovery		Mean Arrival Time (d)		Swept Volume (L)	
	Lower Zone	Upper Zone	Lower Zone	Upper Zone	Lower Zone	Upper Zone
41	23%	9%	0.48	2.25	740	3470
44	8%	6%	1.17	2.13	810	1470
46	34%	18%	0.25	0.86	550	1850
51	11%	18%	0.43	1.03	660	1570
54	11%	20%	0.29	0.75	520	1330
56	10%	15%	0.35	0.90	550	1430
Total	97%	87%	-	-	3830	11120

Table 4-5. Pre-flushing partitioning tracer test, common lower zone partitioning tracer results.

Well	n-Hexanol				2,4-Dimethyl-3-Pentanol				2-Octanol			
	M	R	S_N	V_N	M	R	S_N	V_N	M	R	S_N	V_N
41	22%	1.01	0.0008	0.6	24%	1.15	0.0051	3.7	24%	1.42	0.0035	2.6
44	8%	0.98	-	-	9%	1.05	0.0015	1.2	9%	1.10	0.0008	0.7
46	33%	1.15	0.0190	10.5	34%	1.30	0.0010	5.5	37%	1.90	0.0074	4.1
51	11%	1.23	0.0280	18.5	11%	1.42	0.0138	9.2	12%	2.08	0.0089	5.9
54	11%	1.14	0.0171	8.9	11%	1.19	0.0062	3.2	11%	1.16	0.0013	0.7
56	10%	1.34	0.0406	22.3	10%	1.48	0.0157	8.6	11%	2.20	0.0099	5.4
Total	95%	-	-	60.8	100%	-	-	31.4	104%	-	-	19.4

M = mass recovery (%), R – Retardation factor, S_N = NAPL saturation, and V_N = NAPL volume (L).

Table 4-6. Pre-flushing partitioning tracer test, upper-zone reactive tracer (n-heptanol) results. The corrected mass recovery is based on a first-order degradation model.

Well	Mass Recovery	R	Corrected Mass Recovery	Corrected R	S_N	V_N
41	5%	0.89	10%	1.03	0.0010	3.9
44	3%	0.74	5%	0.78	-	-
46	17%	1.04	23%	1.29	0.0095	16.2
51	16%	0.91	22%	1.31	0.0101	19.2
54	17%	0.82	21%	0.95	-	-
56	14%	0.88	19%	1.02	0.0005	0.8
Total	72%	-	100%	-	-	40.2

is 19.4 L. This is based on using the tracer with the largest measured retardation (2-Octanol). Using individual tracers showed high variability ranging form 31.4 L for DMP to 60.8 L for n-hexanol.

The upper zone tracers showed a retardation of less than one in all extraction wells except EW 46 (Table 4-6). However, the non-reactive tracer, isopropanol (IPA), and the partitioning tracer, n-heptanol, showed poor recovery (87% and 72%, respectively). This is likely due to tracer degradation since straight–chain alcohols tend to degrade more rapidly in the environment. These tracers were not in the original suite of tracers designed for this test but were substituted for pentaflourobenzoic acid and 2,6-dimethyl-4-heptanol when regulatory approval for those tracers was denied. In order to provide an estimate of the volume of PCE in the upper swept zone, some correction for tracer degradation was required. The simplest approach is to assume a first-order degradation model and estimate the degradation-rate constant by recovering the zeroth

moment using the BTC of the degraded tracer. Each concentration measurement in the BTC is adjusted using

$$C_{adj} = \frac{C}{e^{-kt}} , \qquad (4\text{-}1)$$

where C is the measured concentration, C_{adj} is the estimated concentration with no degradation, k is the decay coefficient, and t is the time that the sample was collected after the mean of the tracer-pulse injection. Applying this adjustment and recalculating the zeroth moment of each tracer, the degradation coefficient was adjusted until the mass recovery matched the mass injected. This approach has several critical assumptions. The degradation is assumed to be first order and can be described by a single value for the entire cell. The approach used here ignores the width of the tracer pulse assuming the width is small and injection occurred at one-half the tracer pulse. This approximation should have minimal impact on the adjusted moments.

The degradation corrected moments for all wells were tabulated in Table 4-6. These results were based on a temporal moment analysis in order to simplify the degradation corrections necessary to obtain 100% mass recovery. The NAPL saturations in two of the extraction wells remained less than zero, and these values were assumed zero for estimating the total NAPL volume present in the cell. The total volume of PCE estimated using the degradation corrected BTCs was 40.2 L. This represents a significant portion of the total 60 L of PCE estimated to be in the cell. The degradation correction therefore takes on significant importance. This also indicates that a substantial fraction of the PCE present in the cell was in the upper swept zone. This may indicate that PCE was located higher in the cell than anticipated based on the release locations, however,

another explanation is that the upper zone tracers in fact traveled down into the target zone between 10.7 and 12.2 m bgs.

The issue of uncertainty associated with the current estimate, 60 L, must be assessed. In general the estimated volume in the lower zone is more reliable than the upper zone because of the degradation problem and the significant size of the upper swept zone, 11,000 L compared to 3,800 L for the lower zone. General sources of measurement uncertainty associated with the NAPL volume estimates include BTC volumes, BTC concentrations, tracer-pulse volumes, tracer partitioning coefficients, and the background-retardation estimate. The combined extraction well effluent was discharged to storage tanks, and cumulative volume measurements were made based on the volume in the storage tanks. Flow meters were also used on each well, but were considered less reliable measures of cumulative volume compared to the storage tanks because flow rates were often near the lower operational limit of the instruments. Instead, the flow meters were used to estimate the flow distribution between the wells, and this distribution along with the cumulative volume estimated from the storage tanks was used to estimate the cumulative volume produced at each well. Uncertainties in BTC volume measurements were therefore based on one-half of the smallest division of the tank-volume scale (± 25 L). Uncertainties in BTC concentration measurements were conservatively assumed to be 0.15 of the measured concentration. Uncertainty in the tracer-pulse volume was assumed negligible due to the controlled conditions under which the measurement was made. It was assumed that the uncertainty in partitioning coefficients was described using a coefficient of variation equal to 0.15. Uncertainty in the background retardation factor was neglected. The BTCs were extrapolated to

improve estimates of the normalized first moments. The uncertainty of the extrapolated portion of the BTC should be based on the measurements used in the extrapolation process. However, as an approximation, it was assumed that each extrapolated volume-concentration measurement had the same relative uncertainty as the measured points.

Propagation of these uncertainties using the methods from Chapters 2 and 3 produced an uncertainty estimate of 19.4 ± 1.5 L for the lower zone. Those methods, however, neglect the estimation of uncertainty associated with degradation of the tracers. This can be partially addressed by looking at the sensitivity of the results to the degradation parameter and the model assumed. This was done and indicated that significant errors on the order of 25% can be introduced. Based on this, the estimate of PCE in the upper zone can be presented as 40 ± 10 L. This gives a revised total estimate of 60 ± 10 L.

The extraction well results can be used to estimate the spatial distribution of PCE within the cell. The six extraction wells have unique swept zones and the unique tracers applied to the two injection wells can further delineate swept zones to eight separate zones within the lower portion of the cell. The results of the unique tracer suites are presented in Table 4-7. The results of the spatial analysis based on extraction wells are presented in Figure 4-5.

Comparison to Release Locations and Volumes

The total release volume, 92 ± 1 L, after reduction to 86 ± 1 L (see Table 4-2) by mass removed prior to the start of the partitioning tracer test, should be compared with the estimate of 60 ± 10 L. Approximately 2 L of PCE may have been resident in solution when the tracer test was initiated and would not be part of the tracer estimate.

Table 4-7. Pre-flushing partitioning tracer test, summary of unique tracer pairs injected into wells 45 and 55.

Well	Non-reactive Tracer mass recovery		Swept Zone (L)		NAPL Volume (L)	
	IW 45	IW 55	IW 45	IW 55	IW 45	IW 55
41	46%	0.02%	798	-	2.1	-
44	17%	0.01%	793	-	1.2	-
46	24%	39%	971	513	6.5	5.6
51	0.1%	22%	-	737	-	7.3
54	0.02%	23%	-	631	-	1.6
56	12%	9%	615	605	5.7	12.1
Total	100%	93%	3177	2486	15.5	26.6

The non-reactive and partitioning tracers injected into well 45 were tert-butyl alcohol and n-octanol, and the non-reactive and partitioning tracers injected into well 55 were isobutyl alcohol and 3-heptanol.

The spatial injection pattern of the PCE release can be compared to the spatial resolutions based on the extraction well data (Figures 4-3 and 4-5). The comparison must be made recognizing that the DNAPL may have migrated to different regions of the cell based on the geologic structure of the media in the cell. In general, the spatial pattern of the PCE distribution based on the extraction wells agrees with the release data. Higher saturation zones are located in the swept zones of wells 51 and 56 where significant mass was released.

Summary of Post-Flushing Partitioning Tracer Test

Two months after the cosolvent flood, a final post-flushing partitioning tracer test was conducted. The procedure followed was the same as the pre-flushing test with the exception that unique tracers were not used in wells 45 and 55. The tracer suite used was also modified to reduce degradation problems experienced with the first tracer test, since those tracers planned for use in the first test were given regulatory approval.

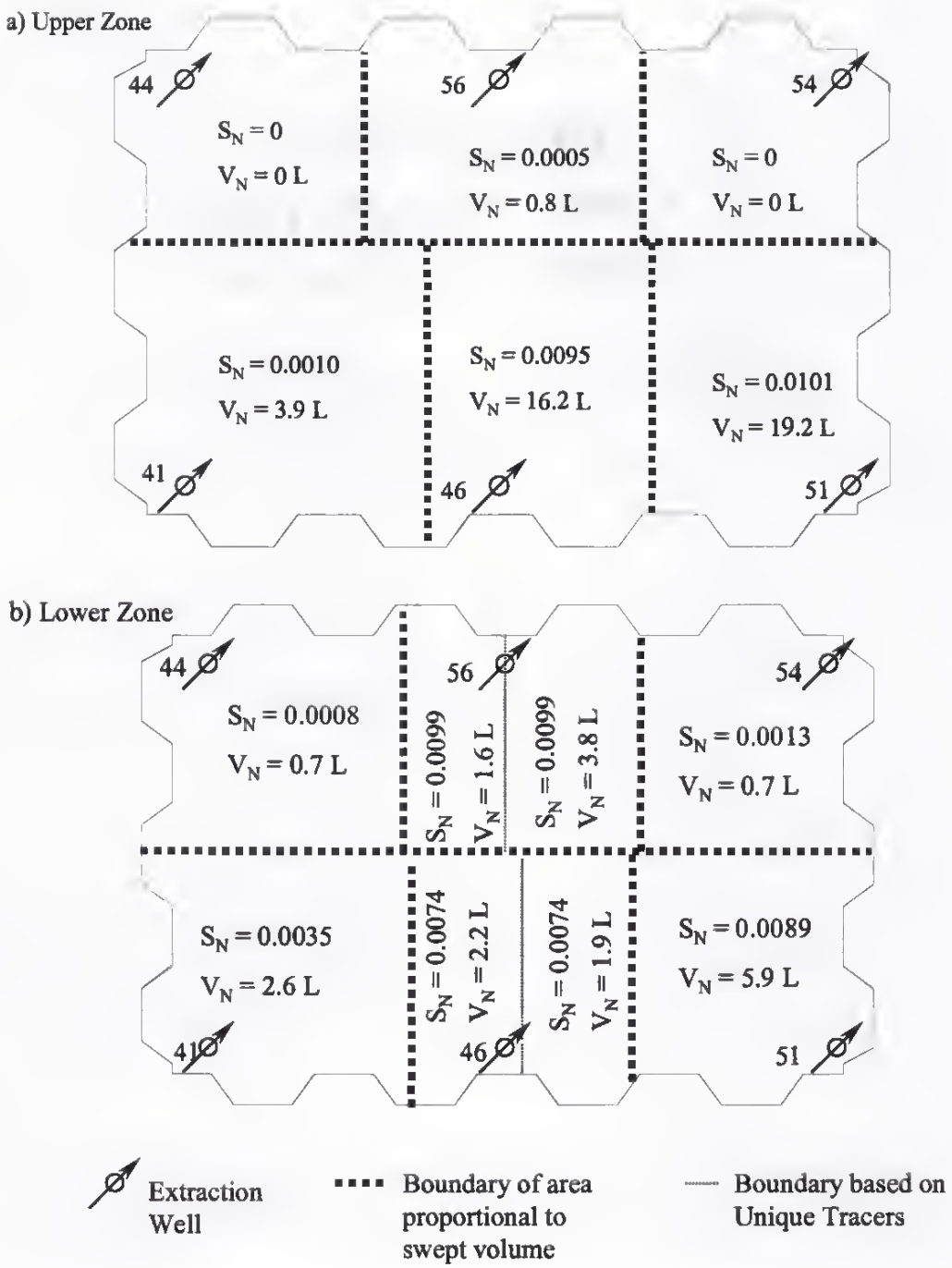

Figure 4-5. Pre-flushing PITT estimate of a) upper zone and b) lower zone spatial distribution of NAPL based on extraction well data.

The mass balance from the cosolvent flood (discussed in Chapter 5) indicated that 30 ± 1 L of PCE remained in the cell prior to the final tracer test (see Table 4-2). The results of the final partitioning tracer test are summarized in Table 4-8. The swept volume estimated from methanol was approximately 17% larger in the post-flushing tracer test compared to the pre-flushing tracer test. A total of 4.9 ± 0.4 L of PCE was estimated based on upper and lower zone tracers.

Discussion

It is apparent that both the pre- and post-flushing tracer tests underestimated the volume of PCE present in the cell by approximately 25 L. This might suggest that 25 L of PCE was not accessible to the tracers. This NAPL could have been pooled on the clay or located in isolated corners or regions of the cell. The fact that the pre-flushing tracer test has high uncertainties caused by degradation of the upper zone tracers must be recognized when reaching this conclusion.

The volume of PCE present in the cell represents relatively low average NAPL saturations. When expressed as NAPL saturation within the lower-swept zone, the pre- and post-flushing saturations are 0.005 and 0.0008 respectively. If averaged over the entire swept zone these drop to 0.004 and 0.0003. While these are very low saturations, tracers with high partitioning coefficients such as 3,5,5 TMH (K_{NW} = 265) would provide a retardation of 1.2 at the lower saturation. Even though this retardation is within the range considered acceptable for tracer applications (Jin et al., 1995), it should be recognized that the tracer technology was generally being tested under conditions that

Table 4-8. Post-flushing partitioning tracer test summary.

Well	Lower Zone						Upper Zone					
	Non-reactive (Methanol)			Reactive (3,5,5-TM-3-H)			Non-reactive (Isobutyl Alcohol)			Reactive (2-E-1-H)		
	M	AT	SV	M	S_N	V_N	M	AT	SV	M	S_N	V_N
41	27%	0.51	880	26%	0.0008	0.7	11%	1.94	3320	11%	-	-
44	6%	1.54	710	6%	0.0005	0.3	2%	0.87	1490	2%	0.0004	0.7
46	11%	0.32	650	13%	0.0013	0.9	17%	0.85	1450	18%	-	-
51	14%	0.51	840	20%	0.0008	0.7	18%	0.83	1420	18%	0.0002	0.3
54	20%	0.29	510	22%	0.0010	0.5	17%	0.89	1520	16%	0.0001	0.1
56	11%	0.46	1020	11%	0.0008	0.8	26%	0.70	1200	25%	-	-
Total	89%	-	4610	97%	-	3.9	91%	-	10400	91%	-	1.1

3,5,5-TM-3-H = 3,5,5-Trimethyl-3-hexanol; 2-E-1-H = 2-Ethyl-1-hexanol; M = Mass recovery (%); AT = Arrival time (d); SV = swept volume (L).

approached the limits of its application.

The trend in NAPL volume estimates as a function of the tracer partitioning coefficients is illustrated in Figure 4-6. Tracers with higher partitioning coefficients predicted less NAPL volume. The tracer with the lowest partitioning coefficient, hexanol (K_{NW} = 8) predicted the NAPL volume closest to the release volume. However, this tracer had the lowest retardation factor, and consequently, the corresponding NAPL volume estimate has a higher uncertainty than estimates from the other tracers. Furthermore, this tracer overestimated the volume of NAPL in the cell after the ethanol flood. This trend could be the result of neglecting background retardation estimates. Another possible explanation for this observation is that the tails of the BTCs from the higher K_{NW} tracers were not properly characterized. In order to investigate the uncertainty in BTC extrapolation, three different approaches to log-linear extrapolation were compared. The first log-linear extrapolation, used to estimate all moments reported

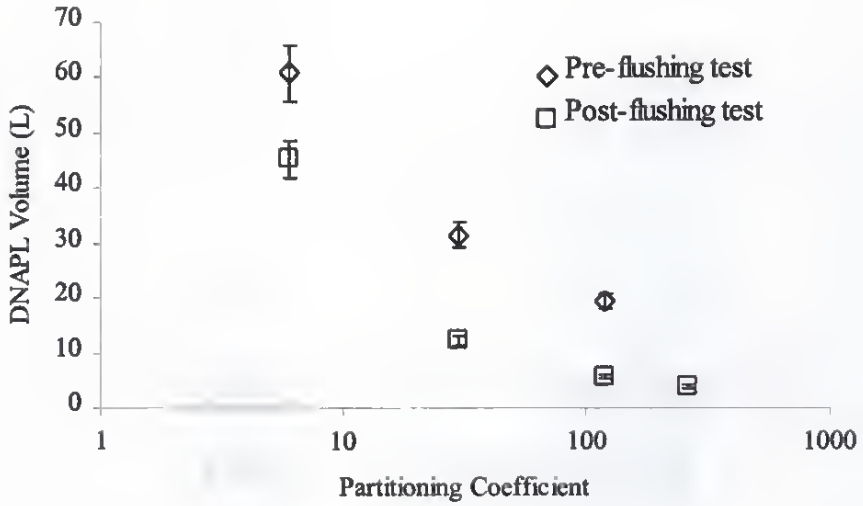

Figure 4-6. DNAPL volume estimated from the pre- and post-partitioning tracer tests as a function of the tracer partitioning coefficient.

thus far, was based on the most "reasonable" fit to the data in the BTC tail. This was a somewhat subjective approach based on log-linear regression using those data points that visually produced the best over-all fit to the BTC tails. The second approach was to extrapolate from that portion of the BTC tail that yielded the largest retardation factor. The final extrapolation scheme was based on log-linear regression using the last ten data points above the method detection limit (estimated as 1 mg/L). Results from moment calculations without extrapolation were also used for comparison. The NAPL volumes estimated from the pre-flushing, lower zone tracers are shown in Table 4-9. As an estimate of the uncertainty due to the extrapolation procedure, the average and standard deviation of the NAPL volume predicted for each tracer is shown in Figure 4-7. While there is more overlap of the estimates by this approach, the trend of smaller NAPL volume predictions with increasing partitioning coefficients is still apparent.

Table 4-9. Comparison in NAPL volume (L) estimates based on four schemes of log-linear BTC extrapolation.

Extrapolation	2-Octanol (K_{NW} = 120)	2,4-DM-3-P (K_{NW} = 30)	Hexanol (K_{NW} = 6)
None	17.4	30.4	55.6
General	19.7	32.1	67.8
Maximum	42.6	57.0	178.6
10 points >1mg/L	24.1	25.2	33.2
Average	26.0	36.2	83.8
Standard Deviation	11.4	14.2	64.8

2,4-DM-3-P = 2,4-Dimethyl-3-pentanol

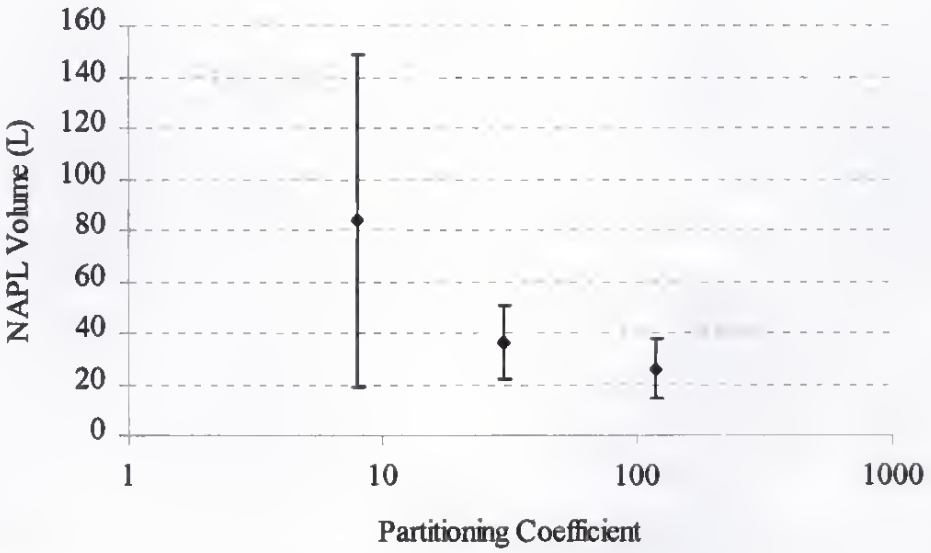

Figure 4-7. Average and standard deviation in NAPL volume from four different extrapolation schemes.

Conclusions

The best estimate of the volume of DNAPL in the cell prior to the first partitioning tracer test (pre-ethanol flushing tracer test) was 86 ± 1 L based on the release information, while the partitioning-tracer test results predicted a NAPL volume of 60 ± 10 L. This represents an error of approximately 30%, which is considered very encouraging. The post-flushing partitioning-tracer test predicted only 4.9 ± 0.4 L of the estimated 30 ± 1 L remaining. This represents an error of approximately 83%, which is certainly less encouraging. However, both the pre- and post-flushing tests underestimated the DNAPL by approximately 25 L. This discrepancy can most likely be explained by the possibility that contact between the tracers and this volume of DNAPL was prevented due to geological conditions.

Partitioning tracer tests are limited by geological considerations. In theory, partitioning tracers with higher partitioning coefficients could be used to predict smaller volumes of NAPL. However, this is predicated on the assumption that the tracer will contact the NAPL. In some situations, it can easily be envisioned that the DNAPL is distributed in regions of low conductivity, especially following remediation efforts, such that tracer-NAPL contact is prevented. Partitioning tracer predictions of NAPL volume should always be qualified with the statement that the NAPL volume is that predicted in the swept-zone of the tracer. The swept-zone of the tracer and the target area of investigation are not always the same. These results caution against the use of partitioning tracer tests as detection methods.

Neither the pre- nor post-partitioning tracer test results agreed with the PCE mass estimated from mass balance within the calculated limits of uncertainty. This highlights

the fact that the calculated uncertainty is based only on measurement uncertainty. It does not account for uncertainty that may arise from conditions contrary to the assumptions used in the partitioning tracer test. In this sense, the estimates of uncertainty provide the minimum level of uncertainty associated with partitioning tracer predictions. As conditions deviate from those necessary to meet the assumptions, the resulting uncertainty will grow, however, this will not be reflected in the uncertainty estimates based on the methods presented in Chapters 2 and 3.

CHAPTER 5
FIELD-SCALE COSOLVENT FLUSHING OF DNAPL FROM A CONTROLLED RELEASE

Introduction

Nonaqueous phase liquids (NAPLs), such as fuels, oils, and industrial solvents, may act as long-term sources of groundwater pollution when released into aquifers because of their low aqueous solubilities. Dense nonaqueous phase liquids (DNAPLs) are denser than water, and are more difficult to remedy because of their tendency to sink and pool in the aquifer. Conventional remediation such as pump-and-treat can take many decades to remove DNAPLs (Mackay and Cherry, 1989). Enhanced source-zone remediation can expedite the removal of contaminants. One enhanced source-zone remediation technique is in-situ cosolvent flushing, which involves the addition of miscible organic solvents to water to increase the solubility or mobility of the NAPL (Imhoff et al., 1995; Falta et al., 1999; Lunn and Kueper, 1997; Rao et al., 1997; Augustijn et al., 1997; Lowe et al., 1999). In the case of DNAPLs, increased mobility can result in greater contaminant risk due to the potential for downward migration, and density modification of the NAPL has been proposed to prevent this risk (Roeder et al., 1996; Lunn and Kueper, 1997; Lunn and Kueper, 1999). Alcohols have principally been used as cosolvents for enhanced source-zone remediation (Lowe et al., 1999).

A limited number of field-scale, cosolvent-flushing demonstrations have been conducted. Two cosolvent-flushing demonstrations were conducted at Hill AFB, Utah in

isolated test cells installed in a sand and gravel aquifer contaminated with a multi-component NAPL (Rao et al., 1997; Sillan et al., 1998a; Falta et al., 1999). Rao et al. (1997) demonstrated NAPL remediation by enhanced dissolution. The test cell was approximately 4.3 m long by 3.6 m wide, and the clay confining unit was 6 m below grade. A total of 40,000 L of a ternary cosolvent mixture (70% ethanol, 12% pentanol, and 18% water) was injected into the cell over a ten-day period. Based on several remediation performance measures (target contaminant concentrations in soil cores, target contaminant mass removed at extraction wells, and pre- and post-flushing target contaminant groundwater concentrations), the cell-averaged reduction in contaminant mass was reported as >85%. They also reported an approximate 81% reduction in NAPL saturation based on pre- and post-flushing partitioning interwell tracer tests (PITTs). Falta et al. (1999) presented results from a second cosolvent-flushing study at Hill AFB wherein the remedial mechanisms were NAPL mobilization and enhanced dissolution. Their test cell was approximately 5 m long by 3 m wide, and the clay-confining unit was 9 m below grade. They injected 28,000 L of a ternary cosolvent mixture (80% tert-butanol, 15% n-hexanol, and 5% water) over a 7-day period. Reductions in target contaminant concentrations measured from pre- and post-flushing soil cores were reported to range from 70% to >90%, and an 80% reduction in total NAPL content was reported based on pre-and post-flushing PITTs.

Jawitz et al. (2000) and Sillan et al. (1999) described a third cosolvent-flushing field demonstration conducted at a former dry cleaning facility in Jacksonville, Florida that was contaminated with PCE. It was reported to be the first field-scale demonstration of DNAPL remediation by cosolvent flushing. Furthermore, no physical barriers were

used. Based on a PITT conducted prior to the demonstration, it was estimated that 68 L of DNAPL were located in the 17,000 L swept zone of the study. A total of 34,000 L of alcohol solution (95% ethanol and 5% water) was injected over an 8-day period, removing 43 L of DNAPL (63% of the PCE initially present). A post-flushing PITT indicated 26 L of PCE remained. Soil cores were also used to assess remedial performance, and indicated a 67% reduction in the amount of PCE initially present.

The remedial performance assessments of these three demonstrations were determined from comparisons between pre- and post-flushing contaminant characterization techniques (e.g., soil cores, PITTs, and groundwater samples), and from comparing the amount of contaminant removed during in-situ flushing to the pre-flushing estimated amount. The accuracy of the remedial performance assessment for these studies was, thus, hindered by uncertainties in the characterization methods used to estimate the amount and distribution of the NAPL.

A controlled release experiment, in which a known volume of NAPL is carefully released into an isolated test cell, provides a unique opportunity to better evaluate remediation techniques, as well as source-zone characterization techniques. Several controlled-release experiments have been conducted in the unconfined, sand aquifer at Canadian Forces Base, Borden, Ontario, but the purpose of these investigations was characterization, not remediation (Poulsen and Kueper, 1992; Rivett et al., 1992; Kueper et al., 1993; Broholm et al., 1999). Furthermore, PITTs were not used in these tests to characterize the NAPL. Poulsen and Kueper (1992) and Kueper et al. (1993) investigated the distribution of DNAPL resulting from a release, and Rivett et al. (1992) and Broholm

et al. (1999) investigated the aqueous dissolution of DNAPL components resulting from a release.

The present field-scale test was conducted at the DNTS, located at Dover AFB in Dover, Delaware. The DNTS is a field-scale laboratory, designed as a national test site for evaluating remediation technologies (Thomas, 1996). This demonstration was the first in a series of tests designed to compare the performance of several DNAPL remediation technologies. Each demonstration will follow a similar test protocol. Researchers from the Environmental Protection Agency (EPA) begin each test by releasing a known quantity of PCE into an isolated test cell. However, the amount and spatial distribution of the release are not revealed to the researchers conducting the remedial demonstration until they have completed the characterization and remediation components of their test protocol. After a release, a PITT is completed to characterize the volume and distribution of PCE, followed by the remedial demonstration, and finally, a post-demonstration PITT is conducted to evaluate the remedial performance. Since multiple remedial technologies were planned for each test cell, DNAPL characterization using soil cores was not feasible. The first demonstration, enhanced dissolution by ethanol flushing, was completed in the spring of 1999. The purpose of this chapter is to present the results of the ethanol flushing test.

Methods

PCE Volume Initially Present

The volume of PCE released into the cell by EPA (91.7 ± 0.5 L) was given in Chapter 4. A total of 5.6 ± 0.1 L of PCE was removed by dissolution during the pre-

flushing tracer tests (Conservative Interwell Tracer Test (CITT) and pre-flushing PITT). Before the start of the pre-flushing PITT, all of the well sumps were checked for DNAPL using a Solinst interface probe (model number 122). The only well in which DNAPL was detected was well 56, from which 2.8 ± 0.2 L of PCE was removed from the well sump. An additional 0.2 ± 0.05 L of free-phase PCE was produced from the MLSs prior to the start of the flushing demonstration. Therefore, the volume of PCE in the test cell at the start of the alcohol flushing test was 83.1 ± 0.6 L. The performance of the alcohol-flushing test was judged using this value.

System Description

A double five-spot pattern, which consisted of injection wells along the cell perimeter and extraction wells in the center (Figure 4-2a in Chapter 2), was used to inject and extract fluids from the cell during alcohol flushing. This pattern was used because of the flexibility it afforded to target the ethanol to specific regions in the cell. Inflatable packers were placed in each injection and extraction well to minimize dilution of the ethanol solution by separating the flow through the cell into upper and lower zones. The system was designed with flow control on each injection and extraction zone to provide the flexibility necessary to optimize the alcohol flood.

Alcohol solution and water were pumped into the test cell using Cole Parmer, Master Flex variable speed peristaltic pumps (I/P series) from holding tanks in a nearby tank storage area. An air-powered drive was used to pump the alcohol solution to minimize the explosion hazard associated with potential fugitive ethanol vapors. Water was injected above the packers into the upper zone and alcohol solution was injected below the packers into the lower zone. The lower- and upper-zone effluents were

pumped from the cell using Marschalk Corporation air-displacement bladder pumps (Minnow, Aquarius, and Aquarius II models, with a 99000 Main Logic Controller) to designated holding tanks in the tank storage area.

The upper-zone fluid was recycled by pumping it through two Advanced Recovery Technologies activated carbon drums (model number ARTCORP D16) in series. The lower-zone fluid was recycled by pumping it through either two or three activated carbon drums in series, or during the latter part of the demonstration, an ORS Environmental Systems, Lo-Pro™ II Low Profile air stripper and an activated carbon drum. Upper-zone recycling started after a sufficient volume of effluent pumped from the upper zone had been stored (1.0 day), and lower-zone cosolvent recycling started after the effluent ethanol content was high enough (approximately 70%) to make recycling feasible (6.9 days). Prior to lower-zone recycling, new 95% ethanol solution was injected into the lower zone. The recycled alcohol solution was augmented with new 95% ethanol solution as needed to maintain the ethanol content in the influent around 70%. A target ethanol content of 70% was used to maintain a large PCE dissolution capacity in the solution, yet facilitate cosolvent recycling by minimizing the need to augment treated effluent with the fresh 95% ethanol solution.

The demonstration was conducted for 38.8 days and consisted of five phases, which are summarized in Table 5-1. In general, the strategy was to initially target the alcohol solution to the bottom 0.6 m of the test cell in order to dissolve PCE near the clay, and to dissolve any PCE mobilized from the higher zones during the test. Packers were used in both injection and extraction wells to accomplish this. The target zone thickness was gradually increased by raising the packers until the full flood-zone height

Table 5-1. Phases of the flushing demonstration.

Phase	Duration (Days)	Purpose
1. Flush Initiation	0 to 0.8	Establish a layer of cosolvent along the bottom of the cell that would dissolve PCE near the clay and capture any PCE mobilized from the higher zones.
2. Flood Zone Development	0.8 to 6.9	Transition period until the ethanol content in the lower zone effluent was sufficient to start lower-zone recycling.
3. Lower Zone Recycling	6.9 to 27.7	Flush the contaminated portion of the cell with recycled cosolvent solution.
4. Hot Spot Targeting	27.7 to 34.7	Target cosolvent to specific locations of elevated PCE concentrations.
5. Water Flood	34.7 to 38.8	Flush out the resident cosolvent solution with water.

was achieved. The full height corresponded to the bottom of the release points, 10.7 m below grade.

Performance Monitoring

Samples were collected at regular intervals from the injection wells, extraction wells, MLSs, and the recycling treatment processes during the demonstration. Samples were refrigerated onsite, and then shipped overnight in coolers to the University of Florida for ethanol and PCE analysis. Samples were analyzed for ethanol by gas chromatography (GC) using a J&W capillary column (DB-624) and a flame ionization detector (FID). Samples were analyzed for PCE by a similar GC/FID method, as well as liquid chromatography using a Supelco packed column (PAH C18), UV detection, and a metbanol (70%) and HPLC grade water (30%) mixture as the mobile phase. If free phase

PCE was observed in sample vials in the laboratory, an acetone extract was used to dissolve the free phase PCE, and the sample was then analyzed by the GC/FID method.

Samples were collected from the extraction wells and MLSs over the entire test duration. Samples were collected from the injection wells during recycling treatment to monitor the amount of PCE and ethanol that was re-injected into the cell. Influent and effluent samples were collected from each carbon drum and from the air stripper to monitor treatment performance. Selected samples were analyzed in the field using a field SRI GC (8610B GC with an auto sampler) to provide real-time information for operational decisions. Density measurements were also taken in the field using Fisher Scientific specific-gravity hydrometers.

Injection and extraction flow rates, and water levels in the test cell were monitored throughout the demonstration to maintain a steady flow field to the extent possible. Injection and extraction rates were monitored using tank-volume data, flow-meter readings, and volumetric measurements at the wells. Water levels in the cell were monitored using pressure transducers in selected wells, as well as periodic measurements from well 42 with a Solinst interface probe. Adjustments to influent flow rates were made in accordance with these data to minimize water-level fluctuations in the cell.

Results and Discussion

System Hydraulics

The water level in monitoring well 42 during the test averaged 8.2 m below grade, with a standard deviation of 0.2 m. Figure 5-1a shows the cumulative volume of fluid

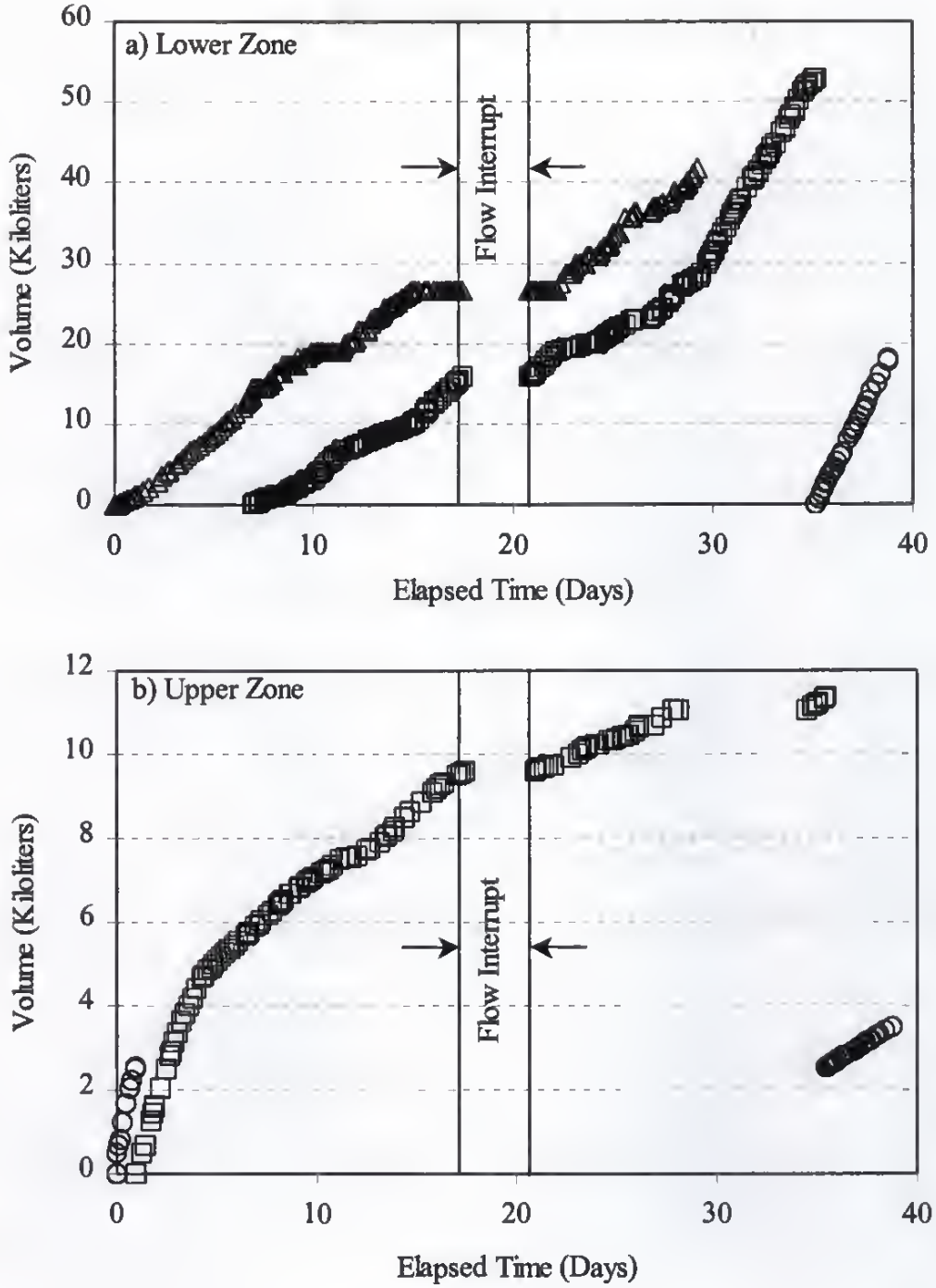

Figure 5-1. Cumulative volume injected into a) the lower zone, and b) the upper zone. Injected fluid consists of new ethanol (triangles), recycled ethanol (squares), and water (circles) for the lower zone; and re-cycled water (squares) and water (circles) for the upper zone.

injected into the lower zone during the demonstration. Three different fluids are indicated: ethanol (new 95% ethanol solution as delivered to the site), recycled ethanol (ethanol solution extracted from the cell, treated and then re-injected), and water (injected at the end of the demonstration to flush out the remaining ethanol). Recycled ethanol accounted for 47% of the fluid injected into the lower zone. The break from 17.5 to 20.9 days represents a flow interrupt that was conducted to investigate mass-transfer limitations to PCE dissolution. Figure 5-1b shows the cumulative volume of water and recycled water injected into the upper zone during the test. The recycled water is the fluid extracted from the upper zone, treated, and then re-injected. Recycling accounted for 77% of the fluid injected into the upper zone. The total amount of fluid injected into the lower zone was approximately eight times greater than that injected into the upper zone. Estimates of the number of pore volumes flushed through the upper and lower zones separately are not possible because the location of the separation between the two zones in the cell was not known. However, using the combined upper- and lower-zone extraction volumes, an average water table position of 4 m above the clay, and an effective porosity of 0.20, approximately 10 pore volumes were flushed through the test cell.

In theory, a symmetric double-five spot pattern would have produced a stagnation point in the center of the test cell, assuming homogeneous hydraulic conductivity and balanced flow rates in the injection and extraction wells. The center of the cell was swept, however, by changing the flow system as done during the Hot-Spot Targeting Phase (Phase 4). During this phase, injection into wells 41, 51, and 54 was stopped and injection into wells 41, 46, and 56 was increased. In addition, well 51 was converted to

an extraction well from 30.2 to 34.2 days. PCE concentrations in samples collected from the extraction wells and MLSs during Phase 4 suggested that contaminant was not trapped in the center of the test cell by the double-five spot pattern.

Mass Recovery

PCE concentrations and the ethanol percentages from extraction well samples are plotted in Figure 5-2. The ethanol content in the lower zone increased over the first 5 days as the new 95% ethanol solution displaced the resident water in the test cell. Changes in the ethanol content after approximately 5 days resulted from changes in flushing operations (i.e., ethanol recycling, ethanol augmentation, and changes in packer positions). Ethanol content and PCE concentrations from well 51 during the period it was converted to an extraction well are not shown in Figure 5-2. The ethanol content in the effluent from this well varied between 58 to 65%, and the PCE concentration varied from 1300 to 2300 mg/L.

The ratio of aqueous PCE concentration to PCE solubility limit for extraction wells 45 and 55 are plotted in Figure 5-3 as a function of time. The PCE solubility limit, which is a function of the ethanol content, was based on PCE solubility limits reported by Van Valkenburg (1999). The ratio of aqueous PCE concentration to PCE solubility limits for well 51 (not shown in Figure 5-3) ranged from 0.04 to 0.08. PCE concentrations above PCE solubility limits are evident in the lower-zone effluent for a short period from approximately 1 to 2 days, and in the upper-zone effluent from approximately 2 to 13 days. The volume of free-phase PCE represented by a ratio greater than unity is 0.04 ± 0.004 L for the lower zone and 3.2 ± 0.1 L for the upper zone. Gravity separators were

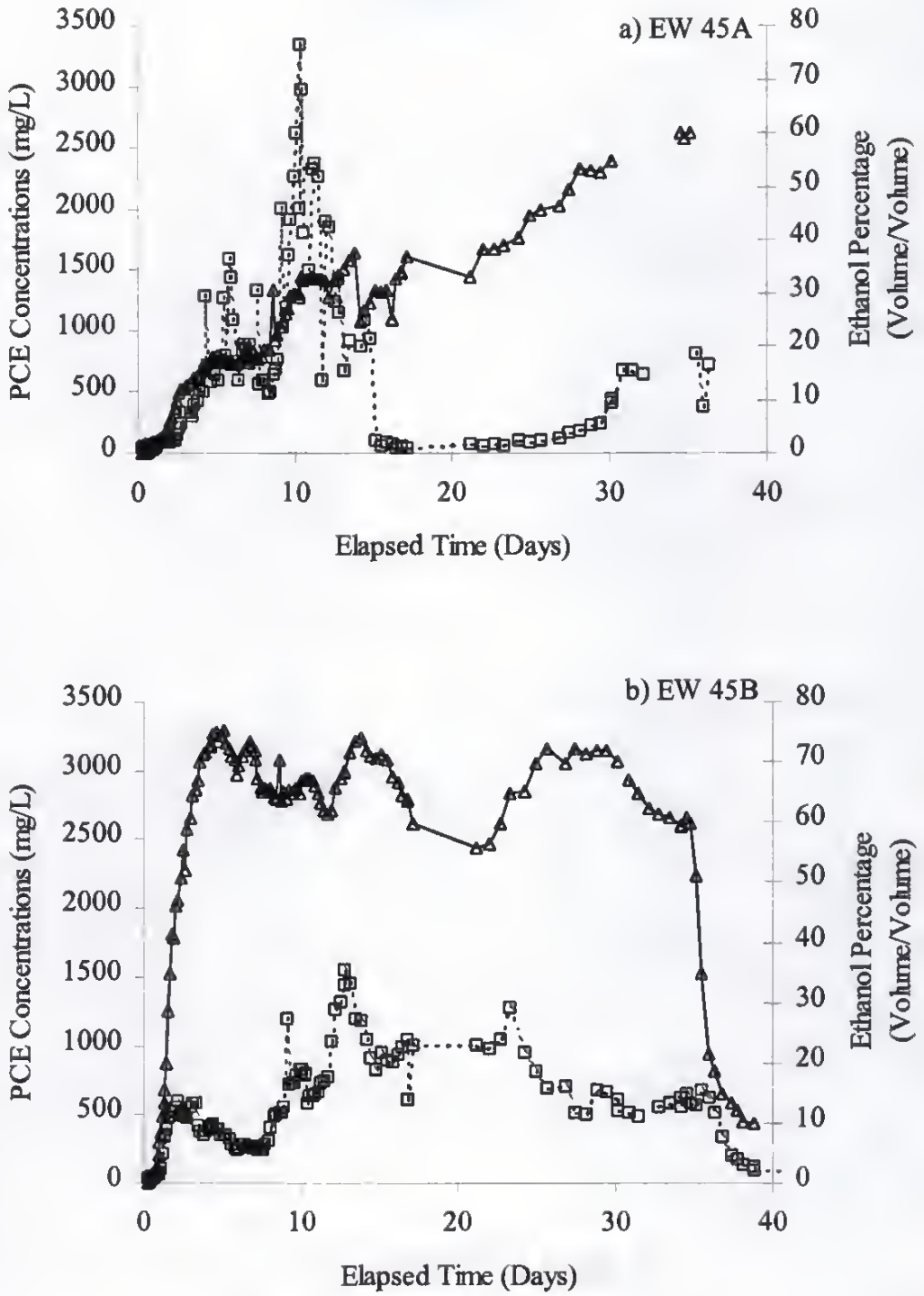

Figure 5-2. PCE concentrations (squares) and ethanol percentages (triangles) from a) upper zone extraction well 45A, and b) lower zone extraction well 45B.

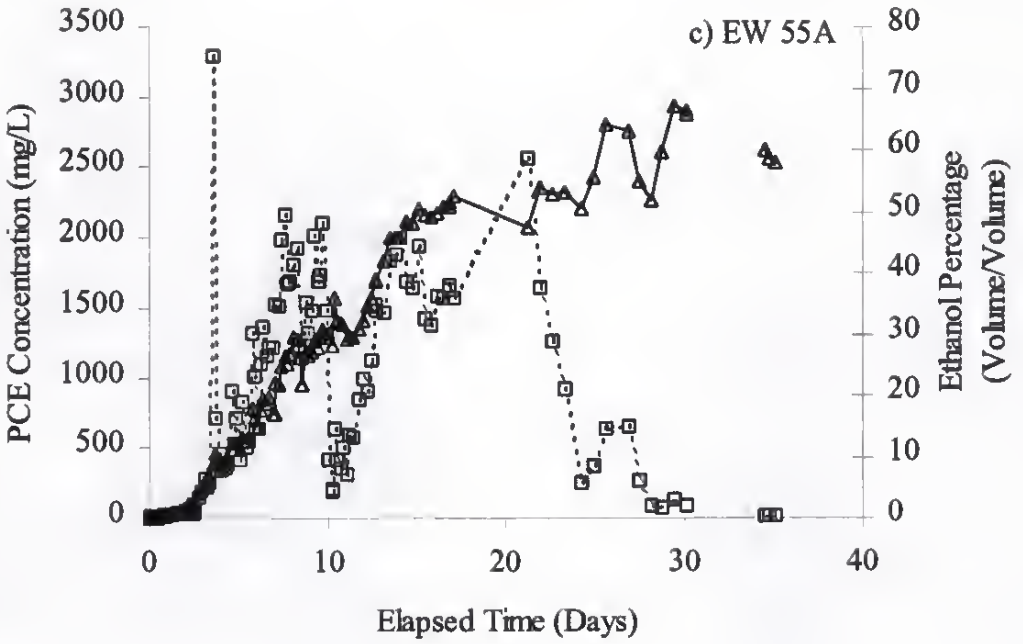

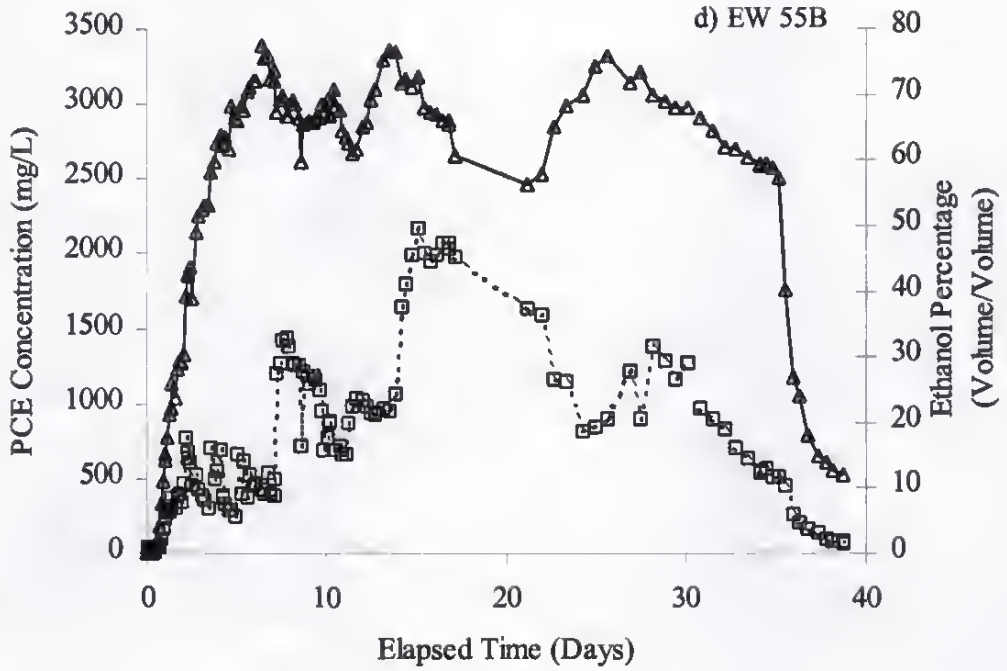

Figure 5-2 continued. PCE concentrations (squares) and ethanol percentages (triangles) from c) upper zone extraction well 55A, and d) lower zone extraction well 55B.

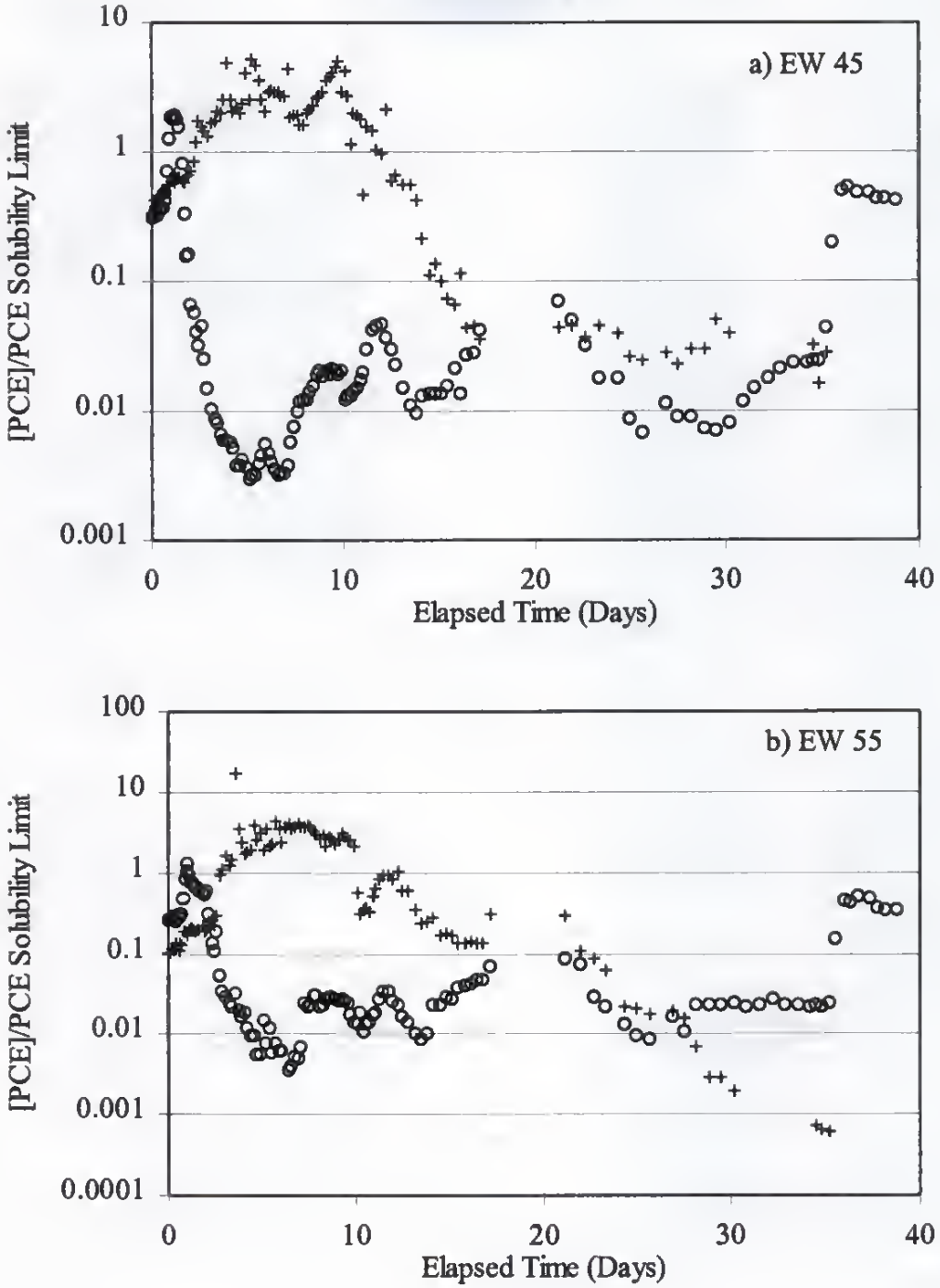

Figure 5-3. Ratio of PCE concentration to PCE solubility limit for upper zone (plus signs) and lower zone (circles) samples from extraction wells a) 45 and b) 55. The PCE solubility limits are a function of ethanol content, and were based on values reported by VanValkenburg (1999).

installed in the extraction well effluent lines to remove any free-phase PCE from the effluent. Over the course of the entire test, only 0.35 ± 0.01 L of free-phase PCE was collected from the upper-zone separators, and no free-phase PCE was collected from the lower-zone separators. The relatively small volume of free-phase PCE collected from the separators was supported by the fact that free-phase PCE was not observed when extraction well effluent samples were collected. The formation of an emulsion is the most likely explanation for the discrepancy between free-phase PCE volumes observed during the test, and those estimated from the laboratory samples. It is suspected that the emulsion formed in the extraction wells, rather than in the aquifer, due to mixing which diluted the ethanol content in the well, resulting in free-phase PCE formation and subsequent emulsification.

Free phase PCE was observed in only 16 of more than 5000 MLS samples collected, and only at selected depths in MLS locations 12 and 14. The majority of these observations occurred within the first day after the start of alcohol flushing. The PCE ranged from small drops, approximately 1 mm or smaller in diameter, to slugs no greater than 20 mL in volume. PCE concentrations in excess of estimated PCE solubility limits occurred in 56 samples (out of approximately 1500 samples analyzed) at selected depths in MLS locations 12, 14, 21, 25, 32, 41, 43, and 63. However, only at MLS locations 12, 14, 25, 41, and 63 were concentrations observed significantly higher than the solubility limit (>1.5 times the solubility limit). The difference in the number of observations of free-phase PCE during sample collection, and the number of samples with PCE concentrations greater than PCE solubility limits is also attributed to the formation of an emulsion as pore fluids converged and mixed in the samplers. The majority of these

samples occurred within the first 5 days after the start of alcohol flushing. Furthermore, free-phase PCE was not detected in the well sumps using the interface probe when they were investigated prior to the start of the post-flushing PITT. Based on this evidence, it is considered that limited mobilization occurred during alcohol flushing.

The PCE concentrations in the lower-zone extraction well effluent were well below the PCE solubility limits after approximately 3 days (Figure 5-3). The low PCE concentrations relative to PCE solubility could have resulted from mixing at the extraction wells, or from mass-transfer limitations. During the demonstration, the longest flow interrupt occurred from 17.5 to 20.9 days, when the system was intentionally turned off to investigate mass-transfer limitations. In general, evidence of mass-transfer limitations are manifested by increases in effluent contaminant concentrations after the flow interrupt (Brusseau et al., 1997). No evidence of mass-transfer limitation is apparent from the breakthrough curves shown in Figure 5-2. Localized mass-transfer limitations may have occurred, but were not observed as elevated PCE concentrations in the extraction well effluent. Therefore, effluent PCE concentrations were most likely observed to be less than the PCE solubility limit due to mixing at the extraction wells.

Ethanol Recovery

A total of 41,700 L of 95% ethanol solution was delivered to the test cell. Through recycling operations, the total amount of ethanol injected into the test cell over the course of the test was 69,400 L. A total of 62,500 L of ethanol, or 90% of that injected, was recovered from the test cell during alcohol flushing and water flooding, and an additional 3,800 L was removed during the post-demonstration PITT, yielding a total ethanol recovery of 96%.

PCE Recovery

Approximately 52.6 ± 0.7 L of PCE were removed from the test cell, based on the zeroth moment of the PCE breakthrough curves measured at the extraction wells. The error estimate for the amount of PCE extracted was based on the propagation of errors in volume and concentration measurements through the zeroth moment calculations. Errors in volume measurements (±25 L) were based on one half of the smallest division of the tank volume scale, and errors in concentration were conservatively assumed to be ±15% of the measured concentration. Using an average PCE concentration (2096 ± 51 mg/L) based on all MLS samples analyzed, the total volume of fluid removed by the MLSs during the test (916 ± 42 L), and the volume of free-phase PCE removed through the MLSs (0.08 ± 0.04 L), the total amount of PCE removed by the MLSs was estimated at 1.3 ± 0.1 L. Thus, the total amount of PCE removed from the test cell by the extraction wells and the MLSs was 53.9 ± 0.7 L, while that injected during alcohol recycling was estimated at 0.5 ± 0.04 L. Therefore, the net amount of PCE removed from the cell was estimated to be 53.4 ± 0.7 L.

All extracted fluids were stored in three tanks at the end of the demonstration. Samples were collected from each tank and were analyzed for PCE and ethanol. A second estimate of the PCE removed from the test cell was obtained by adding the amount of PCE in the storage tanks to the amount of PCE removed by activated carbon and air stripping treatment. Based on the tank volumes and PCE concentrations, the mass of PCE in the tanks at the end of the demonstration was 19 ± 3 L. Based on influent and effluent treatment samples, the volume of PCE removed by activated carbon was 16.6 ±

0.9 L, and the amount removed by air stripping was 11.1 ± 0.8 L. The preceding errors are based on assumed errors of 15% for the treatment volumes and 15% for the influent and effluent concentrations. This tank-based approach yielded an estimate of 47 ± 3 L of PCE, which is 11% less than the 53 L estimated from the extraction well and MLS samples. The tank-based estimate could be less because the tank samples were collected from valves located on the bottom of the tanks, and density-driven vertical segregation of fluids may have occurred. This would result in a non-uniform distribution of PCE within the tank, as more PCE would tend to dissolve in the higher ethanol fraction fluid accumulated at the top of the tank due to its lower density. Due to such potential bias in the tank-based estimate, the previous estimate of 53 L is considered to be more robust.

The flushing demonstration removed 53.4 ± 0.7 L of PCE, which is 64% of the 83.1 ± 0.6 L of PCE estimated in the test cell at the start of the test. Therefore, approximately 29.7 ± 0.9 L of PCE remained in the cell at the end of the demonstration. Figure 5-4 presents the aqueous PCE concentrations from field analysis of MLS samples collected 32.3 days after the start of the test. Based on this figure, areas of high concentrations are evident near MLS locations 25 and 12, which supports the conclusion that a significant volume of PCE was left in the test cell.

Results from the pre- and post-flushing PITTs presented here are limited to PCE volume estimates based on the normalized, first temporal moments of tracer BTCs measured at the extraction wells (Table 5-2). Both the pre-flushing and the post-flushing PITTs used an inverted five-spot flow pattern, resulting in six extraction wells (41, 44, 46, 51, 54, and 56), and two injection wells (45 and 55). An inverted five-spot pattern was used in the PITTs because it afforded better spatial resolution of the NAPL

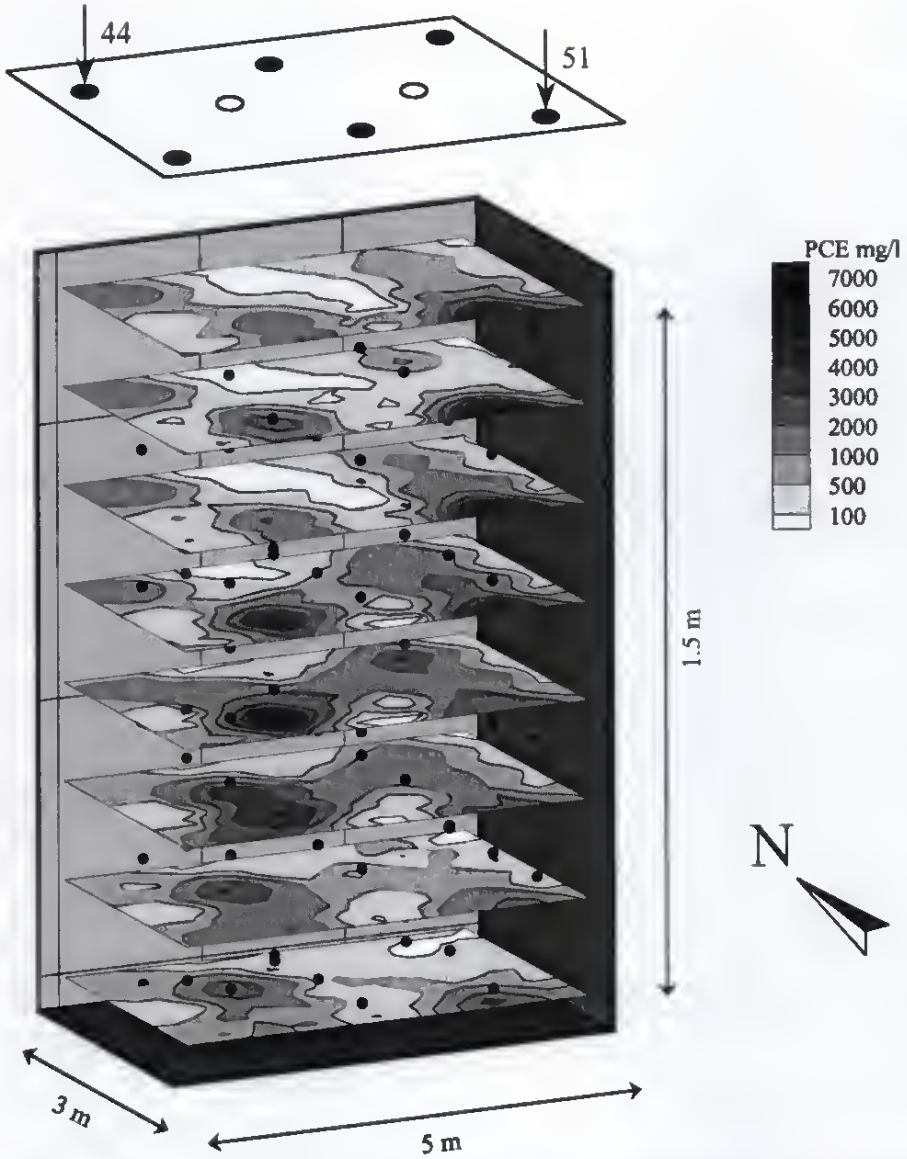

Figure 5-4. Aqueous PCE distribution based on MLS samples from the end of the flushing demonstration. The concentration contours were created using an inverse distance contouring method in the TechPlot software package.

distribution through six extraction well breakthrough curves. Background retardation of the tracers was assumed to be negligible. Multiple tracers were used in both PITTs, but the PCE volume estimates were based only on those partitioning tracers with reasonable recovery (approximately 90% to 110%), and with the consistently highest retardation values (retardation > 1.1). Tracers used in the upper zone of the pre-flushing PITT decayed as indicated by poor mass recovery from extraction well BTCs. An effort was made to estimate the volume of DNAPL in the upper tracer swept zone by correcting for tracer degradation (see Chapter 4). Because of the high uncertainty of this estimate, focus is given only to the lower zone tracer comparison of pre- and post-flushing PITT results to assess performance of the alcohol flood (Table 5-2). This performance assessment of the alcohol flood based on the PITT results assumes each test had a common swept zone.

Jawitz et al. (1997) defined removal effectiveness as the fraction of cumulative volume removed within a swept zone. The overall average reduction in PCE volume from the lower zone in the test cell was 80%, based on the pre- and post-flushing PITTs (This estimate increases to 92% if the upper zone tracer results are included). This remedial performance estimate is higher than the performance estimate (64%) based on the comparison of released and extracted PCE volumes. It is concluded that both PITTs underestimated the PCE volume in the test cell, and the underestimate of PCE volume in the post-flushing PITT is the principle reason for the overestimate of remedial performance. Factors which limited contact between the tracers and PCE may also have limited contact between the alcohol solution and the PCE, which may explain the low PCE recovery (64%) for the alcohol flood.

Table 5-2. Summary of PCE Volumes predicted from Pre-and Post flushing PITTs

Extraction Well	PCE Volume		PCE Removal Effectiveness
	Pre-Flushing	Post-Flushing	
	(Liters)	(Liters)	(%)
41	3	0.7	73%
44	0.7	0.3	57%
46	4	0.9	78%
51	6	0.7	88%
54	0.7	0.5	25%
56	5	0.8	85%
Total	19	4	80%

Treatment Efficiency

The contaminant volume removed divided by the volume of flushing fluid has been used to describe the efficiency of in-situ flushing remediation systems (Jawitz et al., 1997; Sillan et al., 1998b). Efficiency is defined here as the cumulative volume of DNAPL removed per cumulative volume of applied remedial fluid. If the volume of remedial fluid is limited to the ethanol delivered to the test cell, then the cell-averaged removal efficiency was $1x10^{-3}$ liters of PCE per liter of ethanol (53 L PCE/ 41,700L ethanol). If the volume of remedial fluid includes the total amount of ethanol and water injected from the start of the demonstration to the start of the final water flood, then the removal efficiency was $6x10^{-4}$ liters of PCE per liter of injected fluid (53 L PCE/ 94,500 L ethanol and water). An estimate of pump-and-treat performance in the test cell can be made based on the amount of PCE removed during the pre-flushing PITT. A removal efficiency of $2x10^{-5}$ is obtained by the ratio of PCE removed to the volume of water

flushed through the cell. Therefore, the removal efficiency for alcohol flushing was 30 times better than the pump-and-treat efficiency.

Removal efficiencies, calculated as cumulative PCE volume removed per cumulative extracted volume, are shown for each well in Figure 5-5 as a function of time. Once the extraction well packers were raised to their maximum height at 13.9 days, the removal efficiencies in extraction wells 45A, 45B, and 55A remained constant at approximately $4x10^{-4}$ to $5x10^{-4}$, while the removal efficiency in 55B remained constant at approximately $6x10^{-4}$ to $7x10^{-4}$. This indicates that PCE mass removal was fairly constant during the demonstration. This further suggests that continued flushing should have increased removal effectiveness, but this was prevented because of personnel limitations, project schedule, and budget considerations. Based on the constant removal efficiencies indicated in Figure 5-5, it is estimated that a significant portion of the remaining PCE could have been removed if the demonstration had been continued. Neglecting decreases in performance resulting from diminishing NAPL content, it is estimated that the majority of the remaining PCE would have been removed if the system had been operated for another 3 weeks. However, this prediction is inconsistent with the fact that both pre- and post-flushing PITTs underestimated the volume of DNAPL by approximately 25 L, which suggests the removal efficiency may have substantially decreased due to contact limitations before the majority of the remaining DNAPL was removed. Temporary extraction well 51B had the highest removal efficiency of approximately $1x10^{-3}$, which may suggest an advantage to changing the flow field during flushing when hot spots are identified.

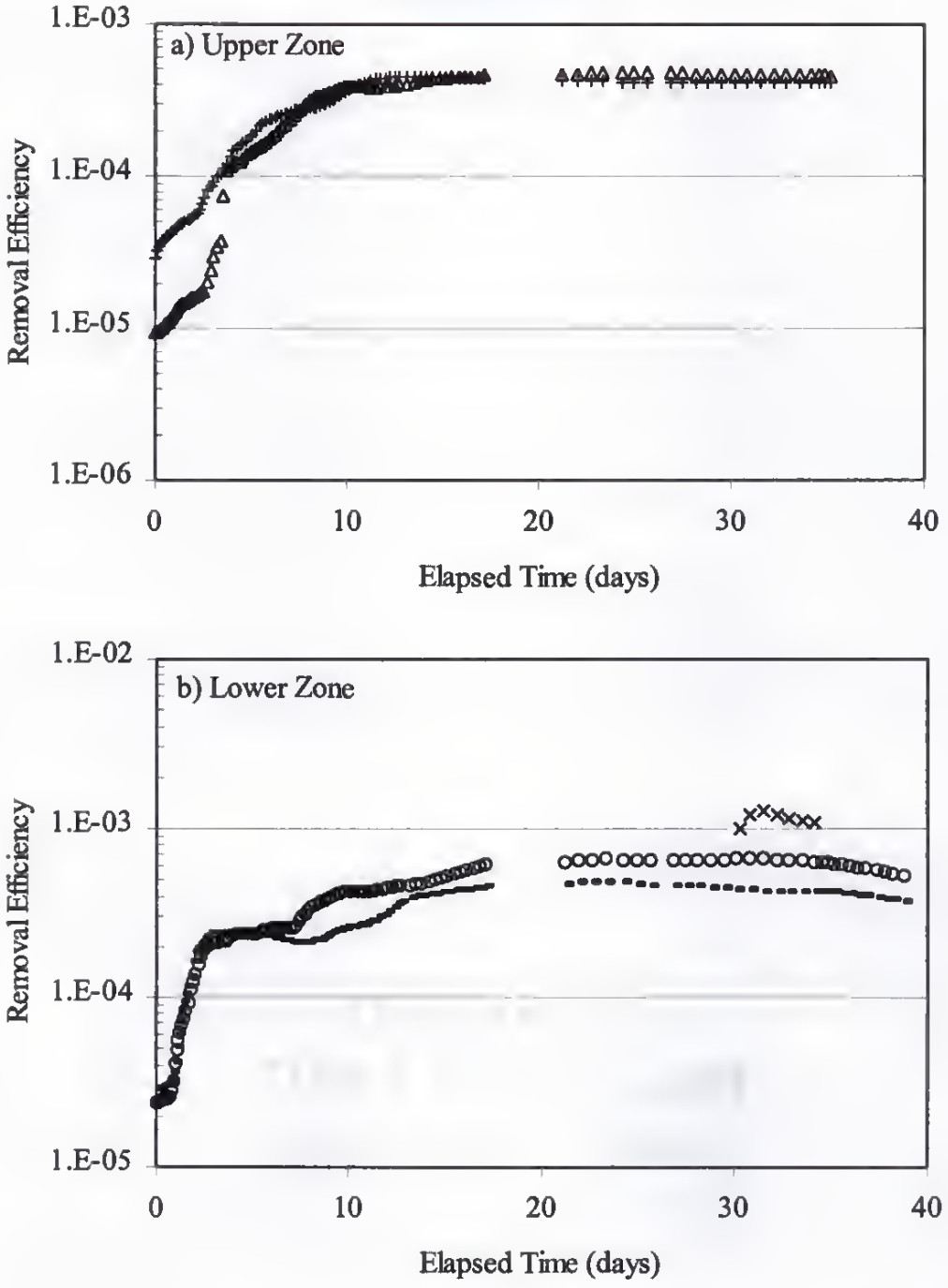

Figure 5-5. Removal efficiency for a) upper zone: 45A (plus symbols) and 55A (triangles); and b) lower zone: 45B (minus symbol), 55B (circles), and 51B (x).

Changes in Aqueous PCE Concentrations

The flux-averaged aqueous PCE concentrations from extraction well samples collected at the end of the pre-flushing PITT ranged from 8 mg/L (EW 44) to 47 mg/L (EW 51). Subsequent to flushing, reductions in aqueous concentrations were observed in all extraction wells. The flux-averaged aqueous PCE concentrations from extraction well samples collected at the end of the post-flushing PITT ranged from 6 mg/L (EW 44) to 19 mg/L (EW 41). The aqueous PCE concentrations changed the least in extraction wells 41, 44, and 54 (percent reductions of 37%, 25%, and 23%, respectively). These three wells also had the lowest PCE removal effectiveness based on the PITT results (Table 5-2). Larger decreases in aqueous PCE concentration were observed in extraction wells 46, 51, and 56 (percent reductions of 79%, 77%, and 72%, respectively), which correspond to the wells with the higher values of removal effectiveness (Table 5-2). The apparent correlation between removal effectiveness and flux-averaged aqueous concentrations (Figure 5-6) supports the use of removal effectiveness as a measure of remedial performance. More importantly, these data suggest that partial reductions in DNAPL mass can result in decreased flux-averaged aqueous PCE concentrations, at least under forced-gradient conditions.

Recycling Treatment

This is the first cosolvent-flushing demonstration in which an alcohol cosolvent effluent was treated and re-injected. Activated carbon drums were used to treat the effluent alcohol solution for the first two-thirds of the demonstration. Influent and effluent aqueous PCE concentrations from each drum were monitored and drums were

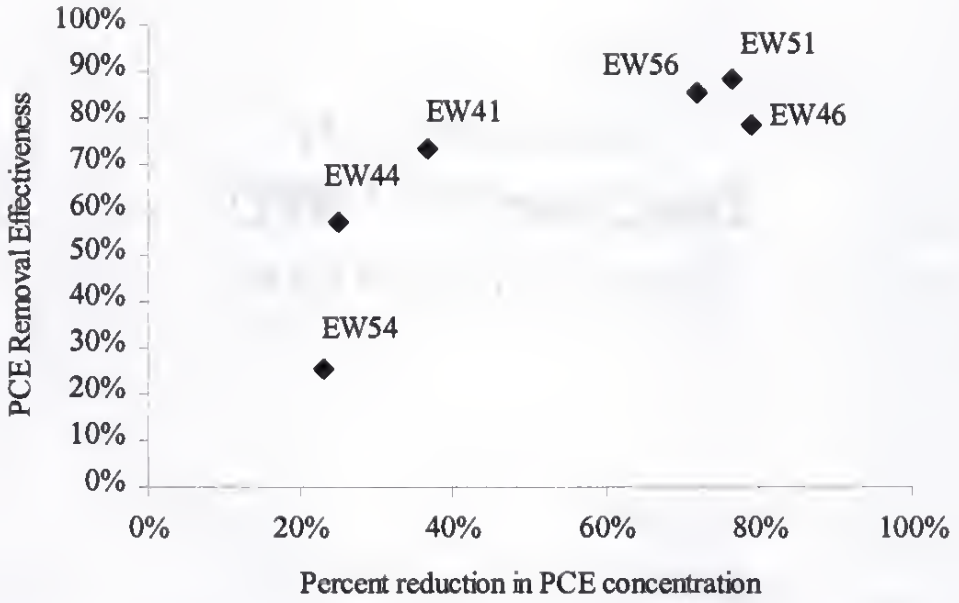

Figure 5-6. DNAPL removal effectiveness versus reduction in PCE concentrations.

removed from service once the effluent PCE concentration equaled the influent PCE concentration. Approximately 3 to 6 L of PCE was adsorbed in each drum before PCE breakthrough occurred. For the final third of the demonstration, a series combination of air stripping and activated carbon was used to evaluate cosolvent recycling by air stripping. The average air-stripping treatment efficiency was 91%. Ethanol content was not significantly affected by either the activated-carbon or air-stripping treatment processes. The ethanol content in the effluent samples after the treatment processes was reduced by an average of approximately 1% relative to the influent ethanol content. Cosolvent recycling was a significant factor in this demonstration, as evident by the fact

that the volume of alcohol solution delivered to the test cell, and consequently, the volume of PCE removed from the test cell, were approximately doubled by recycling.

Conclusions

This chapter presents field test results for enhanced dissolution of PCE by an ethanol solution in a hydraulically isolated test cell. By mass balance, it was estimated that 83 L of PCE were present in the test cell at the start of the test. Over a 40-day period, 64% of the PCE was removed by flushing with the alcohol solution. High removal efficiencies at the end of the demonstration indicated that more PCE could have been removed if the demonstration had continued. Results from pre- and post-flushing PITTs overestimated the treatment performance, however, both PITTs missed significant amounts of PCE. Inaccessibility of the tracers to PCE may also mean that some PCE was inaccessible to the alcohol solution, which may explain the limited amount of PCE removed by the alcohol flush. The flux-averaged aqueous PCE concentrations were reduced by a factor of 3 to 4 in the extraction wells that showed the highest PCE removal. The ethanol solution extracted from the test cell was recycled using activated carbon and air stripping treatment. Both treatment processes were successful in removing PCE for recycling purposes, while having minimal impact on the solution ethanol content.

CHAPTER 6
CONCLUSIONS

The analysis method presented in Chapter 2 can be used to estimate uncertainty in absolute and normalized moments resulting from measurement uncertainty. It is based on the assumption that moments are calculated directly from the BTC by numerical integration using the trapezoidal rule. Provided this requirement is met, the method can be used to estimate the uncertainty of results from a variety of tracer studies. Compared to previous work, it has the advantage of application to volume-based moments, accounting for uncertainty in the volume measurements. The analysis indicates that the relative uncertainty is reduced as it is propagated from measured values to calculated moments. As presented in Chapter 3, the method was extended to quantify the uncertainty of NAPL volume estimates based on partitioning tracers. Previous work has reported uncertainty in NAPL saturation, but not NAPL volume.

There are several areas where additional work in tracer test uncertainty analysis should prove beneficial. Relative to the work introduced in Chapter 2, additional efforts should focus on estimating the uncertainty associated with BTC extrapolation, explicitly accounting for the covariance between the truncated and extrapolated portions of the BTC. Given the improved accuracy of equation (2-4a) over (2-5) in approximating absolute moments (especially the higher moments), it would be useful to develop the uncertainty equations associated with equation (2-4a). Furthermore, due to the complexity of analytical uncertainty expressions for higher moments, the use of delta

method approximations may prove to be more practical. Relative to the work introduced in Chapter 3, future efforts in uncertainty analysis associated with partitioning tracers could investigate the use of published techniques to explicitly account for measurement uncertainty in least-squares regression curve-fitting techniques. A method is also needed to estimate the correlation between the non-reactive normalized first moment and NAPL saturation when least-squares regression curve-fitting techniques are used to estimate NAPL volume from partitioning tracer test data.

The cosolvent flushing demonstration removed 64% of the PCE from the cell over a 40-day period. High removal efficiencies at the end of the demonstration indicated that more PCE could have been removed if the demonstration had continued. However, the fact that both pre- and post-partitioning tracer tests missed approximately 25 L of PCE suggests that all of the released PCE would not have been recovered. The flux-averaged aqueous PCE concentrations were reduced by a factor of 3 to 4 in the extraction wells that showed the highest PCE removal. The ethanol solution extracted from the cell was recycled using activated carbon and air stripping treatment. Both treatment processes were successful in removing PCE for recycling purposes, while having minimal impact on the solution ethanol content.

The success of the cosolvent flushing test is dependent upon the metric used in making the judgment. One metric that could be applied is the state of the cell after the remedial test, simply stated as, "is the cell clean?" The answer to this question is of course dependent on the definition of clean. Using the regulatory approach of maximum contaminant levels, the cell was not clean after the demonstration, and hence the test was unsuccessful. However, it is questionable whether any technology at the moment could

reach this extreme measure of success. Certainly the cell was cleaner, but the merit of a relative comparison is debatable. Another success metric could be the comparison of the test performance to conventional technology performance. Certainly the test would be considered successful in that its performance was better than that of pump-and-treat based on the amount of PCE removed over the test duration. From a qualitative standpoint, the fact that the test was successful by this metric is not surprising. However, the test results do serve as a benchmark for quantitatively defining success relative to pump-and-treat performance. Another success metric is the comparison of the performance to other DNAPL source-zone remediation techniques. This, of course, was the purpose of the entire project and the verdict of success by this comparison cannot be answered at this time since the project is still in progress.

Partitioning tracer tests offer an alternative method for quantifying NAPL. They offer the advantage of characterizing a much larger subsurface volume compared to more conventional NAPL characterization techniques. For the demonstration presented, the best estimate of the volume of DNAPL in the cell prior to the first partitioning tracer test (pre-ethanol flushing tracer test) was 86 ± 1 L, while the partitioning tracer test results predicted a NAPL volume of 60 ± 10 L. This represents an error of approximately 30%, which is considered very encouraging. This result is also supported by the fact that the volume of DNAPL removed by the flushing demonstration was 53 L, or 88% of the volume predicted by the tracers. The post-flushing partitioning-tracer test predicted only 5 L of the estimated 30 L remaining. This represents an error of approximately 83%, which is certainly less encouraging. However, the consistency between the PCE volume discrepancy in the pre-flushing partitioning tracer test, flushing test, and post-flushing

partitioning tracer test (26, 30, and 25 L, respectively) suggest the possibility that contact between flushing fluids and a certain volume of DNAPL was hindered by geological constraints. Partitioning-tracer predictions of NAPL volume should always be qualified with the rather obvious statement that the NAPL volume is that predicted in the swept-zone of the tracer. What can be too easily neglected is the fact that the swept-zone of the tracer and the target area of investigation are not always the same.

Were the partitioning tracer tests successful? As discussed for the ethanol flood, the success of the partitioning tracer tests is dependent upon the metric used in making the judgment. One success metric could be the comparison of the predicted DNAPL volume based on the tracer test results to the DNAPL volume in the cell based on the release information. In other words, did the tracers tests accurately predict the DNAPL volume? If accuracy is defined as an agreement in DNAPL volumes within the limits of the estimated uncertainty, it would have to be concluded that the tracers tests were unsuccessful. However, if a less stringent definition of accuracy is used, such as the accuracy that could be expected from more conventional DNAPL characterization technologies, predicting 60 L out of 83 L should be considered a successful result. To a certain degree, even predicting 5 L out of 30 L could be considered successful, in light of the influence of geologic heterogeneities on DNAPL contamination. Conclusions about the reliability of tracer tests to achieve this level of accuracy (whether deemed good or poor) at other sites should be made cautiously. Potential tracer degradation issues, site specific geology, DNAPL volume, and the choice of injection/extraction schemes hinder extrapolation of these tests results to general conclusions about tracer tests.

For partitioning tracer tests, future work should investigate the apparent difference in DNAPL volume estimates as a function of tracer partitioning coefficients. For cosolvent flushing, future work should focus on recycling in order to improve the efficiency of the technique. Design equations to predict cosolvent recycling performance by air stripping would be useful for practical applications. Efficient and economical means to separate the alcohol cosolvent from the water during cosolvent flushing operations would certainly improve its utility. Results in Chapter 5 touched on partial source-zone removal and its impact on aqueous groundwater concentrations. This is a very important topic for future research, and one that may have the most influence over future use of all source-zone characterization and remediation efforts.

APPENDIX A
SYSTEMATIC ERRORS

Constant Systematic Errors in Volume Measurements

Let "a" represent a constant, systematic error in volume measurements, such that

$$V_i = V_i^t + a \ . \qquad \text{(A-1)}$$

The value of a is constrained such that $a \geq -V_{min}$, where V_{min} is the smallest volume measurement. The change in volume between the i^{th} and $(i+1)^{th}$ measurements is

$$\Delta V_i = \left(V_{i+1}^t + a\right) - \left(V_i^t + a\right) = \Delta V_i^t \ , \qquad \text{(A-2a)}$$

Consequently, in light of equation (2-4b),

$$m_0 = m_0^t \ . \qquad \text{(A-2b)}$$

Therefore, constant systematic errors in volume measurements have no effect on the absolute zeroth moment. The average volume over the i^{th} interval is

$$\overline{V}_i = \frac{1}{2}\left[\left(V_{i+1}^t + a\right) + \left(V_i^t + a\right)\right] = \overline{V}_i^t + a \ . \qquad \text{(A-3a)}$$

The absolute first moment is therefore

$$m_1 = \sum_{i=1}^{n-1} \Delta V_i \left(\overline{V}_i^t + a\right)\overline{c}_i = \sum_{i=1}^{n-1} \left(\Delta V_i \overline{V}_i^t \overline{c}_i + a\Delta V_i \overline{c}_i\right) = m_1^t + a m_0^t \ . \qquad \text{(A-3b)}$$

Combining equations (A-2b) and (A-3b) and accounting for the tracer pulse volume give the pulse-corrected, normalized first moment:

$$\mu_1' = \frac{m_1^t + a m_0^t}{m_0^t} - \frac{V_p}{2} \ , \qquad \text{(A-3c)}$$

$$\mu_1' = \mu_1^{t'} + a \ . \qquad \text{(A-3d)}$$

Equation (A-3d) neglects systematic errors in the tracer pore volume. The retardation factor can now be expressed as

$$R = \frac{\mu_1^{R,t'} + a}{\mu_1^{NR,t'} + a} \ . \qquad \text{(A-4)}$$

Saturation, S, therefore becomes

$$S^t = \frac{\left(\frac{\mu_1^{R,t'} + a}{\mu_1^{NR,t'} + a}\right) - 1}{\left(\frac{\mu_1^{R,t'} + a}{\mu_1^{NR,t'} + a}\right) - 1 + K_{NW}}, \qquad \text{(A-5a)}$$

which, can be rearranged to

$$S^t = \frac{\mu_1^{R,t'} - \mu_1^{NR,t'}}{\mu_1^{R,t'} - \mu_1^{NR,t'} + K_{NW}\left(\mu_1^{NR,t'} + a\right)}. \qquad \text{(A-5b)}$$

Using equations (4-3), (A-3d), (defined in terms of the non-reactive tracer) and (A-5b), the NAPL volume is

$$V_N = \frac{\left(\mu_1^{R,t'} - \mu_1^{NR,t'}\right)\left(\mu_1^{NR,t'} + a\right)}{\mu_1^{R,t'} - \mu_1^{NR,t'} + K_{NW}\left(\mu_1^{NR,t'} + a\right)} \qquad \text{(A-6)}$$

Proportional Systematic Errors in Volume Measurements

The relationship between a proportional, systematic error in volume measurements, α', and the true volume measurements can be expressed as

$$V_i = V_i^t + \alpha' V_i^t = V_i^t\left(1 + \alpha'\right) \ . \qquad \text{(A-7a)}$$

For simplicity, let $\alpha = (1+\alpha')$, therefore,

$$V_i = \alpha V_i^t \ . \qquad \text{(A-7b)}$$

The difference in the i^{th} and $(i+1)^{th}$ cumulative volume measurement is

$$\Delta V_i = \alpha V_{i+1}^t - \alpha V_i^t = \alpha \Delta V_i^t \ , \qquad \text{(A-8a)}$$

and the absolute zeroth moment becomes

$$m_0 = \alpha m_0^t \ . \qquad \text{(A-8b)}$$

The average volume over the i^{th} interval is

$$\overline{V}_i = \frac{1}{2}\left[\alpha V_{i+1}^t + \alpha V_i^t\right] = \alpha \overline{V}_i^t \ , \qquad \text{(A-9a)}$$

so, the absolute first moment is therefore

$$m_1 = \sum_{i=1}^{n-1} \alpha \Delta V_i^t \alpha \overline{V}_i^t \overline{c}_i = \alpha^2 m_1^t \ . \qquad \text{(A-9b)}$$

Combining equations (2-6), (A-8b) and (A-9b) and accounting for the tracer-pulse volume give the pulse-corrected, normalized first moment:

$$\mu_1' = \frac{\alpha^2 m_1^t}{\alpha m_0^t} - \frac{V_p}{2} = \frac{\alpha m_1^t}{m_0^t} - \frac{V_p}{2} \ , \qquad \text{(A-9c)}$$

The true normalized first moment can be expressed as

$$\mu_1^{t'} = \frac{m_1^t}{m_0^t} - \frac{V_p}{2} \ , \qquad \text{(A-9d)}$$

which can be rearranged as

$$\frac{V_p}{2} = \frac{m_1^t}{m_0^t} - \mu_1^{t'} \ . \qquad \text{(A-9e)}$$

Substituting equation (A-9e) into (A-9c) and rearranging result in

$$\mu_1' = \mu_1^{t'} + \frac{m_1^t}{m_0^t}(\alpha - 1) = \mu_1^{t'} + \frac{m_1^t}{m_0^t}\alpha' \qquad \text{(A-9f)}$$

Equation (A-9f) neglects a systematic error in the tracer-pulse volume. Using equations (3-1a) and (A-9f), the retardation factor becomes

$$R = \frac{\mu_1^{R,t'} + \frac{m_1^{R,t}}{m_0^{R,t}}(\alpha - 1)}{\mu_1^{NR,t'} + \frac{m_1^{NR,t}}{m_0^{NR,t}}(\alpha - 1)} . \qquad \text{(A-10)}$$

The saturation, S, then becomes

$$S = \frac{\left[\frac{\mu_1^{R,t'} + m_1^{R,t}/m_0^{R,t}(\alpha - 1)}{\mu_1^{NR,t'} + m_1^{NR,t}/m_0^{NR,t}(\alpha - 1)}\right] - 1}{\left[\frac{\mu_1^{R,t'} + m_1^{R,t}/m_0^{R,t}(\alpha - 1)}{\mu_1^{NR,t'} + m_1^{NR,t}/m_0^{NR,t}(\alpha - 1)}\right] - 1 + K_{NW}} , \qquad \text{(A-11a)}$$

which can also be written as

$$S = \frac{\mu_1^{R,t'} - \mu_1^{NR,t'} + \left(\frac{m_1^{R,t}}{m_0^{R,t}} - \frac{m_1^{NR,t}}{m_0^{NR,t}}\right)(\alpha - 1)}{\mu_1^{R,t'} - \mu_1^{NR,t'} + \left(\frac{m_1^{R,t}}{m_0^{R,t}} - \frac{m_1^{NR,t}}{m_0^{NR,t}}\right)(\alpha - 1) + K_{NW}\left[\mu_1^{NR,t'} + \frac{m_1^{NR,t}}{m_0^{NR,t}}(\alpha - 1)\right]} \qquad \text{(A-11b)}$$

The NAPL volume can then be expressed as the product of the right hand side of equations (A-9f, for the non-reactive tracer) and (A-11b):

$$V_N = \frac{\left[\mu_1^{R,t'} - \mu_1^{NR,t'} + \left(\frac{m_1^{R,t}}{m_0^{R,t}} - \frac{m_1^{NR,t}}{m_0^{NR,t}}\right)(\alpha - 1)\right]\left[\mu_1^{NR,t'} + \frac{m_1^{NR,t}}{m_0^{NR,t}}(\alpha - 1)\right]}{\mu_1^{R,t'} - \mu_1^{NR,t'} + \left(\frac{m_1^{R,t}}{m_0^{R,t}} - \frac{m_1^{NR,t}}{m_0^{NR,t}}\right)(\alpha - 1) + K_{NW}\left[\mu_1^{NR,t'} + \frac{m_1^{NR,t}}{m_0^{NR,t}}(\alpha - 1)\right]} \qquad \text{(A-12)}$$

Constant Systematic Errors in Concentration Measurements

The i^{th} measured concentration, c_i^d, in terms of a constant systematic error, b [ML^{-3}], and the true concentration, $c_i^{d,t}$, is expressed as

$$c_i^d = c_i^{d,t} + b \qquad \text{(A-13a)}$$

Likewise, the injection concentration, c_0, becomes

$$c_0 = c_0^t + b \qquad \text{(A-13b)}$$

Note that the value of b is constrained such that $b \geq -c_{min}$, where c_{min} is the smallest concentration measurement. Therefore, the nondimensional concentration, c_i, is

$$c_i = \frac{c_i^{d,t} + b}{c_0^t + b} \tag{A-13c}$$

By using $c_i^{d,t} = c_i^t c_0^{d,t}$, equation (A-13c) can also be expressed as

$$c_i = c_i^t \left[\frac{c_0^t}{c_0^t + b}\right] + \left[\frac{b}{c_0^t + b}\right] \tag{A-13d}$$

For simplicity, let

$$\phi_1 = \left[\frac{c_0^t}{c_0^t + b}\right], \tag{A-13e}$$

and

$$\phi_2 = \left[\frac{b}{c_0^t + b}\right]. \tag{A-13f}$$

Therefore, equation (A-13d) becomes

$$c_i = c_i^t \phi_1 + \phi_2. \tag{A-13g}$$

Note that ϕ_1 and ϕ_2 are constant for each tracer. Applying equation (A-13g), the average of the i^{th} and $(i+1)^{th}$ concentration is

$$\bar{c}_i = \phi_1 \bar{c}_i^t + \phi_2 \tag{A-14}$$

The absolute, zeroth moment equation then becomes

$$m_0 = \sum_{i=1}^{n-1} \Delta V_i \left(\phi_1 \bar{c}_i^t + \phi_2\right). \tag{A-15a}$$

Assuming no errors in volume measurements, equation (A-15a) becomes

$$m_0 = \phi_1 m_0^t + V_T \phi_2 , \tag{A-15b}$$

where V_T is the total cumulative volume. Similarly, the absolute first moment is

$$m_1 = \phi_1 m_1^t + \phi_2 \sum_{i=1}^{n-1} \Delta V_i \overline{V}_i \ , \qquad \text{(A-16a)}$$

The first normalized moment, defined in terms of the true values, is

$$\mu_1^{t'} = \frac{m_1^t}{m_0^t} - \frac{V_p}{2} \qquad \text{(A-16b)}$$

The first normalized moment in terms of the constant systematic error and the true values is

$$\mu_1' = \frac{\phi_1 m_1^t + \phi_2 \sum_{i=1}^{n-1} \Delta V_i \overline{V}_i}{\phi_1 m_0^t + V_T \phi_2} - \frac{V_p}{2} \ . \qquad \text{(A-16c)}$$

The retardation factor is

$$R = \frac{\mu_1^{R'}}{\mu_1^{NR'}} = \frac{\dfrac{\phi_1^R m_1^{t,R} + \phi_2^R \sum_{i=1}^{n-1} \Delta V_i \overline{V}_i}{\phi_1^R m_0^{t,R} + V_T \phi_2^R} - \dfrac{V_p}{2}}{\dfrac{\phi_1^{NR} m_1^{t,NR} + \phi_2^{NR} \sum_{i=1}^{n-1} \Delta V_i \overline{V}_i}{\phi_1^{NR} m_0^{t,NR} + V_T \phi_2^{NR}} - \dfrac{V_p}{2}} \qquad \text{(A-17)}$$

The saturation, S, is

$$S = \frac{\left[\dfrac{\phi_1^R m_1^{t,R} + \phi_2^R \sum_{i=1}^{n-1} \Delta V_i \overline{V}_i}{\phi_1^R m_0^{t,R} + V_T \phi_2^R} - \dfrac{V_p}{2} \right] - 1}{\left[\dfrac{\phi_1^R m_1^{t,R} + \phi_2^R \sum_{i=1}^{n-1} \Delta V_i \overline{V}_i}{\phi_1^R m_0^{t,R} + V_T \phi_2^R} - \dfrac{V_p}{2} \right] - 1 + K_{NW}} \ . \qquad \text{(A-18a)}$$

which can also be expressed as

$$S = \frac{\dfrac{\phi_1^R m_1^{t,R} + \phi_2^R \sum_{i=1}^{n-1} \Delta V_i \overline{V}_i}{\phi_1^R m_0^{t,R} + V_T \phi_2^R} - \dfrac{\phi_1^{NR} m_1^{t,NR} + \phi_2^{NR} \sum_{i=1}^{n-1} \Delta V_i \overline{V}_i}{\phi_1^{NR} m_0^{t,NR} + V_T \phi_2^{NR}}}{\dfrac{\phi_1^R m_1^{t,R} + \phi_2^R \sum_{i=1}^{n-1} \Delta V_i \overline{V}_i}{\phi_1^R m_0^{t,R} + V_T \phi_2^R} - \dfrac{\phi_1^{NR} m_1^{t,NR} + \phi_2^{NR} \sum_{i=1}^{n-1} \Delta V_i \overline{V}_i}{\phi_1^{NR} m_0^{t,NR} + V_T \phi_2^{NR}} + K_{NW} \left[\dfrac{\phi_1^{NR} m_1^{t,NR} + \phi_2^{NR} \sum_{i=1}^{n-1} \Delta V_i \overline{V}_i}{\phi_1^{NR} m_0^{t,NR} + V_T \phi_2^{NR}} - \dfrac{V_p}{2} \right]}$$

(A-18b)

The NAPL volume is obtained by the product of the right hand side of equation (A-16c, (for the non-reactive tracer) and equation (A-18b):

$$V_N = \frac{\left[\dfrac{\phi_1^R m_1^{t,R} + \phi_2^R \sum_{i=1}^{n-1} \Delta V_i \overline{V}_i}{\phi_1^R m_0^{t,R} + V_T \phi_2^R} - \dfrac{\phi_1^{NR} m_1^{t,NR} + \phi_2^{NR} \sum_{i=1}^{n-1} \Delta V_i \overline{V}_i}{\phi_1^{NR} m_0^{t,NR} + V_T \phi_2^{NR}} \right] \left[\dfrac{\phi_1^{NR} m_1^{t,NR} + \phi_2^{NR} \sum_{i=1}^{n-1} \Delta V_i \overline{V}_i}{\phi_1^{NR} m_0^{t,NR} + V_T \phi_2^{NR}} - \dfrac{V_p}{2} \right]}{\dfrac{\phi_1^R m_1^{t,R} + \phi_2^R \sum_{i=1}^{n-1} \Delta V_i \overline{V}_i}{\phi_1^R m_0^{t,R} + V_T \phi_2^R} - \dfrac{\phi_1^{NR} m_1^{t,NR} + \phi_2^{NR} \sum_{i=1}^{n-1} \Delta V_i \overline{V}_i}{\phi_1^{NR} m_0^{t,NR} + V_T \phi_2^{NR}} + K_{NW} \left[\dfrac{\phi_1^{NR} m_1^{t,NR} + \phi_2^{NR} \sum_{i=1}^{n-1} \Delta V_i \overline{V}_i}{\phi_1^{NR} m_0^{t,NR} + V_T \phi_2^{NR}} - \dfrac{V_p}{2} \right]}$$

(A-19)

Proportional Systematic Errors in Concentration Measurements

Let β represent a proportional systematic concentration error, such that

$$c_i^d = c_i^{d,t} + \beta c_i^{d,t} \ . \qquad \text{(A-20a)}$$

The nondimensional concentration with the proportional systematic error then becomes

$$c_i = \frac{c_i^d + \beta c_i^d}{c_0^d + \beta c_0^d} \ , \qquad \text{(A-20b)}$$

which can also be expressed as

$$c_i = \frac{c_i^{d,t}(1+\beta)}{c_0^{d,t}(1+\beta)} = \frac{c_i^{d,t}}{c_0^{d,t}} = c_i^t \ . \qquad \text{(A-20c)}$$

Therefore, assuming nondimensional concentrations are used in the moment calculations, proportional systematic errors in concentrations have no effect on the moment calculations, nor consequently any effect on NAPL volume estimates.

APPENDIX B
RANDOM ERRORS IN MOMENT CALCULATIONS

The general method for estimating the uncertainty in breakthrough curve moments was presented in Chapter 2, and that method is applied here to the specific case of the zeroth and first absolute moments. The method is based on the premise that the moments are estimated from the experimentally measured data using the Trapezoidal rule. Uncertainty is assumed to result from random errors in the measured data, and is propagated using conventional statistical methods.

Absolute Zeroth Moment

The absolute zeroth moment of the breakthrough curve, m_0 [L^3], can be approximated using the trapezoidal rule:

$$m_0 = \int_0^\infty c dV \cong \sum_{i=1}^{n-1} \bar{c}_i \Delta V_i \qquad \text{(B-1)}$$

where, $\bar{c}_i = (c_i + c_{i+1})/2$ = average dimensionless concentration over the i^{th} interval, and $\Delta V_i = (V_{i+1} - V_i)$ = change in cumulative volume over the i^{th} interval [L^3]. Note that the numerical approximation methods used herein employ a forward difference scheme starting with i = 1. The variance of ΔV_i can be expressed in terms of the variance in the i^{th} and $(i+1)^{th}$ volume measurements by

$$\sigma^2_{\Delta V[i]} = \sigma^2_{V[i]} + \sigma^2_{V[i+1]}. \qquad \text{(B-2)}$$

Note that equation (B-2) reflects that the volume measurements are independent of one another. Likewise, the variance in the average concentration over the i^{th} interval in terms of the variance in the i^{th} and $(i+1)^{th}$ dimensionless concentration is given by

$$\sigma^2_{\bar{c}[i]} = \frac{1}{4}\sigma^2_{c[i]} + \frac{1}{4}\sigma^2_{c[i+1]} \ . \qquad \text{(B-3)}$$

Note that equation (B-3) reflects that concentration measurements (for a given tracer) are independent from one another. Assuming volume and concentration measurements are independent, the variance equation for the i^{th} product $\Delta V\bar{c}$ is

$$\sigma^2_{\Delta V\bar{c}[i]} = \Delta V_i^2\sigma^2_{\bar{c}[i]} + \sigma^2_{\Delta V[i]}\bar{c}_i^2 + \sigma^2_{\Delta V[i]}\sigma^2_{\bar{c}[i]} \ . \qquad \text{(B-4)}$$

The variance of the sum of the i^{th} and $(i+1)^{th}$ products of differential volumes and average concentrations is given by

$$\begin{aligned} &\mathrm{var}\left[\Delta V_i\bar{c}_i + \Delta V_{i+1}\bar{c}_{i+1}\right] = \\ &\mathrm{var}\left[\Delta V_i\bar{c}_i\right] + \mathrm{var}\left[\Delta V_{i+1}\bar{c}_{i+1}\right] + 2\,\mathrm{cov}\left[\Delta V_i\bar{c}_i, \Delta V_{i+1}\bar{c}_{i+1}\right] \end{aligned} \ . \qquad \text{(B-5)}$$

The sum of the i^{th} and $(i+1)^{th}$ products of differential volumes and average concentrations are not independent since they both use the $(i+1)^{th}$ measure of cumulative volume and concentration. The general definition of covariance is

$$\sigma_{xy} = \mathrm{cov}[x,y] = E\left[(x-\mu_x)(y-\mu_y)\right] = E[xy] - \mu_x\mu_y \ . \qquad \text{(B-6)}$$

Applying equation (B-6) to the i^{th} and $(i+1)^{th}$ products of differential volumes and average concentrations yields

$$\mathrm{cov}\left[\Delta V_i\bar{c}_i, \Delta V_{i+1}\bar{c}_{i+1}\right] = E\left[\Delta V_i\bar{c}_i\Delta V_{i+1}\bar{c}_{i+1}\right] - \Delta V_i'\bar{c}_i'\Delta V_{i+1}'\bar{c}_{i+1}' \ , \qquad \text{(B-7)}$$

Volume differentials and average concentrations can be expressed in terms of their mean value and zero-meaned error term as

$$\Delta V = \Delta V' + e_{\Delta V} \ , \qquad \text{(B-8)}$$

and

$$\bar{c} = \bar{c}^{t} + e_{\bar{c}}. \tag{B-9}$$

Applying equations (B-8) and (B-9) to equation (B-7) yields

$$\begin{aligned}&\mathrm{cov}\left[\Delta V_i \bar{c}_i, \Delta V_{i+1} \bar{c}_{i+1}\right] = \\ &E\left[(\Delta V_i^t + e_{\Delta V[i]})(\bar{c}_i^t + e_{\bar{c}[i]})(\Delta V_{i+1}^t + e_{\Delta V[i+1]})(\bar{c}_{i+1}^t + e_{\bar{c}[i+1]})\right] . \\ &- \Delta V_i^t \bar{c}_i^t \Delta V_{i+1}^t \bar{c}_{i+1}^t\end{aligned} \tag{B-10}$$

Expanding the first term on the right hand side of equation (B-10) results in an equation with 16 terms. Noting that the expected values of zero-meaned terms are zero, and assuming errors in concentrations and volumes are independent, the expanded form of equation (B-10) can be reduced to

$$\begin{aligned}&\mathrm{cov}\left[\Delta V_i \bar{c}_i, \Delta V_{i+1} \bar{c}_{i+1}\right] = \\ &E\begin{bmatrix}\Delta V_i^t \bar{c}_i^t \Delta V_{i+1}^t \bar{c}_{i+1}^t + \Delta V_i^t e_{\bar{c}[i]} \Delta V_{i+1}^t e_{\bar{c}[i+1]} + \\ e_{\Delta V[i]} \bar{c}_i^t e_{\Delta V[i+1]} \bar{c}_{i+1}^t + e_{\Delta V[i]} e_{\bar{c}[i]} e_{\Delta V[i+1]} e_{\bar{c}[i+1]}\end{bmatrix} . \\ &- \Delta V_i^t \bar{c}_i^t \Delta V_{i+1}^t \bar{c}_{i+1}^t\end{aligned} \tag{B-11a}$$

Equation (B-11a) can be simplified to

$$\begin{aligned}&\mathrm{cov}\left[\Delta V_i \bar{c}_i, \Delta V_{i+1} \bar{c}_{i+1}\right] = \\ &\Delta V_i^t \Delta V_{i+1}^t E\left[e_{\bar{c}[i]} e_{\bar{c}[i+1]}\right] + \bar{c}_i^t \bar{c}_{i+1}^t E\left[e_{\Delta V[i]} e_{\Delta V[i+1]}\right] + E\left[e_{\Delta V[i]} e_{\Delta V[i+1]}\right] E\left[e_{\bar{c}[i]} e_{\bar{c}[i+1]}\right] .\end{aligned} \tag{B-11b}$$

To further simplify equation (B-11b), it is necessary to express the errors in average concentrations and differential volumes in terms of the errors in concentration and cumulative volume measurements. Starting with the first expectation term on the right-hand side of equation (B-11b):

$$\begin{aligned}&E\left[e_{\bar{c}[i]} e_{\bar{c}[i+1]}\right] = E\left[(\bar{c}_i - \bar{c}_i^t)(\bar{c}_{i+1} - \bar{c}_{i+1}^t)\right] = \\ &E\left[\left\{\left[\frac{1}{2}(c_i + c_{i+1})\right] - \bar{c}_i^t\right\}\left\{\left[\frac{1}{2}(c_{i+1} + c_{i+2})\right] - \bar{c}_{i+1}^t\right\}\right] .\end{aligned} \tag{B-12a}$$

Expressing each dimensionless concentration in terms of zero-meaned error yields

$$E\left[e_{\bar{c}[i]}e_{\bar{c}[i+1]}\right]=$$
$$E\left[\begin{array}{l}\{[\frac{1}{2}((c_i^t+e_{c[i]})+(c_{i+1}^t+e_{c[i+1]})]-\bar{c}_i^t\}\times \\ \{[\frac{1}{2}((c_{i+1}^t+e_{c[i+1]})+(c_{i+2}^t+e_{c[i+2]}))]-\bar{c}_{i+1}^t\}\end{array}\right], \qquad \text{(B-12b)}$$

which reduces to

$$\mathrm{E}\left[\mathrm{e}_{\bar{c}[i]}\mathrm{e}_{\bar{c}[i+1]}\right]=\frac{1}{4}\mathrm{E}\left[\mathrm{e}_{c[i]}\mathrm{e}_{c[i+1]}+\mathrm{e}_{c[i]}\mathrm{e}_{c[i+2]}+\mathrm{e}_{c[i+1]}\mathrm{e}_{c[i+2]}+\mathrm{e}_{c[i+1]}^2\right]. \qquad \text{(B-12c)}$$

Assuming errors associated with each measurement of concentration are independent, the first three terms on the right-hand side of equation (B-12c) are zero, and the equation is reduced to

$$\mathrm{E}\left[\mathrm{e}_{\bar{c}[i]}\mathrm{e}_{\bar{c}[i+1]}\right]=\frac{1}{4}\mathrm{E}\left[\mathrm{e}_{c[i+1]}^2\right]. \qquad \text{(B-12d)}$$

Likewise, the second expectation term on the right-hand side of equation (B-11b) expands to

$$\begin{array}{l}\mathrm{E}\left[\mathrm{e}_{\Delta V[i]}\mathrm{e}_{\Delta V[i+1]}\right]=\mathrm{E}\left[(\Delta V_i-\Delta V_i^t)(\Delta V_{i+1}-\Delta V_{i+1}^t)\right]= \\ \mathrm{E}\left[\{(V_{i+1}-V_i)-\Delta V_i^t\}\{(V_{i+2}-V_{i+1})-\Delta V_{i+1}^t\}\right]\end{array} \qquad \text{(B-13a)}$$

Expressing each cumulative volume measurement in terms of zero-meaned error yields

$$E\left[e_{\Delta V[i]}e_{\Delta V[i+1]}\right]=$$
$$E\left[\begin{array}{l}\{[(V_{i+1}^t+e_{V[i+1]})-(V_i^t+e_{V[i]})]-\Delta V_i^t\}\times \\ \{[(V_{i+2}^t+e_{V[i+2]})-(V_{i+1}+e_{V[i+1]})]-\Delta V_{i+1}^t\}\end{array}\right], \qquad \text{(B-13b)}$$

which reduces to

$$\mathrm{E}\left[\mathrm{e}_{\Delta V[i]}\mathrm{e}_{\Delta V[i+1]}\right]=\mathrm{E}\left[\mathrm{e}_{V[i+1]}\mathrm{e}_{V[i+2]}-\mathrm{e}_{V[i+1]}^2-\mathrm{e}_{V[i]}\mathrm{e}_{V[i+2]}-\mathrm{e}_{V[i]}\mathrm{e}_{V[i+1]}\right]. \qquad \text{(B-13c)}$$

Assuming errors associated with each measurement of volume are independent, equation (B-13c) is reduced to

$$\mathrm{E}\left[\mathrm{e}_{\Delta V[i]}\mathrm{e}_{\Delta V[i+1]}\right]=-\mathrm{E}\left[\mathrm{e}_{V[i+1]}^2\right]. \qquad \text{(B-13d)}$$

Therefore, the covariance of the i^{th} and $(i + 1)^{th}$ products of differential volumes and average concentrations is

$$\begin{aligned}&\mathrm{cov}\left[\Delta V_i \bar{c}_i, \Delta V_{i+1} \bar{c}_{i+1}\right] = \\ &\frac{1}{4}\Delta V_i^t \Delta V_{i+1}^t E\left[e_{c[i+1]}^2\right] - \bar{c}_i^t \bar{c}_{i+1}^t E\left[e_{V[i+1]}^2\right] - E\left[e_{c[i+1]}^2\right] E\left[e_{V[i+1]}^2\right],\end{aligned} \tag{B-14a}$$

or applying equation (2-9b),

$$\mathrm{cov}\left[\Delta V_i \bar{c}_i, \Delta V_{i+1} \bar{c}_{i+1}\right] = \frac{1}{4}\Delta V_i^t \Delta V_{i+1}^t \sigma_{c[i+1]}^2 - \bar{c}_i^t \bar{c}_{i+1}^t \sigma_{V[i+1]}^2 - \frac{1}{4}\sigma_{c[i+1]}^2 \sigma_{V[i+1]}^2 \tag{B-14b}$$

The variance of the absolute zeroth moment estimated using the trapezoidal rule is therefore

$$\mathrm{var}\left[m_0\right] = \sum_{i=1}^{n-1} \mathrm{var}\left[\Delta V_i \bar{c}_i\right] + 2\sum_{i=1}^{n-2} \mathrm{cov}\left[\Delta V_i \bar{c}_i, \Delta V_{i+1} \bar{c}_{i+1}\right] . \tag{B-15}$$

Absolute First Moment

The absolute first moment of the breakthrough curve, m_1 $[L^6]$, can be approximated using the trapezoidal rule:

$$m_1 = \int_0^\infty cV dV \cong \sum_{i=1}^{n-1} \Delta V_i \bar{V}_i \bar{c}_i \quad , \tag{B-16}$$

where, $\bar{V}_i = (V_i + V_{i+1})/2$ = average cumulative volume over the i^{th} interval $[L^3]$. The variance of $\bar{V}_i$ in terms of the variance in the i^{th} and $(i+1)^{th}$ volume measurements is given by

$$\sigma_{\bar{V}[i]}^2 = \frac{1}{4}\sigma_{V[i]}^2 + \frac{1}{4}\sigma_{V[i+1]}^2 . \tag{B-17}$$

Formally, equations (2-12a) and (2-13) from Chapter 2 would be used to determine the expected value and variance of the product $\Delta V_i \overline{V}_i \overline{c}_i$. An alternative approach is to first calculate the variance of the product $\Delta V_i \overline{V}_i$:

$$\begin{aligned}&\sigma^2(\overline{V}_i \Delta V_i) = \\ &(\overline{V}_i)^2 \sigma^2(\Delta V_i) + (\Delta V_i)^2 \sigma^2(\overline{V}_i) + [\sigma(\overline{V}_i, \Delta V_i)]^2 \\ &+ 2\overline{V}_i \Delta V_i \sigma(\overline{V}_i, \Delta V_i) + \sigma^2(\overline{V}_i)\sigma^2(\Delta V_i)\end{aligned}, \qquad \text{(B-18)}$$

The covariance between ΔV_i and $\overline{V}_i$ is given by:

$$\text{cov}[\Delta V_i, \overline{V}_i] = E[\Delta V_i \overline{V}_i] - \Delta V_i^t \overline{V}_i^t \; . \qquad \text{(B-19a)}$$

Expressing the differential volume and average volume in terms of their means and errors yields

$$\text{cov}[\Delta V_i, \overline{V}_i] = E[(\Delta V_i^t + e_{\Delta V[i]})(\overline{V}_i^t + e_{\overline{V}[i]})] - \Delta V_i^t \overline{V}_i^t , \qquad \text{(B-19b)}$$

which simplifies to

$$\text{cov}[\Delta V_i, \overline{V}_i] = E[e_{\Delta V[i]} e_{\overline{V}[i]}]. \qquad \text{(B-19c)}$$

Equation (B-19c) can also be expressed as

$$\text{cov}[\Delta V_i, \overline{V}_i] = E[(\Delta V_i - \Delta V_i^t)(\overline{V}_i - \overline{V}_i^t)] , \qquad \text{(B-19d)}$$

or, expanding ΔV_i and $\overline{V}_i$ in terms of cumulative volume measurements,

$$\text{cov}[\Delta V_i, \overline{V}_i] = E\left[\left\{(V_{i+1} - V_i) - \Delta V_i^t\right\}\left\{\frac{1}{2}(V_{i+1} + V_i) - \overline{V}_i^t)\right\}\right], \qquad \text{(B-19e)}$$

and cumulative volume measurements in terms of true values and errors:

$$\begin{aligned}&\text{cov}[\Delta V_i, \overline{V}_i] = \\ &E\left[\begin{array}{l}\left\{((V_{i+1}^t + e_{V[i+1]}) - (V_i^t + e_{V[i]})) - \Delta V_i^t\right\} \times \\ \left\{\frac{1}{2}((V_{i+1}^t + e_{V[i+1]}) + (V_i^t + e_{V[i]})) - \overline{V}_i^t)\right\}\end{array}\right],\end{aligned} \qquad \text{(B-19f)}$$

which simplifies to

$$\mathrm{cov}\left[\Delta V_i, \overline{V}_i\right] = E\left[\left\{e_{V[i+1]} - e_{V[i]}\right\}\left\{\frac{1}{2}\left(e_{V[i+1]} + e_{V[i]}\right)\right\}\right]. \quad \text{(B-19g)}$$

Therefore,

$$\mathrm{cov}\left[\Delta V_i, \overline{V}_i\right] = \frac{1}{2}E\left[e^2_{V[i+1]} - e^2_{V[i]}\right], \quad \text{(B-19h)}$$

which can also be expressed as

$$\mathrm{cov}\left[\Delta V_i, \overline{V}_i\right] = \frac{1}{2}\left(E\left[e^2_{V[i+1]}\right] - E\left[e^2_{V[i]}\right]\right). \quad \text{(B-19i)}$$

Applying equation (2-9b) to equation (B-19i) yields

$$\mathrm{cov}\left[\Delta V_i, \overline{V}_i\right] = \frac{1}{2}\left(\sigma^2_{V[i+1]} - \sigma^2_{V[i]}\right). \quad \text{(B-19j)}$$

Since volume measurements and concentration measurements are independent, the variance of the product of $\Delta V_i \overline{V}_i$ and $\overline{c}_i$ can then be calculated using

$$\sigma^2_{\Delta V \overline{V}[i]\overline{c}[i]} = \left(\Delta V_i\ \overline{V}_i\right)^2 \sigma^2_{\overline{c}[i]} + \sigma^2_{\Delta V \overline{V}[i]} \overline{c}_i^2 + \sigma^2_{\Delta V \overline{V}[i]} \sigma^2_{\overline{c}[i]} \quad . \quad \text{(B-20)}$$

The terms $\Delta V_i \overline{V}_i \overline{c}_i$ and $\Delta V_{i+1} \overline{V}_{i+1} \overline{c}_{i+1}$ are not independent, since they are both based on the $(i+1)^{th}$ measure of cumulative volume and concentration. The covariance between $\Delta V_i \overline{V}_i \overline{c}_i$ and $\Delta V_{i+1} \overline{V}_{i+1} \overline{c}_{i+1}$ is defined as

$$\begin{aligned} &\mathrm{cov}\left[\Delta V_i \overline{V}_i \overline{c}_i, \Delta V_{i+1} \overline{V}_{i+1} \overline{c}_{i+1}\right] = \\ &E\left[\Delta V_i \overline{V}_i \overline{c}_i, \Delta V_{i+1} \overline{V}_{i+1} \overline{c}_{i+1}\right] - \Delta V_i^t \overline{V}_i^t \overline{c}_i^t \Delta V_{i+1}^t \overline{V}_{i+1}^t \overline{c}_{i+1}^t \end{aligned} \quad , \quad \text{(B-21)}$$

The average volume can be expressed in terms of it's mean by

$$\overline{V} = \overline{V}^t + e_{\overline{V}}. \quad \text{(B-22)}$$

Applying equations (B-8), (B-9), and (B-22) to (B-21), and then expanding the expression results in an equation with 64 terms. Noting that the expected values of zero-

mean terms are zero, and assuming each measurement of volume and concentration are independent, the expanded equation reduces to

$$\begin{aligned}
&\mathrm{cov}\left[\Delta V_i \overline{V}_i \overline{c}_i, \Delta V_{i+1} \overline{V}_{i+1} \overline{c}_{i+1}\right] = \Delta V_i^t \overline{V}_i^t \overline{c}_i^t \overline{c}_{i+1}^t E\left[e_{\Delta V[i+1]} e_{\overline{V}[i+1]}\right] + \\
&\Delta V_i^t \overline{V}_i^t \Delta V_{i+1}^t \overline{V}_{i+1}^t E\left[e_{\overline{c}[i]} e_{\overline{c}[i+1]}\right] + \Delta V_i^t \overline{V}_i^t E\left[e_{\Delta V[i+1]} e_{\overline{V}[i+1]}\right] E\left[e_{\overline{c}[i]} e_{\overline{c}[i+1]}\right] + \\
&\Delta V_i^t \Delta V_{i+1}^t \overline{c}_i^t \overline{c}_{i+1}^t E\left[e_{\overline{V}[i]} e_{\overline{V}[i+1]}\right] + \Delta V_i^t \overline{V}_{i+1}^t \overline{c}_i^t \overline{c}_{i+1}^t E\left[e_{\overline{V}[i]} e_{\Delta V[i+1]}\right] + \\
&\Delta V_i^t \Delta V_{i+1}^t E\left[e_{\overline{V}[i+1]} e_{\overline{V}[i+1]}\right] E\left[e_{\overline{c}[i]} e_{\overline{c}[i+1]}\right] + \Delta V_i^t \overline{V}_{i+1}^t E\left[e_{\overline{V}[i]} e_{\Delta V[i+1]}\right] E\left[e_{\overline{c}[i]} e_{\overline{c}[i+1]}\right] + \\
&\overline{V}_i^t \Delta V_{i+1}^t \overline{c}_i^t \overline{c}_{i+1}^t E\left[e_{\Delta V[i]} e_{\overline{V}[i+1]}\right] + \overline{V}_i^t \overline{V}_{i+1}^t \overline{c}_i^t \overline{c}_{i+1}^t E\left[e_{\Delta V[i]} e_{\Delta V[i+1]}\right] + \\
&\overline{V}_i^t \Delta V_{i+1}^t E\left[e_{\Delta V[i]} e_{\overline{V}[i+1]}\right] E\left[e_{\overline{c}[i]} e_{\overline{c}[i+1]}\right] + \Delta V_{i+1}^t \overline{V}_{i+1}^t \overline{c}_i^t \overline{c}_{i+1}^t E\left[e_{\Delta V[i+1]} e_{\overline{V}[i]}\right] + \\
&\overline{c}_i^t \overline{c}_{i+1}^t E\left[e_{\Delta V[i]} e_{\overline{V}[i]}\right] E\left[e_{\Delta V[i+1]} e_{\overline{V}[i+1]}\right] + \Delta V_{i+1}^t \overline{V}_{i+1}^t E\left[e_{\Delta V[i]} e_{\overline{V}[i]}\right] E\left[e_{\overline{c}[i]} e_{\overline{c}[i+1]}\right] + \\
&E\left[e_{\Delta V[i]} e_{\overline{V}[i]}\right] E\left[e_{\Delta V[i+1]} e_{\overline{V}[i+1]}\right] E\left[e_{\overline{c}[i]} e_{\overline{c}[i+1]}\right]
\end{aligned} \quad \text{(B-23a)}$$

There are four expectation terms involving average volume errors, which need to be expressed in terms of volume measurement errors. This process is analogous to the expansion and simplification shown above in equations (B-12) and (B-13). The resulting equations are

$$E\left[e_{\Delta V[i+1]} e_{\overline{V}[i+1]}\right] = \frac{1}{2} E\left[e^2_{V[i+2]} - e^2_{V[i+1]}\right] = \frac{1}{2} E\left[e^2_{V[i+2]}\right] - \frac{1}{2} E\left[e^2_{V[i+1]}\right], \quad \text{(B-23b)}$$

$$E\left[e_{\overline{V}[i]} e_{\overline{V}[i+1]}\right] = \frac{1}{4} E\left[e^2_{V[i+1]}\right], \quad \text{(B-23c)}$$

$$E\left[e_{\overline{V}[i]} e_{\Delta V[i+1]}\right] = -\frac{1}{2} E\left[e^2_{V[i+1]}\right], \quad \text{(B-23d)}$$

and,

$$E\left[e_{\Delta V[i]} e_{\overline{V}[i+1]}\right] = \frac{1}{2} E\left[e^2_{V[i+1]}\right]. \quad \text{(B-23e)}$$

Therefore, the covariance of the i^{th} and $(i+1)^{th}$ products of differential volumes, average volumes, and average concentrations is

$$\begin{aligned}
&\operatorname{cov}\left[\Delta V_i \bar{V}_i \bar{c}_i, \Delta V_{i+1} \bar{V}_{i+1} \bar{c}_{i+1}\right] = \frac{1}{2}\Delta V_i' \bar{V}_i' \bar{c}_i' \bar{c}_{i+1}' \left(E\left[e_{V[i+2]}^2\right] - E\left[e_{V[i+1]}^2\right]\right) + \\
&\frac{1}{4}\Delta V_i' \bar{V}_i' \Delta V_{i+1}' \bar{V}_{i+1}' E\left[e_{c[i+1]}^2\right] + \frac{1}{8}\Delta V_i' \bar{V}_i' E\left[e_{c[i+1]}^2\right]\left(E\left[e_{V[i+2]}^2\right] - E\left[e_{V[i+1]}^2\right]\right) + \\
&\frac{1}{4}\Delta V_i' \bar{c}_i' \Delta V_{i+1}' \bar{c}_{i+1}' E\left[e_{V[i+1]}^2\right] - \frac{1}{2}\Delta V_i' \bar{c}_i' \bar{V}_{i+1}' \bar{c}_{i+1}' E\left[e_{V[i+1]}^2\right] + \\
&+ \frac{1}{16}\Delta V_i' \Delta V_{i+1}' E\left[e_{V[i+1]}^2\right] E\left[e_{c[i+1]}^2\right] - \frac{1}{8}\Delta V_i' V_{i+1}' E\left[e_{c[i+1]}^2\right] E\left[e_{V[i+1]}^2\right] + \\
&\frac{1}{2}\bar{V}_i' \bar{c}_i' \Delta V_{i+1}' \bar{c}_{i+1}' E\left[e_{V[i+1]}^2\right] - \bar{V}_i' \bar{c}_i' \bar{V}_{i+1}' \bar{c}_{i+1}' E\left[e_{V[i+1]}^2\right] + \\
&\frac{1}{8}\bar{V}_i' \Delta V_{i+1}' E\left[e_{c[i+1]}^2\right] E\left[e_{V[i+1]}^2\right] - \frac{1}{4}\bar{V}_i' \bar{V}_{i+1}' E\left[e_{V[i+1]}^2\right] E\left[e_{c[i+1]}^2\right] + \\
&\frac{1}{2}\bar{c}_i' \Delta V_{i+1}' \bar{V}_{i+1}' \bar{c}_{i+1}' \left(E\left[e_{V[i+1]}^2\right] - E\left[e_{V[i]}^2\right]\right) + \\
&\frac{1}{4}\bar{c}_i' \bar{c}_{i+1}' \begin{pmatrix} E\left[e_{V[i+1]}^2\right] E\left[e_{V[i+2]}^2\right] - E\left[e_{V[i+1]}^4\right] - \\ E\left[e_{V[i]}^2\right] E\left[e_{V[i+2]}^2\right] + E\left[e_{V[i]}^2\right] E\left[e_{V[i+1]}^2\right] \end{pmatrix} + \\
&\frac{1}{8}\Delta V_{i+1}' \bar{V}_{i+1}' \left(E\left[e_{V[i+1]}^2\right] - E\left[e_{V[i]}^2\right]\right) E\left[e_{c[i+1]}^2\right] + \\
&\frac{1}{16} E\left[e_{c[i+1]}^2\right] \begin{pmatrix} E\left[e_{V[i+1]}^2\right] E\left[e_{V[i+2]}^2\right] - E\left[e_{V[i+1]}^4\right] - \\ E\left[e_{V[i]}^2\right] E\left[e_{V[i+2]}^2\right] + E\left[e_{V[i]}^2\right] E\left[e_{V[i+1]}^2\right] \end{pmatrix}
\end{aligned} \qquad \text{(B-23f)}$$

Assuming a normal distribution for the volume errors, it can be shown that

$$E\left[e_V^4\right] = 3\sigma_V^4 \qquad \text{(B-24)}$$

Using equations (2-9b) and (B-24) equation (B-23f) becomes

$$\begin{aligned}
&\mathrm{cov}\left[\Delta V_i \overline{V}_i \overline{c}_i, \Delta V_{i+1} \overline{V}_{i+1} \overline{c}_{i+1}\right] = \\
&\frac{1}{2}\Delta V_i^t \overline{V}_i^t \overline{c}_i^t \overline{c}_{i+1}^t \left(\sigma^2_{V[i+2]} - \sigma^2_{V[i+1]}\right) + \frac{1}{4}\Delta V_i^t \overline{V}_i^t \Delta V_{i+1}^t \overline{V}_{i+1}^t \sigma^2_{c[i+1]} + \\
&\frac{1}{8}\Delta V_i^t \overline{V}_i^t \sigma^2_{c[i+1]}\left(\sigma^2_{V[i+2]} - \sigma^2_{V[i+1]}\right) + \frac{1}{4}\Delta V_i^t \overline{c}_i^t \Delta V_{i+1}^t \overline{c}_{i+1}^t \sigma^2_{V[i+1]} - \frac{1}{2}\Delta V_i^t \overline{c}_i^t \overline{V}_{i+1}^t \overline{c}_{i+1}^t \sigma^2_{V[i+1]} + \\
&\frac{1}{16}\Delta V_i^t \Delta V_{i+1}^t \sigma^2_{V[i+1]} \sigma^2_{c[i+1]} - \frac{1}{8}\Delta V_i^t V_{i+1}^t \sigma^2_{c[i+1]} \sigma^2_{V[i+1]} + \frac{1}{2}\overline{V}_i^t \overline{c}_i^t \Delta V_{i+1}^t \overline{c}_{i+1}^t \sigma^2_{V[i+1]} + \\
&-\overline{V}_i^t \overline{c}_i^t \overline{V}_{i+1}^t \overline{c}_{i+1}^t \sigma^2_{V[i+1]} + \frac{1}{8}\overline{V}_i^t \Delta V_{i+1}^t \sigma^2_{c[i+1]} \sigma^2_{V[i+1]} - \frac{1}{4}\overline{V}_i^t \overline{V}_{i+1}^t \sigma^2_{V[i+1]} \sigma^2_{c[i+1]} + \\
&\frac{1}{2}\overline{c}_i^t \Delta V_{i+1}^t \overline{V}_{i+1}^t \overline{c}_{i+1}^t \left(\sigma^2_{V[i+1]} - \sigma^2_{V[i]}\right) + \\
&\frac{1}{4}\overline{c}_i^t \overline{c}_{i+1}^t \left(\sigma^2_{V[i+1]} \sigma^2_{V[i+2]} - 3\sigma^4_{V[i+1]} - \sigma^2_{V[i]} \sigma^2_{V[i+2]} + \sigma^2_{V[i]} \sigma^2_{V[i+1]}\right) + \\
&\frac{1}{8}\Delta V_{i+1}^t \overline{V}_{i+1}^t \left(\sigma^2_{V[i+1]} - \sigma^2_{V[i]}\right)\sigma^2_{c[i+1]} + \\
&\frac{1}{16}\sigma^2_{c[i+1]}\left(\sigma^2_{V[i+1]} \sigma^2_{V[i+2]} - 3\sigma^4_{V[i+1]} - \sigma^2_{V[i]} \sigma^2_{V[i+2]} + \sigma^2_{V[i]} \sigma^2_{V[i+1]}\right) \qquad . \qquad \text{(B-25)}
\end{aligned}$$

The variance of the sum of the i^{th} and $(i+1)^{th}$ product of $\Delta V \overline{V} \overline{c}$ is therefore

$$\begin{aligned}
&\mathrm{var}\left[\Delta V_i \overline{V}_i \overline{c}_i + \Delta V_{i+1} \overline{V}_{i+1} \overline{c}_{i+1}\right] = \\
&\mathrm{var}\left[\Delta V_i \overline{V}_i \overline{c}_i\right] + \mathrm{var}\left[\Delta V_{i+1} \overline{V}_{i+1} \overline{c}_{i+1}\right] + 2\,\mathrm{cov}\left[\Delta V_i \overline{V}_i \overline{c}_i, \Delta V_{i+1} \overline{V}_{i+1} \overline{c}_{i+1}\right],
\end{aligned} \qquad \text{(B-26)}$$

and the variance of the absolute first moment estimated by the trapezoidal rule is

$$\mathrm{var}\left[m_1\right] = \sum_{i=1}^{n-1} \mathrm{var}\left[\Delta V_i \overline{V}_i \overline{c}_i\right] + 2\sum_{i=1}^{n-2} \mathrm{cov}\left[\Delta V_i \overline{V}_i \overline{c}_i, \Delta V_{i+1} \overline{V}_{i+1} \overline{c}_{i+1}\right] . \qquad \text{(B-27)}$$

APPENDIX C
DELTA METHOD FORMULAS

Approximations to statistical moments based on Taylor-series expansions are discussed in probability and statistical textbooks such as Kendal and Stuart (1977) and Papoulis (1991). The general method has been referred to as the delta method, and the specific case of the first-order variance approximation has been referred to as the propagation of error formula. Lynch and Walsh (1998) provide a useful summary of delta method formulas in Appendix A of their work. Several articles have also been published on the accuracy of this method (Winzer, 2000; Asbjornsen, 1986, and Park and Himmelblau, 1980). The purpose of this appendix is to present a brief overview of the method, and to apply it to the derivation of formulas used to estimate uncertainty in BTC moments.

General Expressions

A Taylor series expansion for a random variable, x, about its mean, μ_x, is given by

$$f(x) = \sum_{m=0}^{\infty} \frac{f^{(m)}(\mu_x)}{m!}(x - \mu_x)^m \quad , \qquad \text{(C-1)}$$

where $f^{(m)}$ denotes the m^{th} derivative of the function f. Equation (C-1) assumes f has derivatives of all orders at μ_x. For n variables, equation (C-1a) becomes

$$f(x_1,\ldots,x_i,\ldots,x_n) = \sum_{m=0}^{\infty} \frac{f^{(m)}\left(\mu_{x[1]},\ldots,\mu_{x[1]},\ldots,\mu_{x[n]}\right)}{m!}\left(x_1 - \mu_{x[1]}\right)^m \ldots \left(x_i - \mu_{x[i]}\right)^m \ldots \left(x_n - \mu_{x[n]}\right)^m \quad . \qquad \text{(C-2)}$$

Taking the expectation of both sides of equation (C-1) yields

$$E[f(x)] = f(\mu_x) + E[(x-\mu_x)]\frac{\partial f(\mu_x)}{\partial x} + E[(x-\mu_x)^2]\frac{\partial^2 f(\mu_x)}{2\partial x^2} + \ldots \quad . \qquad \text{(C-3)}$$

Ignoring higher order terms, and noting that $E[x-\mu_x]$ is zero and that $E[(x-\mu_x)^2]$ is the variance, σ_x^2, equation (C-3) becomes

$$E[f(x)] \cong f(\mu_x) + \sigma_x^2 \frac{\partial^2 f(\mu_x)}{2\partial x^2} \quad . \qquad \text{(C-4)}$$

Noting that $E[(x-\mu_x)(y-\mu_y)]$ is the covariance, $\sigma(x,y)$, the expectation of both sides of equation (C-2) is

$$E[f(x_1,\ldots,x_i,\ldots,x_n)] \cong \hat{f} + \sum_{i=1}^{n} \sigma_{x[i]}^2 \frac{\partial^2 \hat{f}}{2\partial x_i^2} + \sum_{i=1}^{n}\sum_{j>i}^{n} \sigma(x_i x_j)\frac{\partial^2 \hat{f}}{\partial x_i \partial x_j} \quad , \qquad \text{(C-5)}$$

where the superscript caret over the f indicates the function is evaluated using the mean values of x_i.

The variance of a random variable x is defined as

$$\sigma_x^2 = E[(x-\mu_x)^2] = E[x^2] - \mu_x^2 \quad , \qquad \text{(C-6a)}$$

which, for the function f, can be expressed as

$$\sigma_f^2 = E[(f - E[f])^2] = E[f^2] - \{E[f]\}^2 \quad . \qquad \text{(C-6b)}$$

Substituting a truncated Taylor series for f (first two terms on the right hand side of equation C-1b), and using equation (C-4) for E[f], equation (C-6b) becomes

$$\sigma_f^2 = E\left[\left(\left(f(\mu_x) + (x-\mu_x)\frac{\partial f(\mu_x)}{\partial x}\right) - \left(f(\mu_x) + \sigma_x^2 \frac{\partial^2 f(\mu_x)}{2\partial x^2}\right)\right)^2\right] \quad , \qquad \text{(C-7a)}$$

or

$$\sigma_f^2 = E\left[\begin{array}{l}\left((x-\mu_x)\frac{\partial f(\mu_x)}{\partial x}\right)^2 - \\ \left((x-\mu_x)\sigma_x^2\right)\frac{\partial f(\mu_x)}{\partial x}\frac{\partial^2 f(\mu_x)}{2\partial x^2} + \left(\sigma_x^2\frac{\partial^2 f(\mu_x)}{2\partial x^2}\right)^2\end{array}\right]. \qquad \text{(C-7b)}$$

Ignoring terms with second-order derivatives reduced equation (C-7b) to

$$\sigma_f^2 \cong E\left[(x-\mu_x)^2\left(\frac{\partial f(\mu_x)}{\partial x}\right)^2\right] = \sigma_x^2\left(\frac{\partial f(\mu_x)}{\partial x}\right)^2. \qquad \text{(C-7c)}$$

Equation (C-7c) is often referred to as the propagation of error formula. Likewise, ignoring all terms with second order derivatives and higher, the variance of a function f with n independent variables can also be estimated from equation (C-6b) using equations (C-2b) and (C-5):

$$\sigma_f^2 \cong$$
$$E\left[\left(\sum_{i=1}^{n}(x_i-\mu_{x[i]})\frac{\partial \hat{f}}{\partial x_i}\right)^2\right] = E\left[\sum_{i=1}^{n}\sum_{j=1}^{n}(x_i-\mu_{x[i]})(x_j-\mu_{x[j]})\frac{\partial \hat{f}}{\partial x_i}\frac{\partial \hat{f}}{\partial x_j}\right], \qquad \text{(C-8a)}$$

which becomes

$$\sigma_f^2 \cong \sum_{i=1}^{n}\sum_{j=1}^{n}\sigma(x_i,x_j)\frac{\partial \hat{f}}{\partial x_i}\frac{\partial \hat{f}}{\partial x_j}. \qquad \text{(C-8b)}$$

Equation (C-8b) can be used to derive estimates of the variance of the product and ratio of two random variables. Applying the function f = xy, where x and y are random variables (n = 2) to equation (C-8b) results in

$$\sigma_f^2 \cong \sigma_x^2\left(\frac{\partial \hat{f}}{\partial x}\right)^2 + 2\sigma(x,y)\frac{\partial \hat{f}}{\partial x}\frac{\partial \hat{f}}{\partial y} + \sigma_y^2\left(\frac{\partial \hat{f}}{\partial y}\right)^2 \qquad \text{(C-9a)}$$

$$\sigma_f^2 \cong \sigma_x^2 y^2 + \sigma_y^2 x^2 + 2xy\sigma(x,y) \qquad \text{(C-9b)}$$

Equation (C-9a) can also be used to derive the equation for the variance of the ratio of two random variables (f = x/y):

$$\sigma_f^2 \cong \sigma_x^2\left(\frac{1}{y}\right)^2 - 2\sigma(x,y)\frac{1}{y}\frac{x}{y^2} + \sigma_y^2\left(-\frac{x}{y^2}\right)^2 , \qquad \text{(C-10a)}$$

which can be rearranged to yield

$$\sigma_f^2 \cong \frac{x^2}{y^2}\left[\frac{\sigma_x^2}{x^2} + \frac{\sigma_y^2}{y^2} - \frac{2\sigma(x,y)}{xy}\right] . \qquad \text{(C-10b)}$$

Second-order approximations to the product and ratio of two random variables can be estimated by including the second-order derivatives in equation (C-7c) through (C-8b). Note that a second-order Taylor-series approximation to the product xy variance is equal to the analytical expression of the product xy variance. Winzer (2000) presented the following for the second-order approximation of the variance of the function f = x/y:

$$\sigma_f^2 \cong \frac{x^2}{y^2}\left[\frac{\sigma_x^2}{x^2} + \frac{\sigma_y^2}{y^2} - \frac{2\sigma(x,y)}{xy} - \frac{\sigma_y^4}{y^4}\left(\frac{y\sigma(x,y)}{x\sigma_y^2} - 1\right)^2\right] . \qquad \text{(C-10c)}$$

However, he noted that the accuracy of the first- and second-order approximations to the variance were comparable for $x/\sigma_x = y/\sigma_y$, $y/\sigma_y \leq 12$, and $0 \leq \sigma(x,y)/\sigma_x\sigma_y \leq 0.75$.

The covariance between two random variables x and y is defined as

$$\sigma(x,y) = E\left[(x-\mu_x)(y-\mu_y)\right] = E[xy] - \mu_x\mu_y \qquad \text{(C-11)}$$

The covariance between two functions based on the same set of n independent variables can be estimated using equations (C-2b), (C-5), and (C-11):

$$\sigma(f,g) = E\left[\left\{\hat{f} + \sum_{i=1}^{n}(x_i - \mu_{x[i]})\frac{\partial \hat{f}}{\partial x_i} + \ldots\right\}\left\{\hat{g} + \sum_{i=1}^{n}(x_i - \mu_{x[i]})\frac{\partial \hat{g}}{\partial x_i} + \ldots\right\}\right] - \left\{\hat{f} + \sum_{i=1}^{n}\sigma_{x[i]}^2\frac{\partial^2 \hat{f}}{2\partial x_i^2}\right\}\left\{\hat{g} + \sum_{i=1}^{n}\sigma_{x[i]}^2\frac{\partial^2 \hat{g}}{2\partial x_i^2}\right\} , \qquad \text{(C-12a)}$$

which, ignoring second-order and higher derivative terms, becomes

$$\sigma(f,g) \cong \sum_{i=1}^{n}\sum_{j=1}^{n}\sigma(x_i,x_j)\frac{\partial \hat{f}}{\partial x_i}\frac{\partial \hat{g}}{\partial x_j} \quad . \tag{C-12b}$$

Derivation of Zeroth Moment Variance

The Taylor series expansion for a function f with n variables is given by equations (C-2). If $f = m_0$, where m_0 is approximated using the trapezoidal rule, then

$$m_0^{(k)} = 0 \quad \text{for } k > 2, \text{ and} \tag{C-13a}$$

$$\frac{\partial^2 m_0}{\partial x_i^2} = 0 \quad . \tag{C-13b}$$

However, all second-order mixed derivatives are not zero. Therefore, the Taylor series expansion for m_o is

$$m_0 = \hat{m}_0 + \sum_{i=1}^{n}(x_i - \mu_{x[i]})\frac{\partial \hat{m}_0}{\partial x_i} + \sum_{i=1}^{n}\sum_{j>i}^{n}(x_i - \mu_{x[i]})(x_j - \mu_{x[j]})\frac{\partial^2 \hat{m}_0}{\partial x_i \partial x_j} \quad . \tag{C-14a}$$

The x variables are the measured volume and concentration values

$$\{x_1,\ldots,x_i,\ldots,x_m\} = \{V_1,\ldots,V_i,\ldots,V_m\} \text{ , and} \tag{C-14b}$$

$$\{x_{m+1},\ldots,x_{i+m},\ldots,x_{2m}\} = \{c_1,\ldots,c_i,\ldots,c_m\} \text{ ,} \tag{C-14c}$$

where 2m = n. The first derivatives of the zeroth moment with respect to volume and concentration measurements are (see equations 2-4b)

$$\frac{\partial m_0}{\partial V_1} = -\frac{1}{2}(c_2 + c_1) \text{ ,} \tag{C-14d}$$

$$\frac{\partial m_0}{\partial V_i} = \frac{1}{2}(c_{i-1} - c_{i+1}) \quad \text{for } 2 < i < m\text{-}1, \tag{C-14e}$$

$$\frac{\partial m_0}{\partial V_m} = \frac{1}{2}(c_m + c_{m-1}) \text{ ,} \tag{C-14f}$$

$$\frac{\partial m_0}{\partial c_1} = \frac{1}{2}(V_2 - V_1)\,, \qquad \text{(C-14g)}$$

$$\frac{\partial m_0}{\partial c_i} = \frac{1}{2}(V_{i+1} - V_{i-1}) \quad \text{for } 2 < i < m\text{-}1, \quad \text{and} \qquad \text{(C-14h)}$$

$$\frac{\partial m_0}{\partial c_m} = \frac{1}{2}(V_m - V_{m-1})\,, \qquad \text{(C-14i)}$$

The second derivatives of the zeroth moment are

$$\frac{\partial^2 m_0}{\partial V_1 \partial c_1} = \frac{\partial^2 m_0}{\partial V_{i-1} \partial c_i} = -\frac{1}{2} \quad \text{for } 2 \le i \le m, \text{ and} \qquad \text{(C-14j)}$$

$$\frac{\partial^2 m_0}{\partial V_{i+1} \partial c_i} = \frac{\partial^2 m_0}{\partial V_m \partial c_m} = \frac{1}{2} \quad \text{for } 1 \le i \le m\text{-}1. \qquad \text{(C-14k)}$$

Assuming independence between all n random variables,

$$E[m_0] = \hat{m}_0 \ . \qquad \text{(C-15)}$$

A first-order approximation to the variance can be obtained by neglecting all second-order derivatives, in which case, equation (C-14a) becomes

$$m_0 \cong \hat{m}_0 + \sum_{i=1}^{n} (x_i - \mu_{x[i]}) \frac{\partial \hat{m}_0}{\partial x_i} \qquad \text{(C-16)}$$

Applying equations (C-15) and (C-16) to (C-6b)

$$\sigma^2_{m[0]} \cong E\left[\left(\hat{m}_0 + \sum_{i=1}^{n} (x_i - \mu_{x[i]}) \frac{\partial \hat{m}_0}{\partial x_i}\right)^2\right] - \{\hat{m}_0\}^2 \ , \qquad \text{(C-17a)}$$

which simplifies to

$$\sigma^2_{m[0]} \cong E\left[\left(\sum_{i=1}^{n} (x_i - \mu_{x[i]}) \frac{\partial \hat{m}_0}{\partial x_i}\right)^2\right] \ . \qquad \text{(C-17b)}$$

The square of the sum can be expressed as a double sum:

$$\sigma^2_{m[0]} = E\left[\sum_{i=1}^{n}\sum_{j=1}^{n}(x_i - \mu_{x[i]})(x_j - \mu_{x[j]})\frac{\partial \hat{m}_0}{\partial x_j}\frac{\partial \hat{m}_0}{\partial x_i}\right], \qquad \text{(C-17c)}$$

which can be re-written as

$$\sigma^2_{m[0]} = \sum_{i=1}^{n}\sigma^2_{x[i]}\left(\frac{\partial \hat{m}_0}{\partial x_i}\right)^2 + \sum_{i=1}^{n}\sum_{j>i}^{n}\sigma(x_i, x_j)\frac{\partial \hat{m}_0}{\partial x_j}\frac{\partial \hat{m}_0}{\partial x_i}. \qquad \text{(C-17d)}$$

Noting that x_i and x_j are assumed independent, the first-order, zeroth-moment variance is

$$\sigma^2_{m[0]} \cong \sum_{i=1}^{n}\sigma^2_{x[i]}\left(\frac{\partial \hat{m}_0}{\partial x_i}\right)^2. \qquad \text{(C-17e)}$$

A second-order, zeroth-moment variance is obtained by applying equations (C-14a) and (C-15) to (C-6b):

$$\sigma^2_{m[0]} = E\left[\left(\hat{m}_0 + \sum_{i=1}^{n}(x_i - \mu_{x[i]})\frac{\partial \hat{m}_0}{\partial x_i} + \sum_{i=1}^{n}\sum_{j>i}^{n}(x_i - \mu_{x[i]})(x_j - \mu_{x[j]})\frac{\partial^2 \hat{m}_0}{\partial x_i \partial x_j}\right)^2\right] - \{\hat{m}_0\}^2 \qquad \text{(C-18a)}$$

Assuming independence between variables, and assuming all random variables have symmetric distributions (so that all third-order statistical moments are zero), equation (C-18a) simplifies to

$$\sigma^2_{m[0]} = E\left[\left(\sum_{i=1}^{n}(x_i - \mu_{x[i]})\frac{\partial \hat{m}_0}{\partial x_i}\right)^2 + \left(\sum_{i=1}^{n}\sum_{j>i}^{n}(x_i - \mu_{x[i]})(x_j - \mu_{x[j]})\frac{\partial^2 \hat{m}_0}{\partial x_i \partial x_j}\right)^2\right]. \qquad \text{(C-18b)}$$

Under the assumption of independent variables, the second term on the right hand side of equation (C-18b) can be simplified to

$$\left(\sum_{i=1}^{n}\sum_{j>i}^{n}(x_i-\mu_{x[i]})(x_j-\mu_{x[j]})\frac{\partial^2\hat{m}_0}{\partial x_i\partial x_j}\right)^2 = \sum_{i=1}^{n}\sum_{j>i}^{n}(x_i-\mu_{x[i]})^2(x_j-\mu_{x[j]})^2\left(\frac{\partial^2\hat{m}_0}{\partial x_i\partial x_j}\right)^2 . \quad \text{(C-18c)}$$

Therefore, the second-order, zeroth-moment variance is

$$\sigma^2_{m[0]} = \sum_{i=1}^{n}\sigma^2_{x[i]}\left(\frac{\partial\hat{m}_0}{\partial x_i}\right)^2 + \sum_{i=1}^{n}\sum_{j>i}^{n}\sigma^2_{x[i]}\sigma^2_{x[j]}\left(\frac{\partial^2\hat{m}_0}{\partial x_i\partial x_j}\right)^2 . \quad \text{(C-18d)}$$

Note that under the assumptions used, equation (C-18d) is an exact expression for the zeroth-moment variance.

Derivation of First Absolute Moment Variance

If f = m_1, where m_1 is approximated by the trapezoidal rule, then the first derivatives of the first absolute moment with respect to volume and concentration measurements are

$$\frac{\partial m_1}{\partial V_1} = -\frac{1}{2}(c_2 + c_1)(V_1) , \quad \text{(C-19a)}$$

$$\frac{\partial m_1}{\partial V_i} = \frac{1}{2}(c_{i-1} - c_{i+1})(V_i) \quad \text{for } 2 < i < m\text{-}1, \text{ and} \quad \text{(C-19b)}$$

$$\frac{\partial m_1}{\partial V_m} = \frac{1}{2}(c_m + c_{m-1})(V_m) . \quad \text{(C-19c)}$$

$$\frac{\partial m_1}{\partial c_1} = \frac{1}{4}(V_2^2 - V_1^2) , \quad \text{(C-19d)}$$

$$\frac{\partial m_1}{\partial c_i} = \frac{1}{4}(V_{i+1}^2 - V_{i-1}^2) \quad \text{for } 2 < i < m\text{-}1, \text{ and} \quad \text{(C-19e)}$$

$$\frac{\partial m_1}{\partial c_m} = \frac{1}{4}(V_m^2 - V_{m-1}^2) , \quad \text{(C-19f)}$$

The second derivatives of the first moment are

$$\frac{\partial^2 m_1}{\partial V_1 \partial c_1} = \frac{\partial^2 m_1}{\partial V_1 \partial c_2} = -\frac{1}{2} V_1 \ , \tag{C-19f}$$

$$\frac{\partial^2 m_1}{\partial V_2 \partial c_1} = \frac{1}{2} V_2 \ , \tag{C-19g}$$

$$\frac{\partial^2 m_1}{\partial V_i \partial c_{i-1}} = \frac{1}{2} V_i \quad \text{for } 2 \le i \le m, \tag{C-19h}$$

$$\frac{\partial^2 m_1}{\partial V_i \partial c_{i+1}} = -\frac{1}{2} V_i \quad \text{for } 2 \le i \le m\text{-}1. \text{ and} \tag{C-19i}$$

$$\frac{\partial^2 m_1}{\partial V_m \partial c_m} = \frac{1}{2} V_m \ . \tag{C-19j}$$

For third derivatives

$$\frac{\partial^3 m_1}{\partial x_i^3} = 0 \ , \tag{C-19k}$$

but the third-order, mixed derivatives are not necessarily zero. Finally,

$$m_1^{(k)} = 0 \quad \text{for } k > 4 \ . \tag{C-19l}$$

The Taylor's series approximation to m_1 is therefore

$$\begin{aligned} m_1 = \hat{m}_1 &+ \sum_{i=1}^{n} (x_i - \mu_{x[i]}) \frac{\partial \hat{m}_1}{\partial x_i} + \sum_{i=1}^{n} (x_i - \mu_{x[i]})^2 \frac{\partial^2 \hat{m}_1}{2 \partial x_i^2} \\ &+ \sum_{i=1}^{n} \sum_{j>1}^{n} (x_i - \mu_{x[i]})(x_j - \mu_{x[j]}) \frac{\partial^2 \hat{m}_1}{\partial x_i \partial x_j} + \ldots \end{aligned} \ , \tag{C-20}$$

where all remaining terms are third order, mixed partial derivatives. The x variables are given by equations (C-14b) and (C-14c). Third-order mixed derivatives are not listed because formulas involving those terms will be neglected. Assuming independence between all n random variables, and symmetric distributions, the expected value of m_1 is

$$E[m_1] = \hat{m}_1 + \sum_{i=1}^{n} \sigma_{x[i]}^2 \frac{\partial^2 \hat{m}_1}{2\partial x_i^2} \quad . \tag{C-21}$$

The variance of the absolute first moment is

$$\sigma_{m[1]}^2 = E[m_1^2] - \{E[m_1]\}^2 \quad . \tag{C-22a}$$

Neglecting the third-order mixed partial derivatives, applying equations (C-20a) and (C-21) to (C-22a) yields

$$\sigma_{m[1]}^2 \cong$$
$$E\left[\left(\begin{array}{l} \hat{m}_1 + \sum_{i=1}^{n}(x_i - \mu_{x[i]})\frac{\partial \hat{m}_1}{\partial x_i} + \sum_{i=1}^{n}(x_i - \mu_{x[i]})^2 \frac{\partial^2 \hat{m}_1}{2\partial x_i^2} \\ + \sum_{i=1}^{n}\sum_{j>1}^{n}(x_i - \mu_{x[i]})(x_j - \mu_{x[j]})\frac{\partial^2 \hat{m}_1}{\partial x_i \partial x_j} \end{array}\right)^2\right] \quad . \tag{C-22b}$$
$$-\left\{\hat{m}_1 + \sum_{i=1}^{n}\sigma_{x[i]}^2 \frac{\partial^2 \hat{m}_1}{2\partial x_i^2}\right\}^2$$

Let $\Delta x_i = x_i - \mu_{x[i]}$. Simplifying the right-hand side of equation (C-22b) gives

$$\sigma_{m[1]}^2 =$$
$$2\hat{m}_1 \sum_{i=1}^{n}\sum_{j>1}^{n} \mathrm{cov}(x_i, x_j)\frac{\partial^2 \hat{m}_1}{\partial x_i \partial x_j} + E\left[\left(\sum_{i=1}^{n}\Delta x_i \frac{\partial \hat{m}_1}{2\partial x_i}\right)^2\right]$$
$$+ E\left[2\sum_{i=1}^{n}\Delta x_i \frac{\partial \hat{m}_1}{\partial x_i}\sum_{i=1}^{n}\Delta x_i^2 \frac{\partial^2 \hat{m}_1}{\partial x_i^2}\right] + E\left[2\sum_{i=1}^{n}\Delta x_i \frac{\partial \hat{m}_1}{\partial x_i}\sum_{i=1}^{n}\sum_{j>1}^{n}\Delta x_i \Delta x_j \frac{\partial^2 \hat{m}_1}{\partial x_i \partial x_j}\right] \quad . \tag{C-22c}$$
$$+ E\left[2\sum_{i=1}^{n}\Delta x_i^2 \frac{\partial^2 \hat{m}_1}{2\partial x_i^2}\sum_{i=1}^{n}\sum_{j>1}^{n}\Delta x_i \Delta x_j \frac{\partial^2 \hat{m}_1}{\partial x_i \partial x_j}\right] + E\left[\left(\sum_{i=1}^{n}\sum_{j>1}^{n}\Delta x_i \Delta x_j \frac{\partial^2 \hat{m}_1}{\partial x_i \partial x_j}\right)^2\right]$$

Note that:

$$\sum_{i=1}^{n}\Delta x_i \frac{\partial \hat{m}_1}{\partial x_i}\sum_{i=1}^{n}\Delta x_i^2 \frac{\partial^2 \hat{m}_1}{\partial x_i^2} =$$
$$\sum_{i=1}^{n}\Delta x_i^3 \frac{\partial \hat{m}_1}{\partial x_i}\frac{\partial^2 \hat{m}_1}{\partial x_i^2} + \sum_{i=1}^{n}\sum_{i\neq j}^{n}\Delta x_i^2 \Delta x_j \frac{\partial \hat{m}_1}{\partial x_j}\frac{\partial^2 \hat{m}_1}{\partial x_i^2} \quad . \tag{C-22d}$$

The expected value of the first term on the right hand side of equation (C-22d) is the skewness, which is zero for symmetric distributions. The second term on the right-hand side of equation (C-22d) can be expressed as

$$\sum_{i=1}^{n}\sum_{i\neq j}^{n}\Delta x_i{}^2\Delta x_j\frac{\partial\hat{m}_1}{\partial x_j}\frac{\partial^2\hat{m}_1}{\partial x_i^2}= \sum_{i=1}^{n}\sum_{i\neq j}^{n}\left(\mathrm{cov}(x_i^2,x_j)-2\mu_{x[i]}\,\mathrm{cov}(x_i,x_j)\right)\frac{\partial\hat{m}_1}{\partial x_j}\frac{\partial^2\hat{m}_1}{\partial x_i^2}\quad\text{(C-22e)}$$

which is zero assuming that x_i and x_j are independent. Likewise, under the assumption of symmetric distributions and independence, equation (C-22c) becomes

$$\sigma^2_{m[1]}\cong\sum_{i=1}^{n}\sigma^2_{x[i]}\left(\frac{\partial\hat{m}_1}{\partial x_i}\right)^2+\sum_{i=1}^{n}\sum_{j>i}^{n}\sigma^2_{x[i]}\sigma^2_{x[j]}\left(\frac{\partial^2\hat{m}_1}{\partial x_i\partial x_j}\right)^2\quad\text{(C-22f)}$$

Zeroth and First Absolute Moment Covariance

The zeroth and first absolute moments are not independent since they are based on the same measurements of volume and concentration, and consequently the covariance between the two is needed in order to estimate the variance of the normalized first moment. A Delta-method approximation to the covariance is advantageous due to the complexity involved in deriving an analytical covariance expression. The covariance between the zeroth and first moments is defined as

$$\sigma(m_0,m_1)=E[(m_0-E[m_0])(m_1-E[m_1])]=E[m_0m_1]-E[m_0]E[m_1]\quad\text{(C-23a)}$$

Using equations (C-14a), (C-15), (C-20a), and (C-21), equation (C-23a) can be expressed as

$$\sigma(m_0, m_1) =$$

$$E\left[\left(\hat{m}_0 + \sum_{i=1}^{n}(x_i - \mu_{x[i]})\frac{\partial \hat{m}_0}{\partial x_i} + \sum_{i=1}^{n}\sum_{j>i}^{n}(x_i - \mu_{x[i]})(x_j - \mu_{x[j]})\frac{\partial^2 \hat{m}_0}{\partial x_i \partial x_j}\right)\right.$$

$$\left.*\left(\hat{m}_1 + \sum_{i=1}^{n}(x_i - \mu_{x[i]})\frac{\partial \hat{m}_1}{\partial x_i} + \sum_{i=1}^{n}(x_i - \mu_{x[i]})^2\frac{\partial^2 \hat{m}_1}{2\partial x_i^2}\right.\right.$$

$$\left.\left.+\sum_{i=1}^{n}\sum_{j>1}^{n}(x_i - \mu_{x[i]})(x_j - \mu_{x[j]})\frac{\partial^2 \hat{m}_1}{\partial x_i \partial x_j}\right)\right] \quad . \qquad \text{(C-23b)}$$

$$-\hat{m}_0\left(\hat{m}_1 + \sum_{i=1}^{n}\sigma_{x[i]}^2\frac{\partial^2 \hat{m}_1}{2\partial x_i^2}\right)$$

Using the Δx_i notation once again, equation (C-23b) expands to

$$\sigma(m_0, m_1) = E\left[\hat{m}_0\sum_{i=1}^{n}\sum_{j>i}^{n}\Delta x_i \Delta x_j \frac{\partial^2 \hat{m}_1}{\partial x_i \partial x_j}\right] + E\left[\sum_{i=1}^{n}\Delta x_i \frac{\partial \hat{m}_0}{\partial x_i}\sum_{i=1}^{n}\Delta x_j \frac{\partial \hat{m}_1}{\partial x_i}\right]$$

$$+ E\left[\sum_{i=1}^{n}\Delta x_i \frac{\partial \hat{m}_0}{\partial x_i}\sum_{i=1}^{n}\Delta x_i^2 \frac{\partial \hat{m}_1}{\partial x_i}\right] + E\left[\sum_{i=1}^{n}\Delta x_i \frac{\partial \hat{m}_0}{\partial x_i}\sum_{i=1}^{n}\sum_{j>1}^{n}\Delta x_i \Delta x_j \frac{\partial^2 \hat{m}_1}{\partial x_i \partial x_j}\right]$$

$$+ E\left[\hat{m}_1\sum_{i=1}^{n}\sum_{j>i}^{n}\Delta x_i \Delta x_j \frac{\partial^2 \hat{m}_0}{\partial x_i \partial x_j}\right] + E\left[\sum_{i=1}^{n}\Delta x_i \frac{\partial \hat{m}_1}{\partial x_i}\sum_{i=1}^{n}\sum_{j>1}^{n}\Delta x_i \Delta x_j \frac{\partial^2 \hat{m}_0}{\partial x_i \partial x_j}\right] \quad . \qquad \text{(C-23c)}$$

$$+ E\left[\frac{1}{2}\sum_{i=1}^{n}\Delta x_i^2 \frac{\partial^2 \hat{m}_1}{\partial x_i^2}\sum_{i=1}^{n}\sum_{j>1}^{n}\Delta x_i \Delta x_j \frac{\partial^2 \hat{m}_0}{\partial x_i \partial x_j}\right]$$

$$+ E\left[\left(\sum_{i=1}^{n}\sum_{j>1}^{n}\Delta x_i \Delta x_j \frac{\partial^2 \hat{m}_0}{\partial x_i \partial x_j}\sum_{i=1}^{n}\sum_{j>1}^{n}\Delta x_i \Delta x_j \frac{\partial^2 \hat{m}_1}{\partial x_i \partial x_j}\right)\right]$$

Assuming symmetric probability distributions, and that all random variables are independent, equation (C-23c) reduces to

$$\sigma(m_0, m_1) = \sum_{i=1}^{n}\sigma_{x[i]}^2 \frac{\partial \hat{m}_0}{\partial x_i}\frac{\partial \hat{m}_1}{\partial x_i} + \sum_{i=1}^{n}\sum_{j>i}^{n}\sigma_{x[i]}^2 \sigma_{x[j]}^2 \frac{\partial^2 \hat{m}_0}{\partial x_i \partial x_j}\frac{\partial^2 \hat{m}_1}{\partial x_i \partial x_j} \quad . \qquad \text{(C-23d)}$$

Equation (C-23d) is a second-order approximation to the zeroth and first absolute moment covariance. The first-order covariance approximation simply consists of the first term on the right-hand side of equation (C-23d):

$$\sigma(m_0, m_1) \cong \sum_{i=1}^{2n}\sum_{j=1}^{2n}\sigma(x_i x_j)\left(\frac{\partial \hat{m}_0}{\partial x_i}\right)\left(\frac{\partial \hat{m}_1}{\partial x_j}\right) \quad . \tag{C-24}$$

Normalized First Moment

The pulse-corrected, normalized first moment, μ_1' [L^3] is defined as

$$\mu_1' = \frac{m_1}{m_0} - \frac{V_p}{2}, \tag{C-25}$$

where V_p = tracer pulse volume [L^3]. The variance of the normalized first moment, μ_1, (equal to m_1/m_0) can be estimated by one of two approaches. The first approach is to apply the previous expressions for var[m_0], var[m_1] (either analytical or Delta method formulas), and cov[m_0, m_1] to either equation (C-10b) or (C-10c). Using equation (C-10b), as an example, the variance of μ_1 is

$$\sigma^2_{\mu[1]} = \left(\frac{m_1}{m_0}\right)^2\left(\frac{\sigma^2_{m[0]}}{m_0^2} + \frac{\sigma^2_{m[1]}}{m_1^2} - \frac{2\sigma_{m[0]m[1]}}{m_0 m_1}\right) \quad . \tag{C-26}$$

The other approach is to apply the Delta method directly to the definition of the normalized first moment. For the first-order approximation, this results in (presented without derivation)

$$\sigma^2_{\mu[1]} \cong \sum_{i=1}^{n}\sigma^2_{x[i]}\left(\frac{\partial \hat{\mu}_1}{\partial x_i}\right)^2 = \sum_{i=1}^{n}\sigma^2_{x[i]}\left(\frac{\frac{\partial \hat{m}_1}{\partial x_i}\hat{m}_0 - \frac{\partial \hat{m}_0}{\partial x_i}\hat{m}_1}{\hat{m}_0^2}\right)^2 \tag{C-27}$$

The second-order variance estimate requires the second-order, mixed derivative of μ_1. While technically feasible, this approach was not investigated further because it was not considered to have any advantage over the first approach. Finally, the variance of μ_1' is

$$\sigma^2_{\mu[1]'} = \sigma^2_{\mu[1]} + \sigma^2_{V[p]}, \qquad \text{(C-28)}$$

where $\sigma^2_{V[p]}$ is the variance of one half the tracer-pulse volume, estimated from the field techniques.

REFERENCES

Annable, M. D., P. S. C. Rao, K. Hatfield, W. D. Graham, A. L. Wood, and C. G. Enfield, Partitioning tracers for measuring residual NAPL: Field-scale test results, *Journal of Environmental Engineering*, 124(6), 498-503, 1998.

Asbjornsen, O. A., Error in the propagation of error formula, *AIChE Journal*, 32(2), 332-334, 1986.

Augustijn, D. C. M., L. S. Lee, R. E. Jessup, P. S. C. Rao, M. D. Annable, and A. L. Wood, Remediation of soils and aquifers contaminated with hydrophobic organic chemicals: Theoretical basis for the use of cosolvents, in *Subsurface Restoration*, edited by C. H. Ward, J. A. Cherry, and M. R. Scalf, Ann Arbor Press, Inc., Chelsea, Michigan, 231-250, 1997.

Ball, W. P., G. Xia, D. P. Durfee, R. D. Wilson, M. J. Brown, and D. M. Mackay, Hot methanol extraction for the analysis of volatile organic chemicals in subsurface core samples from Dover Air Force Base, Delaware, *Ground Water Monitoring and Remediation*, 17(1), 104-121, 1997.

Broholm, K., S. Feenstra, and J. A. Cherry, Solvent release into a sandy aquifer. 1. Overview of source distribution and dissolution, *Environmental Science Technology*, 33(5), 681-690, 1999.

Brooks, S. C., D. L. Taylor, and P. M. Jardine, Thermodynamics of bromide exchange on ferrihydrite: Implications for bromide transport, *Soil Science Society of America Journal*, 62(5), 1275-1279, 1998.

Brusseau, M. L., N. T. Nelson, and R. B. Cain, The partitioning tracer method for in-situ detection and quantification of immiscible liquids in the subsurface, in *Innovative Subsurface Remediation, Field Testing of Physical, Chemical, and Characterization Technologies*, ACS Symposium Series 725, edited by M. L. Brusseau, D. A. Sabatini, J. S. Gierke, and M. D. Annable, American Chemical Society, Washington, D.C., 208-225, 1999a.

Brusseau, M. L., Q. Hu, and R. Srivastava, Using flow interruption to identify factors causing nonideal contaminant transport, *Journal of Contaminant Hydrology*, 24(3-4), 205-219, 1997.

Brusseau, M. L., L. H. Xie, and L. Li, Biodegradation during contaminant transport in porous media: 1. Mathematical analysis of controlling factors, *Journal of Contaminant Hydrology*, 37(3-4), 269-293, 1999b.

Cain, R. B., G. R. Johnson, J. E. McCray, W. J. Blanford, and M. L. Brusseau, Partitioning tracer tests for evaluating remediation performance, *Ground Water*, 38(5), 752-761, 2000.

Cooke, C. E., Jr., Method for determining residual oil saturation, U.S. Patent 3,590,923., U.S. Patent Office, Washington, D.C., 1971.

Dean, H. A., Method for determining fluid saturation in reservoirs, U.S. Patent 3,623,842, U.S. Patent Office, Washington, D.C., 1971.

Dwarakanath, V., N. Deeds, and G. A. Pope, Analysis of Partitioning Interwell Tracer Tests, *Environmental Science and Technology*, 33(21), 3829-3836, 1999.

Eikens, D. I., and P. W. Carr, Application of the equation of error propagation to obtaining nonstochastic estimates for the reproducibility of chromatographic peak moments, *Analytical Chemistry*, 61(10), 1058-1062, 1989.

Fahim, M. A., and N. Wakao, Parameter estimation from tracer response measurements, *The Chemical Engineering Journal*, 25(1), 1-8, 1982.

Falta, R. W., C. M. Lee, S. E. Brame, E. Roeder, J. T. Coates, C. Wright, A. L. Wood, and C. G. Enfield, Field test of high molecular weight alcohol flushing for subsurface nonaqueous phase liquid remediation, *Water Resources Research*, 35(7), 2095-2108, 1999.

Funk, W., V. Dammann, G. Donnevert, *Quality Assurance in Analytical Chemistry*, translated by A. Gray, VCH Verlagsgesellschaft, Weinheim, 238 pp., 1995.

Gelhar, L. W., *Stochastic Subsurface Hydrology*, Prentice Hall, Englewood Cliffs, New Jersey, 390 pp., 1993.

Haas, C. N., Moment analysis of tracer experiments, *Journal of Environmental Engineering*, 122(12), 1121-1123, 1996.

Haas, C. N., J. Joffe, M. S. Heath, and J. Jacangelo, Continuous flow residence time distribution function characterization, *Journal of Environmental Engineering*, 123(2), 107-114, 1997.

Hayden, N. J., and H. C. Linnemeyer, Investigation of partitioning tracers for determining coal tar saturation in soils, in *Innovative Subsurface Remediation, Field Testing of Physical, Chemical, and Characterization Technologies*, ACS Symposium Series 725, edited by M. L. Brusseau, D. A. Sabatini, J. S. Gierke,

and M. D. Annable, American Chemical Society, Washington, D.C., 208-225, 1999.

Helms, A. D., Moment estimates for imperfect breakthrough data: Theory and application to a field-scale partitioning tracer experiment, Masters Thesis, University of Florida, Gainesville, 188 pp., 1997.

Imhoff, P. T., S. N. Gleyzer, J. F. Mcbride, L. A. Vancho, I. Okuda, and C. T. Miller, Cosolvent-enhanced remediation of residual dense nonaqueous phase liquids: Experimental investigations, *Environmental Science and Technology*, 29(8), 1966-1976, 1995.

Jawitz, J. W., R. K. Sillan, M. D. Annable, and P. S. C. Rao, Methods for determining NAPL source zone remediation efficiency of in-situ flushing technologies, in *In Situ Remediation of the Geoenvironment*, Proceedings of the Conference, Minneapolis, Minnesota, Geotechnical Special Publication No. 71, 271-283, 1997.

Jawitz, J. W., R. K. Sillan, M. D. Annable, P. S. C. Rao, and K. Warner, In-situ alcohol flushing of a DNAPL source zone at a dry cleaner site, *Environmental Science and Technology*, 34(17), 3722-3729, 2000.

Jin M., G. W. Butler, R. E. Jackson, P. E. Mariner, J. F. Pickens, G. A. Pope, C. L. Brown, and D. C. McKinney, Sensitivity models and design protocol for partitioning tracer tests in alluvial aquifers, *Ground Water*, 35(6), 964-972, 1997.

Jin, M., M. Delshad, V. Dwarakanath, D. C. McKinney, G. A. Pope, K. Sepehrnoori, and C. E. Tilburg, Partitioning tracer test for detection, estimation, and remediation performance assessment of subsurface nonaqueous phase liquids, *Water Resources Research*, 31(5), 1201-1211, 1995.

Jin, M., R. E. Jackson, and G. A. Pope, The interpretation and error analysis of PITT data, in *Treating Dense Nonaqueous-Phase Liquids (DNAPLs): Remediation of Chlorinated and Recalcitrant Compounds*, The Second International Conference on Remediation of Chlorinated and Recalcitrant Compounds, edited by G. B. Wickramanayake, A. R. Gavaskar, and N. Gupta, Monterey, California, 85-92, May 22-25, 2000.

Kendall, M., and A. Stuart, *The Advanced Theory of Statistics*, Macmillan Publishing Co., Inc., New York, 472 pp., 1977.

Kueper, B. H., D. Redman, R. C. Starr, S. Reitsma, and M. Mah, A field experiment to study the behavior of tetrachloroethylene below the water table: Spatial distribution of residual and pooled DNAPL, *Ground Water*, 31(5), 756-766, 1993.

Lapidus, L., and N. R. Amundson, Mathematics of adsorption in beds. VI. The effect of longitudinal diffusion in ion exchange and chromatographic columns, *The Journal of Physical Chemistry*, 56(8), 984-988, 1952.

Lee, C. M., S. L. Meyers, C. L. Wright, Jr., J. T. Coates, P. A. Haskell, and R. W. Falta, Jr., NAPL compositional changes influence partitioning coefficients, *Environmental Science and Technology*, 32(22), 3574-3578, 1998.

Lowe, D. F., C. L. Oubre, and C. H. Ward, editors, *Surfactants and Cosolvents for NAPL Remediation, A Technology Practices Manual*, Lewis Publishers, Boca Raton, 412 pp., 1999.

Liu, C., and W. P. Ball, Application of inverse methods to contaminant source identification from aquitard diffusion profiles at Dover AFB, Delaware, *Water Resources Research*, 35(7), 1975-1985, 1999.

Lunn, S. R. D., and B. H. Kueper, Manipulation of density and viscosity for the optimization of DNAPL recovery by alcohol flooding, *Journal of Contaminant Hydrology*, 38(4), 427-445, 1999.

Lunn, S. R. D., and B. H. Kueper, Removal of pooled dense, nonaqueous phase liquid from saturated porous media using upward gradient alcohol floods, *Water Resources Research*, 33(10), 2207-2219, 1997.

Lynch, M., and B. Walsh, *Genetics and Analysis of Quantitative Traits*, Sinauer Associates, Inc., Sunderland, Massachusetts, 980 pp., 1998.

MacKay, D. M., and J. A. Cherry, Groundwater contamination: Pump-and-treat remediation, *Environmental Sciences and Technology*, 23(6), 630-636, 1989.

Massey, B. S., *Measures in Science and Engineering: Their Expression, Relation and Interpretation*, John Wiley & Sons, New York, 216 pp., 1986.

Nelson, N. T., and M. L., Brusseau, Field study of the partitioning tracer method for detection of dense nonaqueous phase liquid in a trichloroethene-contaminated aquifer, *Environmental Science and Technology*, 30(9), 2859-2863, 1996.

Nelson, N. T., M. Oostrom, T. W. Wietsma, and M. L. Brusseau, Partitioning tracer method for the in situ measurement of DNAPL saturation: Influence of heterogeneity and sampling method, *Environmental Science & Technology*, 33(22), 4046-4053, 1999.

Noll, M. R., S. P. Farrington, and T. J. McHale, *Permit Application for United States Air Force Groundwater Remediation Field Laboratory, Cosolvent Solubilization Technology Demonstration*, submitted to the Delaware Department of Natural Resources and Environmental Control, Dover, Delaware, Applied Research

Associates, Inc. and ManTech Environmental Research Services Corp., Dover, Delaware, May, 1998.

Ogata, A., and R. B. Banks, A solution of the differential equation of longitudinal dispersion in porous media, *U.S. Geological Survey Professional Papers*, 411-A, 1961.

Papoulis, A., *Probability, Random Variables, and Stochastic Processes*, 3rd edition, McGraw-Hill, Inc., New York, 666 pp., 1991.

Park, S. W., and D. M. Himmelblau, Error in the propagation of error formula, *AIChE Journal*, 26(1), 168-170, 1980.

Pope, G. A., and R. E. Jackson, Characterization of organic contaminants and assessment of remediation performance in subsurface formations, U.S. Patent 6,003,365, U.S. Patent Office, Washington, D.C., 1999a.

Pope, G. A., and R. E. Jackson, Characterization of organic contaminants and assessment of remediation performance in subsurface formations, U.S. Patent 5,905,036, U.S. Patent Office, Washington, D.C., 1999b.

Poulsen, M. M., and B. H. Kueper, A field experiment to study the behavior of tetrachloroethylene in unsaturated porous media, *Environmental Science and Technology*, 26(5), 889-895, 1992.

Rao, P. S. C., M. D. Annable, and H. Kim, NAPL source zone characterization and remediation technology performance assessment: Recent developments and applications of tracer techniques, 45(1-2), 63-78, 2000.

Rao, P. C. S., M. D. Annable, R. K. Sillan, D. Dai, K. Hatfield, and W. D. Graham, Field-scale evaluation of in situ cosolvent flushing for enhanced aquifer remediation, *Water Resources Research*, 33(12), 2673-2686, 1997.

Roeder, E., S. E. Brame, and R. W. Falta, Swelling of DNAPL by cosolvent to allow its removal as an LNAPL, in *Non-Aqueous Phase Liquids (NAPLs) in Subsurface Environment: Assessment and Remediation*, ASCE Proceedings, edited by L. N. Reddi, Washington, D.C., 333-344, November 12-14, 1996.

Rivett, M. O., S. Feenstra, and J. A. Cherry, Groundwater zone transport of chlorinated solvents: a field experiment, in *Modern Trends in Hydrology*, Conference of the Canadian Chapter, International Association of Hydrogeologist, Hamilton, Ontario, Canada, 1992.

Sillan, R. K., M. D. Annable, and P. S. C. Rao, *Evaluation of in-situ DNAPL remediation and innovative site characterization techniques*, report submitted to the Florida

Center for Solid and Hazardous Waste Management, Gainesville, Florida, 68 pp., 1999.

Sillan, R. K., M. D. Annable, P. S. C. Rao, D. Dai, K. Hatfield, W. D. Graham, A. L. Wood, and C. G. Enfield, Evaluation of in situ cosolvent flushing dynamics using a network of spatially distributed multilevel samplers, *Water Resources Research*, 34(9), 2191-2202, 1998a.

Sillan, R. K., J. W. Jawitz, M. D. Annable, and P. S. C. Rao, Influence of hydrodynamic and contaminant spatial variability on in situ flushing effectiveness and efficiency, *Groundwater Quality: Remediation and Protection*, Proceedings of the GQ'98 Conference, Tübingen, Germany, IAHS Publication no. 250, 407-414, 1998b.

Skopp, J., Estimation of true moments from truncated data, *AIChE Journal*, 30(1), 151-155, 1984.

Starr, R. C., J. A. Cherry, and E. S. Vales, A new steel sheet piling with sealed joints for groundwater pollution control, in 45th Canadian Geotechnical Conference, Canadian Geotechnical Society, Toronto, Ontario, October 26-28, 1992.

Starr, R. C., J. A. Cherry, and E. S. Vales, Sealable joint sheet pile cutoff walls for preventing and remediating groundwater contamination, in Technology Transfer Conference, Ontario Ministry of the Environment, Toronto, 1993.

Tang, J. S., Partitioning tracers and in-situ fluid-saturation measurements, *SPE Formation Evaluation*, 10(1), 33-39, 1995.

Thomas, A., GRFL: An opportunity in groundwater remediation research, *The Civil Engineer*, 4(2), 34-35, 1996.

Valocchi, A. J., Validity of the local equilibrium assumption for modeling sorbing solute transport through homogeneous soils, *Water Resources Research*, 21(6), 808-820, 1985.

Van Valkenburg, M. E., *Solubilization and Mobilization of Perchloroethylene by Cosolvents in Porous Media*, Ph.D. Dissertation, Department of Environmental Engineering Sciences, University of Florida, Gainesville, 159 pp., 1999.

Willson, C. S., O. Pau, J. A. Pedit, and C. T. Miller, Mass transfer rate limitation effects on partitioning tracer tests, *Journal of Contaminant Hydrology*, 45(1-2), 79-97, 2000.

Winzer, P. J., Accuracy of error propagation exemplified with ratios of random variables, *Review of Scientific Instruments*, 71(3), 1447-1454, 2000.

Wise, W. R., NAPL characterization via partitioning tracer tests: quantifying effects of partitioning nonlinearities, *Journal of Contaminant Hydrology*, 36(1-2), 167-183, 1999.

Wise, W. R., D. Dai, E. A. Fitzpatrick, L. W. Evans, P. S. C. Rao, and M. D. Annable, Non-aqueous phase liquid characterization via partitioning tracer tests: A modified Langmuir relation to describe partitioning nonlinearities, *Journal of Contaminant Hydrology*, 36(1-2), 153-165, 1999.

BIOGRAPHICAL SKETCH

Michael Carson Brooks, son of John A. and Betty W. Brooks, was born on July 12, 1965, in Melbourne, Florida. He attended East Bay High School in Gibsonton, Florida, and graduated with the class of 1983. After an indecisive freshman year at the University of South Florida, an interest in water resources resulted in the selection of civil engineering as his undergraduate major. He graduated with a BSCE in December 1988 and spent the following three years working for an environmental consulting company, in large measure, involved in groundwater contaminant characterization work. From this exposure, he developed an interested in groundwater hydrology and returned to school for graduate education in the subject. He attended Auburn University for two years, working to support himself primarily as a graduate teaching assistant responsible for land surveying classes. He completed his course work, and returned to the consulting industry with the intention of completing his master's thesis within six months. The majority of his efforts while working for the second time in the consulting industry were spent on groundwater remedial designs. Almost two years later, he completed his thesis and was awarded a master's degree in civil engineering in August 1995. That same month, he started into the Ph.D. program at the University of Florida. In February of 1996, he was licensed as a Professional Engineer in the state of Florida.

I certify that I have read this study and that in my opinion it conforms to acceptable standards of scholarly presentation and is fully adequate, in scope and quality, as a dissertation for the degree of Doctor of Philosophy.

William R. Wise, Chairman
Associate Professor of Environmental
Engineering Sciences

I certify that I have read this study and that in my opinion it conforms to acceptable standards of scholarly presentation and is fully adequate, in scope and quality, as a dissertation for the degree of Doctor of Philosophy.

Michael D. Annable
Associate Professor of Environmental
Engineering Sciences

I certify that I have read this study and that in my opinion it conforms to acceptable standards of scholarly presentation and is fully adequate, in scope and quality, as a dissertation for the degree of Doctor of Philosophy.

Paul A. Chadik
Associate Professor of Environmental
Engineering Sciences

I certify that I have read this study and that in my opinion it conforms to acceptable standards of scholarly presentation and is fully adequate, in scope and quality, as a dissertation for the degree of Doctor of Philosophy.

Wendy D. Graham
Professor of Agricultural and Biological Engineering

I certify that I have read this study and that in my opinion it conforms to acceptable standards of scholarly presentation and is fully adequate, in scope and quality, as a dissertation for the degree of Doctor of Philosophy.

P. Suresh C. Rao
Graduate Research Professor of Soils and Water Science

The dissertation was submitted to the Graduate Faculty of the College of Engineering and to the Graduate School and was accepted as partial fulfillment of the requirements for the degree of Doctor of Philosophy.

December, 2000

M. J. Ohanian
Dean, College of Engineering

Winfred M. Phillips
Dean, Graduate School

LD
1780
20 .B873
UNIVERSITY OF FLORIDA
3 1262 06554 4699